

Spring 2021

Cationic Metallo-Polyelectrolytes: Synthesis and Application in Self-Assembly and Mechanochemistry

Yujin Cha

Follow this and additional works at: <https://scholarcommons.sc.edu/etd>

 Part of the [Chemistry Commons](#)

Recommended Citation

Cha, Y.(2021). *Cationic Metallo-Polyelectrolytes: Synthesis and Application in Self-Assembly and Mechanochemistry*. (Doctoral dissertation). Retrieved from <https://scholarcommons.sc.edu/etd/6265>

This Open Access Dissertation is brought to you by Scholar Commons. It has been accepted for inclusion in Theses and Dissertations by an authorized administrator of Scholar Commons. For more information, please contact digres@mailbox.sc.edu.

CATIONIC METALLO-POLYELECTROLYTES: SYNTHESIS AND APPLICATION IN
SELF-ASSEMBLY AND MECHANOCHEMISTRY

by

Yujin Cha

Bachelor of Science
Pohang University of Science and Technology, 2008

Master of Science
Pohang University of Science and Technology, 2011

Submitted in Partial Fulfillment of the Requirements

For the Degree of Doctor of Philosophy in

Chemistry

College of Arts and Sciences

University of South Carolina

2021

Accepted by:

Chuanbing Tang, Major Professor

Morgan Stefik, Committee Member

F. Wayne Outten, Committee Member

Alan W. Decho, Committee Member

Tracey L. Weldon, Interim Vice Provost and Dean of the Graduate School

© Copyright by Yujin Cha, 2021
All Rights Reserved.

DEDICATION

To my parents, for their unconditional love, support and wisdom. Without your
sacrifice, nothing would be possible.

To Heasook, my darling wife, I appreciate your support and love.

To Arin, my lovely daughter, you are the reason why I am living.

ACKNOWLEDGEMENTS

First of all, I really want to express my special thanks to Dr. Tang, my advisor. I appreciate him allowing me to work in his research group. During the last 5 years, he has guided me to become a scientist. He has provided lots of advice about research and life. He is an excellent polymer scientist and I have learned a lot from him. Whenever I am in trouble, his advice always encourages me to overcome obstacles in my life.

Second, I would like to thank Dr. Morgan Stefik, Dr. F. Wayne Outten, and Dr. Alan W. Decho for not only serving as my committee members but also providing me with ideas and support for my research, as well as this dissertation. I also want to express my appreciation to Dr. Ian Manners at the University of Victoria for advice on the CDSA project. I want to thank Dr. Tianyu Zhu for his support and friendship throughout graduate school. His kindness always makes me feel not be alone. I would like to thank Dr. Ye Sha for his help. Lastly, I would also like to thank all the members of Dr. Tang's research group; Dr. Peng Yang, Dr. Yufeng Ma, Dr. Parasmani Pageni, Dr. Md Anisur Rahman, Dr. Meghan E. Lamm, Dr. Dustin Goodlett, Dr. Huina Lin, Dr. Yuanyuan Luo, Jihyeon Hwang, Leman Kurnaz, Shayah Bension, Xiaomeng Li, Ian Baxter, Matt Seraydarian, Luis "LD" Ramos. It was a great pleasure to work with you, and I learned a lot from you. And, I would like to thank LG Chem for providing an opportunity to study abroad.

Furthermore, I would like to thank my family. My parents have always supported me for entire my life. I want to express special thanks to my wife, Heasook Kim. Your sacrifice and support have pushed me to go forward. I want to appreciate to my precious

daughter, Arin Cha. You are my inspiration and reason to live. Thank you for being my kid. Finally, I acknowledge all the funding supports from the University of South Carolina, the National Science Foundation (NSF), Department of Energy (DOE).

ABSTRACT

In this dissertation, cationic metallocene-containing polyelectrolytes were investigated for the construction of nano-objects by CDSA and the mechanical force-responsive polymer. The self-assembly behavior and mechanically induced polymer deformation were characterized and discussed.

In Chapter 1, the overall background and recent development of metallocene-containing polymers as well as their applications in self-assembly and polymer mechanochemistry were introduced. Primary research objectives were described.

The first section of the dissertation on the CDSA of cationic metallocene-containing block copolymers was provided in Chapter 2. The preparation of PCL-*b*-PCoAEMAs was achieved through ring-opening polymerization (ROP) of ϵ -caprolactone and reversible addition-fragmentation chain-transfer (RAFT) polymerization of cobaltocenium amidoethylmetacrylate hexafluorophosphate, followed by ion-exchange. The crystallization-driven self-assembly (CDSA) of these block copolymers was described. Moreover, a unique polymer composition-dependent shape transition was studied. The resultant 2D micelles showed unprecedented ionic strength-dependent stability.

The second part of the dissertation is the preparation and characterization of main-chain cobaltocenium-containing copolymers. In Chapter 3, the preparation of cobaltocenium cyclic olefins and main-chain cobaltocenium-containing polymers were described. The diallyl cobaltocenium, a precursor for cyclic olefin, was prepared through

modification of cyclopentadiene (CP) with allyl bromide, followed by coupling with cobalt bromide. The resultant diallyl cobaltocenium showed thermal isomerization in the aqueous solution. The ring-closing metathesis of diallyl cobaltocenium isomers resulted in two different cobaltocenium cyclic olefins; [3]-*asna*- and [4]-*ansa*- cobaltocenophane. The main-chain cobaltocenium-containing copolymers were prepared by ring-opening metathesis polymerization (ROMP) of cobaltocenium cyclic olefin and cyclooctene derivatives, resulting in 2-5 % of labeling ratio. Chapter 4 is dedicated to mechanochemistry of main-chain cobaltocenium-containing metallopolymer. The cobaltocenium-containing polymers were prepared by ROMP. The computational studies proved the mechanistic insight of cobaltocenium mechanophore. A strikingly different dissociation mechanism was further proposed.

Finally, Chapter 5 provides a summary of this dissertation research and outlook for future research.

TABLE OF CONTENTS

Dedication	iii
Acknowledgements	iv
Abstract	vi
List of Figures	x
List of Symbols	xv
List of Abbreviations	xvi
Chapter 1 General Introduction	1
1.1 Metallopolymer	2
1.2 Block Copolymer Self-Assembly.....	6
1.3 Crystallization-Driven Self-Assembly	9
1.4 Polymer Mechanochemistry	12
1.5 Mechanophore	14
1.6 Polymerization Techniques	17
1.7 Research Objectives	22
1.8 References	23
Chapter 2 Crystallization-Driven Self-Assembly of Metallo-Polyelectrolyte Block Copolymer with Polycaprolactone Core-Forming Segment.....	34
2.1 Abstract	35
2.2 Introduction	35
2.3 Experimental	36

2.4 Results and Discussion.....	45
2.5 Conclusion.....	62
2.6 References	63
Chapter 3 Preparation of [3]-, [4]- <i>ansa</i> -Cobaltocenium Hexafluorophoste and Their Application in Ring-Opening Metathesis Polymersization	70
3.1 Abstract	71
3.2 Introduction	71
3.3 Experimental	74
3.4 Results and Discussion.....	80
3.5 Conclusion.....	89
3.6 References	89
Chapter 4 Mechanochemistry of Cationic Metallocene Mechanophore.....	98
4.1 Abstract	99
4.2 Introduction	99
4.3 Experimental	101
4.4 Results and Discussion.....	107
4.5 Conclusion.....	122
4.6 References	123
Chapter 5 Summary and Outlook	131
5.1 Dissertation Summary	132
5.2 Outlook.....	133
Appendix A: Permission to Reprint.....	135

LIST OF FIGURES

Figure 1.1 Electrochemical properties of cobaltocene/cobaltocenium.	3
Figure 1.2 Class of metallocene-containing polymers.....	4
Figure 1.3 Free radical copolymerization of ferrocene ethyl methacrylate and structure of metallocene monomer with various linker structures.....	5
Figure 1.4 Representative structures of metallocene cyclic monomers and main-chain metallocene-containing polymer.....	6
Figure 1.5 Typical structures of block copolymers with two different blocks, A and B.	7
Figure 1.6 Block copolymer phase diagram and representative morphologies	8
Figure 1.7 Block copolymer self-assembly in solution.	9
Figure 1.8 Representative structures of crystallizable polymers.	11
Figure 1.9 Illustration of crystallization-driven self-assembly of the block copolymer	11
Figure 1.10 Illustration of polymer deformation under external force	12
Figure 1.11 Representative structures of mechanophore.....	15
Figure 1.12 Representative modes of mechanical dissociation of mechanophores.....	16
Figure 1.13 Typical ROP of ϵ -caprolactone and representative structures of catalysts used in ROP.....	18
Figure 1.14 General mechanism of RAFT polymerization	20
Figure 1.15 Mechanism of ROMP and structures of Grubbs' catalysts	21
Figure 2.1 GPC trace of polycaprolactone homopolymer (M_n (GPC) = 6,500 g/mol, $D = 1.25$)	40
Figure 2.2 DSC curve of polycaprolactone homopolymer	40

Figure 2.3 FT-IR spectra of PCL-OH (red) and PCL-N ₃ (blue)	42
Figure 2.4 ¹ H-NMR spectrum of PCL- <i>b</i> -PCoAEMAPF ₆	44
Figure 2.5 Synthesis of cobaltocenium-containing block copolymers	46
Figure 2.6 (A) Schematic illustration of the formation of 2D hexagonal platelets by CDSA of block copolymer PCL ₆₁ - <i>b</i> -PCoAEMA ₅₈ . (B) TEM micrograph of hexagonal platelets from PCL ₆₁ - <i>b</i> -PCoAEMA ₅₈ obtained by heating the polymer solution in methanol at 40 °C for 1 h followed by cooling and aging at room temperature for 1 month. (C) TEM SAED of hexagonal platelets. (D) AFTM height image. (E) AFM height profile from image D	48
Figure 2.7 (A) Additional TEM micrograph of elongated hexagonal platelet of PCL ₆₁ - <i>b</i> -PCoAEMA ₅₈ with a concentration of 0.5 mg/mL in methanol and annealing at 40 °C for 1 hour, followed by cooling to 25 °C and then aging for 1 month; and (B) area distribution (average area = 19.6 μm ² , area dispersity = 1.24)	49
Figure 2.8 TEM-EDX analysis of hexagonal platelets	49
Figure 2.9 Time dependent ¹ H NMR spectra of PCL ₆₁ - <i>b</i> -PCoAEMA ₅₈ in methanol- <i>d</i> ₄	50
Figure 2.10 TEM micrographs of PCL ₆₁ - <i>b</i> -PCoAEMA ₅₈ in methanol: (A) before heating; (B) aging for 1 day; (C) aging for 3 days; and (D) aging for 11 days. Plots of (E) area versus aging time and (F) aspect ratio versus aging time	51
Figure 2.11 Illustration of CDSA of PCL- <i>b</i> -PCoAEMA block copolymer toward hexagonal platelet nanostructures	52
Figure 2.12 (A) TEM micrograph of wider hexagonal platelets obtained from PCL ₆₁ - <i>b</i> -PCoAEMA ₂₄₄ in methanol (0.5 mg/mL) with heating at 40 °C for 1 hour, followed by cooling to 25 °C and then aging for 1 month; (B) Electron diffraction; (C) AFM height image; (D) AFM height profile from image C; and (E) area distribution (average area = 2.76 μm ² , area dispersity = 1.05)	54
Figure 2.13 (A) TEM micrograph of diamond-shaped platelets of PCL ₆₁ - <i>b</i> -PCoAEMA ₃₄₄ in methanol (0.5 mg/mL) with heating at 40 °C for 1 hour, followed by cooling to 25 °C and then aging for 1 month; (B) Electron diffraction; (C) AFM height image; (D) AFM height profile from image C; and (E) area distribution (average area = 3.37 μm ² , area dispersity = 1.11)	55

Figure 2.14 TEM micrographs of lenticular structures from PCL ₆₁ - <i>b</i> -PCoAEMA ₃₄₄ in methanol (0.5 mg/mL) obtained by annealing at 40 °C for 1 hour, followed by cooling to 25 °C and then aging for 1 month. Insert: magnified areas from dashed yellow squares	56
Figure 2.15 Schematic of (A, B) lower aspect ratio hexagonal platelet from PCL ₆₁ - <i>b</i> -PCoAEMA ₂₄₄ and diamond-shaped platelet from PCL ₆₁ - <i>b</i> -PCoAEMA ₃₄₄ . TEM micrographs of platelets formed by (C) PCL ₆₁ - <i>b</i> -PCoAEMA ₂₄₄ with an area dispersity of 1.05, (D) PCL ₆₁ - <i>b</i> -PCoAEMA ₃₄₄ with an area dispersity of 1.11, and (E) PCL ₆₁ - <i>b</i> -PCoAEMA ₅₈ in methanol and (F) plot of aspect ratio versus block ratio.....	58
Figure 2.16 TEM micrographs of leaf-like platelet of (A) PCL ₆₁ - <i>b</i> -PCoAEMA ₅₈ ; (A) PCL ₆₁ - <i>b</i> -PCoAEMA ₂₄₄ ; and (C) PCL ₆₁ - <i>b</i> -PCoAEMA ₃₄₄ in methanol (0.5 mg/mL), followed by addition of PCL ₃₈ homopolymer in THF solution	59
Figure 2.17 (A) TEM micrograph of sphere-shaped micelles of PCL ₆₁ - <i>b</i> -PCoAEMA ₅₈ with a concentration of 0.5 mg/mL in water after annealing at 40 °C for 1 hour; (B) area distribution (average area = 19.6 μm ² , area dispersity = 1.24); DLS profiles of spherical micelles from PCL ₆₁ - <i>b</i> -PCoAEMA ₅₈ : (C) in water (red, corresponds to the TEM micrograph in Figure S7, R _h = 36.7 nm); (D) unimers dissolved in DMF (blue, R _h = 8.9 nm) after annealing at 40 °C.....	61
Figure 2.18 (A) Illustration of platelet fragmentation of PCL ₆₁ - <i>b</i> -PCoAEMA ₅₈ caused by charge repulsion and preservation by charge screening in accordance with ionic strength; TEM micrographs: (B) fragmented hexagon by in methanol and water (v/v, 50/50), and (C) preserved hexagons by in methanol and 2.0 M NaCl aq. solution (v/v, 50/50).....	62
Figure 3.1 The reaction of cyclic cobaltoceniums with gas molecules	79
Figure 3.2 Synthesis of diallyl cobaltocenium hexafluorophosphate, cyclic cobaltocenium monomer via RCM, and main-chain cobaltocenium-containing polymers via ROMP	81
Figure 3.3 ¹ H-NMR spectrum of mixture (6.4:3.6 ratio) of 1,1'-diallyl cobaltocenium 1 and 1-allyl-1'-(1-propen-1-yl) cobaltocenium hexafluorophosphate 2	82
Figure 3.4 (A) ¹ H NMR spectra of mixtures of compound 1 and 2 with 8.0:2.0 ratio (bottom blue) and the mixture of compound 1, 2, and 3 with 1.7:5.0:3.3 ratio (top red); (B) 2D COSY ¹ H NMR of compound 1 and 2 with 8.0:2.0 ratio.....	82

Figure 3.5 UV-vis absorption spectra of the isomerized cobaltocenium.....	83
Figure 3.6 ^1H NMR spectra of mixtures of compounds 4 and 5 with 7.0:3.0 ratio (top blue) and 2.2:7.8 ratio (bottom red).....	84
Figure 3.7 (A) Optimized energy of 1, 2, and 3; (B) Ring strain energy of 4, 5, and 6.....	85
Figure 3.8 (A) Synthesis of ROMP for main-chain cobaltocenium-containing polymers; (B) GPC trace of copolymers	86
Figure 3.9 ^1H NMR spectra of (A) P1, (B) P2, and (C) P3; ^{19}F NMR spectra of (D) P1, (E) P2, and (F) P3	88
Figure 4.1 The structure of model cobaltocenium compound	103
Figure 4.2 Structural variation of substituted cobaltocenium	107
Figure 4.3 (A) ^1H NMR; and (B) ^{19}F NMR of cobaltocenium end-labeled PMA with ester linker before (green) and after (red) sonication	108
Figure 4.4 (A) ^1H NMR; and (B) ^{19}F NMR of cobaltocenium end-labeled RAFT agent with triazole linker before (green) and after (red) sonication.....	109
Figure 4.5 Synthesis of cobaltocenium end-labeled PMMA by RAFT polymerization.....	109
Figure 4.6 (A) ^1H NMR spectrum; (B) ^{19}F NMR spectrum (blue: before sonication; red: after sonication); and (C) UV-vis absorption spectrum of P1	110
Figure 4.7 Synthetic scheme of a main-chain cobaltocenium-containing polymer.....	111
Figure 4.8 (A) GPC trace of P2 before and after sonication for 2 h; (B) ^1H NMR spectrum; UV-vis absorption spectrum of P2 (C) with 1,10- phenanthroline (D) without 1,10-phenanthroline	112
Figure 4.9 ^{19}F NMR spectrum of P2 before and after sonication for 2 h in DCM at concentration of 2.5 mg/mL	113
Figure 4.10 Schematic illustration of cobaltocenium dissociation under ultrasonication	113
Figure 4.11 (A) GPC trace; (B) Plot of M_n vs. sonication time of P2 in DCM; (C) GPC trace; and (D) Plot of M_n vs. sonication time of P2 in DCM/MeOH (9/1, v/v) after sonication 30, 60, 90, 120, 150, 180, 210, and 240 min	115

Figure 4.12 Proposed mechanism of back complexation during sonication.....	117
Figure 4.13 (A) Side view; (B) top view for structural evolution of cobaltocenium model compound with stretching distance; (C) representative electrostatic potential map (The contour surface is described based on van der Waals surface with an electron density of 0.001 e/Bohr ³ proposed by Bader; (D) COGEF potential (red symbol) and ion distance (blue symbol) with stretching of end-to-end distance	119
Figure 4.14 COGEF potential of ferrocene model compound with stretching of end-to-end distance	120
Figure 4.15 COGEF force of (A) cobaltocenium; and (B) ferrocene with stretching distance	121
Figure 4.16 (A) COGEF potential of cobaltocenium model compound with stretching and relaxing; (B) optimized geometries at 3.8 Å, 5.6 Å, and 6.5 Å	122
Figure 5.1 Schematic illustration of (A) Shell-crosslinking of 2D micelle and (B) application of di-bridged cobaltocenium for cross-linking of polymers.	133
Figure A.1 Permission to reprint Figure 1.6	136
Figure A.2 Permission to reprint Figure 1.7	137
Figure A.3 Permission to reprint Figure 1.12	138
Figure A.4 Permission to reprint Chapter 2	139

LIST OF SYMBOLS

A_n	Number-average area
A_w	Weight-average area
L_n	Number-average length
W_n	Number-average width
M	Molar concentration
M_n	Number-average molecular weight
M_w	Weight-average molecular weight
\mathcal{D}	Dispersity
E_{cyclic}	Optimized energy of cyclic of cobaltocenium
E_{open}	Optimized energy of di-olefin cobaltocenium
E_{gas}	Optimized energy of ethylene
F_{max}	Force associated with the mechanochemical transformation

LIST OF ABBREVIATIONS

AFM.....	Active Case Detection
AIBN.....	Azobisisobutyronitrile
BDE.....	Bond Dissociation Energy
CDSA.....	Crystallization-Driven Self-Assembly
COGEF	Constrained Geometry Simulating External Force
DCM	Dichlorometane
DFT	Density Functional Theory
DLS	Dynamic Light Scattering
DMF.....	<i>N,N</i> -Dimethylformamide
DSC.....	Differential Scanning Calorimetry
EDG	Electron Donating Group
EVE.....	Ethyl Vinyl Ether
EWG	Electron Withdrawing Group
FTIR.....	Fourier Transform Infrared Spectrometry
GPC.....	Gel Permeation Chromatography
LDA	Lithium Diisopropyl Amide
NMR	Nuclear Magnetic Resonance
PCL	Polycaprolactone
RCM.....	Ring-Closing Metathesis
PMMA	Polymethylmethacrylate
ROMP	Ring-Opening Metathesis Polymerization

ROP	Ring-Opening Polymerization
SAED	Selected Area Electron Diffraction
TEM	Transmission Electron Microscopy
THF	Tetrahydrofuran

CHAPTER 1
GENERAL INTRODUCTION

1.1 Metallopolymer

Metallopolymer is defined as any polymer containing metal. The unique combination of organic and inorganic components makes the metallopolymer an outstanding macromolecule. The metal building blocks are either hydrophobic or hydrophilic, affording desirable material properties by tuning their properties. In past decades, metallopolymers have gained enormous attention as a novel class of polymeric material with the unique electrochemical, optical, responsive, and catalytic properties of the metal component.¹⁻⁴ Especially, metallocene-containing polymers has been in the middle of interest of material research due to the high thermodynamic stability, reversible redox properties, their unique sandwich structure.^{5, 6}

One of the most investigated metallocenes is ferrocene, which has iron as a metal center and two cyclopentadienyl ligands. Since it was first synthesized in 1951,⁷ tremendous efforts have been put into the various metallocene-containing polymers for a broad spectrum of applications in catalyst, sensors, nanolithography, and biomedicine.⁸⁻¹⁴ The introduction of metallocene into polymers is a versatile method for promising materials since it has distinctive characteristics compared to the organic building block. For example, Wurm and coworkers reported that the redox-responsiveness of ferrocene could be utilized for the controlled drug delivery system.¹⁵ The oxidation of ferrocene to ferrocenium can provide the cationic charge into the polymer backbone, resulting in charge-charge repulsion. This behavior can trigger the morphological transition and release the loaded drug to the out of the carrier. Moreover, chemical modification of metallocene has provided a more accessible strategy for the metallocene-containing materials.

Although the majority of metallocene-containing polymers have mainly focused on the neutral metallocene, the charged metallocene, which is called cationic metallocene or metallocenium, recently has attracted considerable attention due to their cationic characteristics. For example, cobaltocenium, an isoelectronic molecule to neutral ferrocene, represents a type of charged metallocene. The unstable 19-e cobaltocene can quickly lose one electron to form the much more stable 18-e cobaltocenium cation (**Figure 1.1**). The cationic metalloceniums are primarily different from neutral metallocenes because they are ionic states and can possess hydrophilic or hydrophobic characteristics, depending on their counterions. The counterion-dependent characteristics of metallocenium-containing polymers give rise to more functional materials. For example, the cobaltocenium-containing polymers show high solubility in water using hydrophilic counterion, which could be more beneficial for biomedical applications.¹⁶⁻²⁰

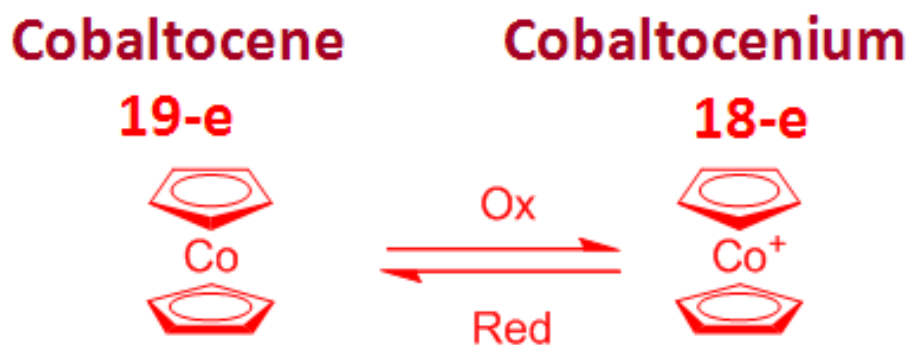


Figure 1.1. Electrochemical properties of cobaltocene/cobaltocenium.

Generally, the metallocene-containing polymers can be classified based on metallocene locations. Rational synthetic strategies and various polymerization techniques allow the precise incorporation of metallocene into the specific position of macromolecules. Most often, the metallocene can be located in the main chain or side-

chain with various chemical linkages. The other types of metallocene polymers are star-shaped and dendritic macromolecules (**Figure 1.2**). Among the types of metallocene-containing polymers, main-chain and side-chain metallocene polymers have been intensively studied.

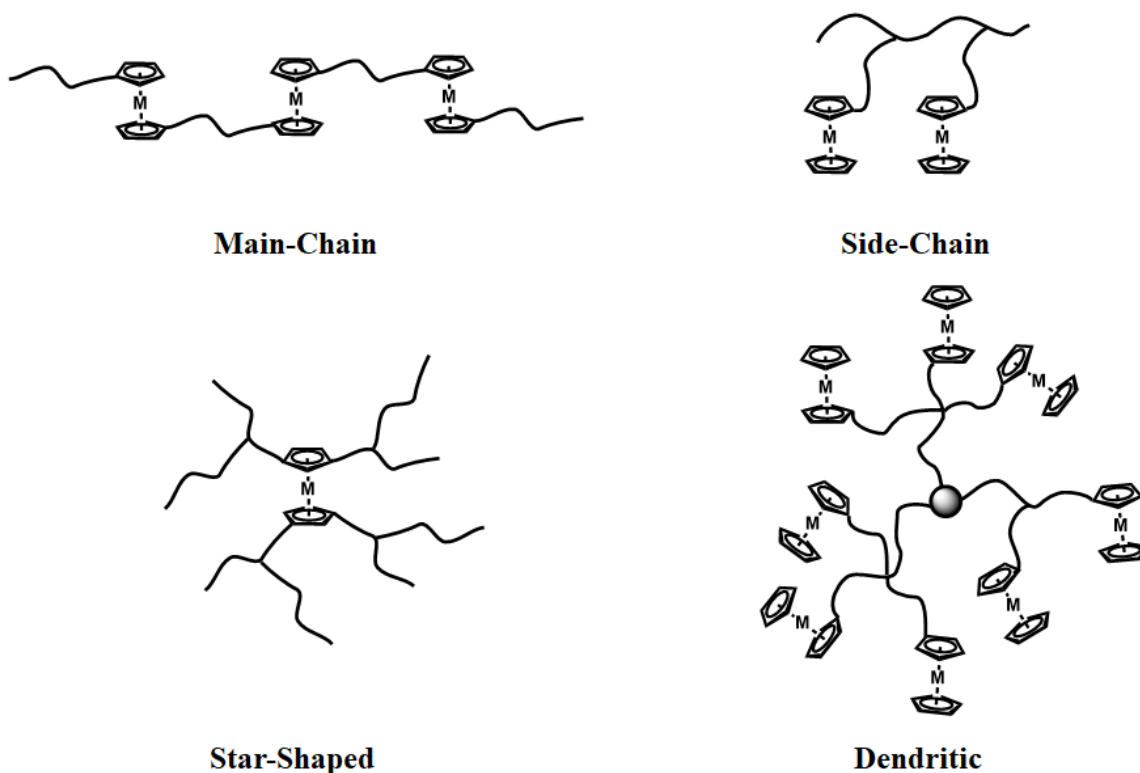


Figure 1.2. Class of metallocene-containing polymers.

Early efforts to prepare metallopolymers with metallocene pendent group mainly focused on through free radical polymerization of vinyl functionalized metallocene.^{21, 22} The homo and copolymerization of ferrocene with acrylate, methacrylate, and styrene monomer was examined using AIBN as an initiator (**Figure 1.3**). Not only free radical polymerization but also controlled radical polymerization has been examined.

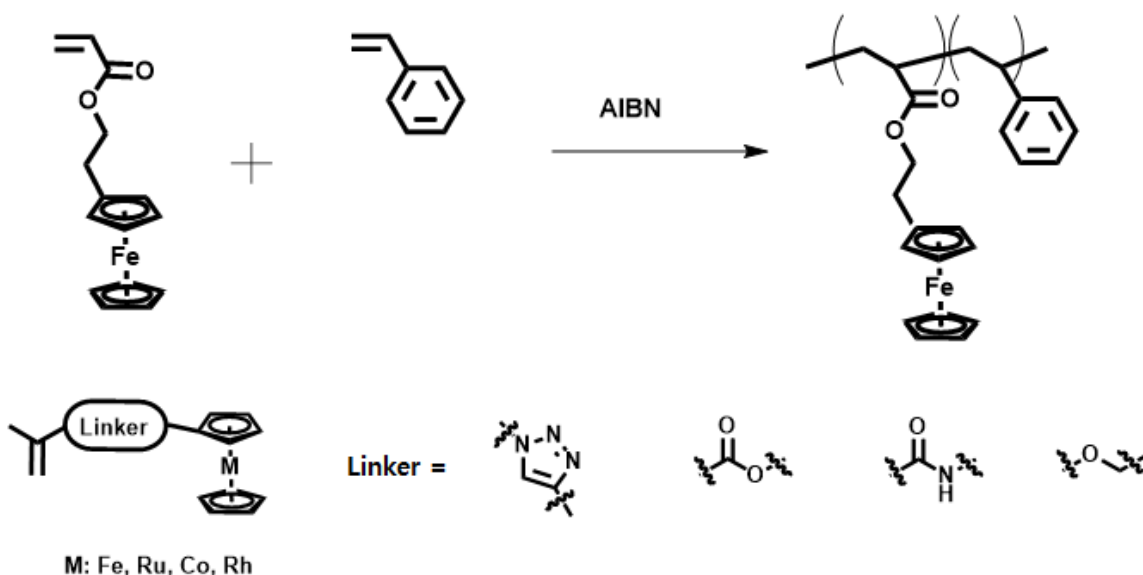


Figure 1.3. Free radical copolymerization of ferrocene ethyl methacrylate and structure of metallocene monomer with various linker structures.

Main-chain metallocene-containing polymers with multiple metallocene building blocks can be prepared the step-growth polymerization of difunctional metallocene units via esterification,²³ amidation,²⁴ and cross-metathesis.²⁵ However, step-growth polymerization is very challenging to obtain high molecular weight due to its sensitivity to monomer conversion and impurities.²⁶ Alternative chain-growth polymerization of cyclic monomers via ring-opening polymerization (ROP) has been successfully developed for main-chain metallocene polymers.^{27, 28} Ring-opening metathesis polymerization (ROMP), one of the most powerful controlled polymerization techniques with mild reaction conditions, has been utilized to prepare main-chain metallocene-containing polymers.²⁹ Cyclic metallocene monomers, which is called *ansa*-metallocenophane, are critical components for developing main-chain metallocene-containing polymer (**Figure 1.4**).³⁰ Highly strained metallocenophanes can be polymerized via an enthalpy-driven ROMP,³¹ whereas less strained metallocenophanes can be incorporated via an entropy-driven (ED) ROMP.³²

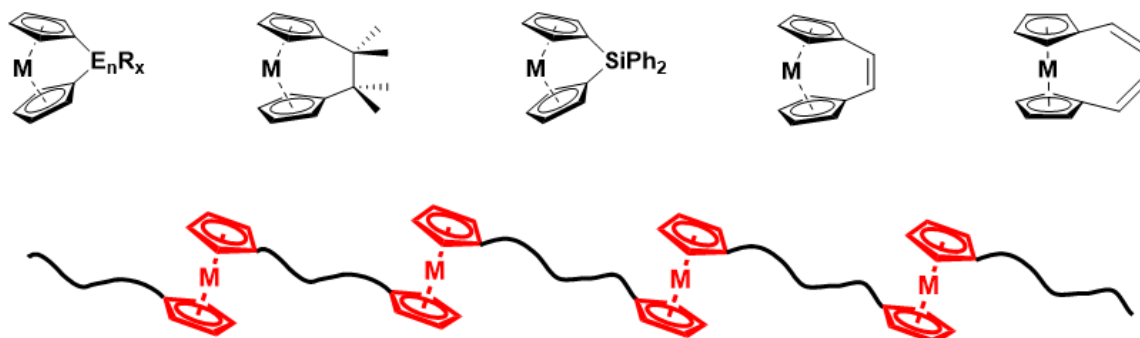


Figure 1.4. Representative structures of metallocene cyclic monomers and main-chain metallocene-containing polymer.

1.2 Block Copolymer Self-Assembly

Self-assembly governs mother nature. Myriads of biomacromolecules are constructed by self-assembly: protein, DNA double helix, lipid bilayers, etc. Most sophisticated natural structures are assembled via weak interactions, such as hydrogen bonding, hydrophobic interactions, and π - π interactions. For the last century, chemists have succeeded in finding many ways to make complex structures by forming and destroying covalent bonds between molecules. However, these approaches are far from what nature does.

From a material science point of view, molecular self-assembly can provide a simple and low-cost bottom-up method to achieve functional materials from pre-fabricated building blocks with reduced steps. Several types of building blocks can be utilized for the self-assembly process from atoms to macromolecules.

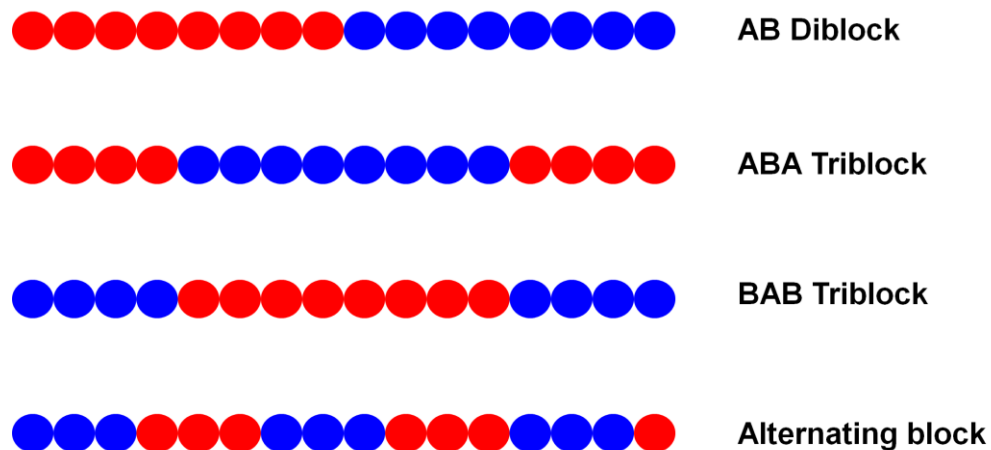


Figure 1.5. Typical structures of block copolymers with two different blocks, A and B.

Among a wide range of different molecules, synthetic block copolymers have gained great attraction from material scientists due to their variety of processability. The block copolymers consist of two or more chemically different and immiscible blocks which are covalently linked (**Figure 1.5**). Block copolymer self-assembly in bulk can afford ordered structures in a series of various morphologies: spheres, gyroid, cylinders, and lamellae (**Figure 1.6**). Self-assembly of these macromolecules depends on their properties, such as molecular weight, composition, inter- or intramolecular interactions.³³

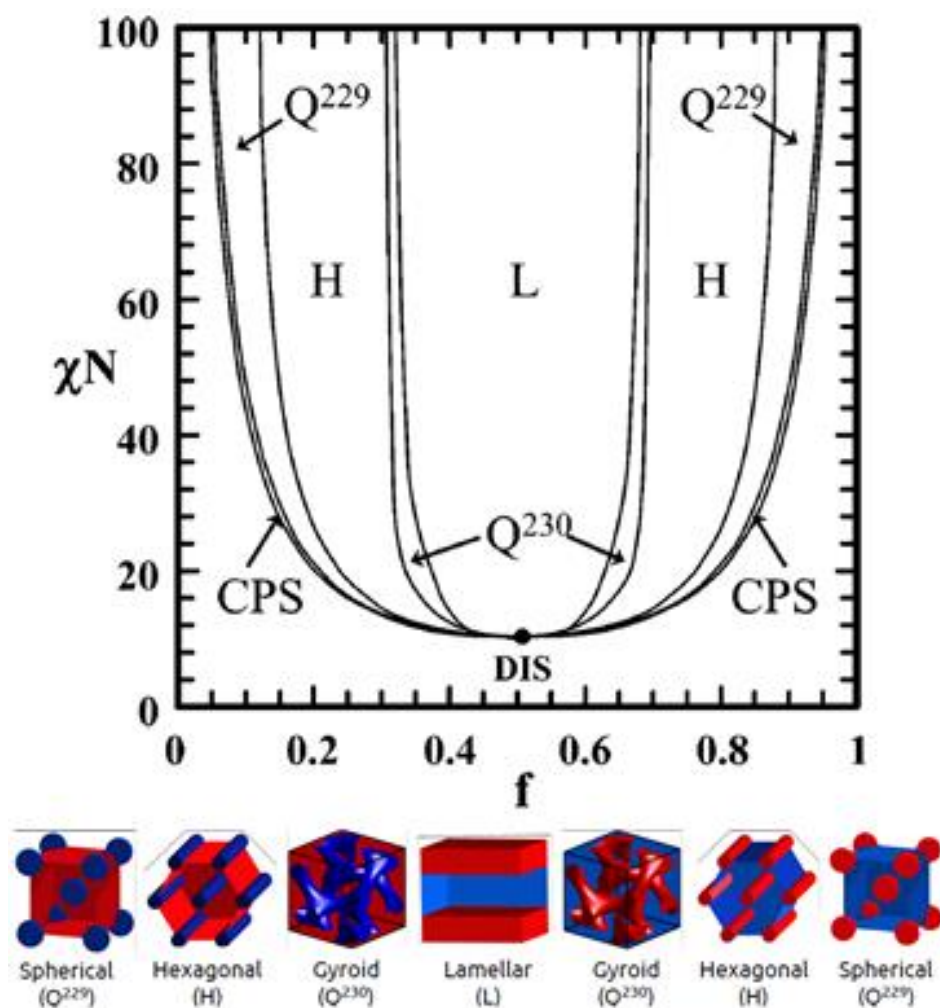


Figure 1.6. Block copolymer phase diagram and representative morphologies. (Adapted with permission from ref [33]. Copyright (2021) American Chemical Society)

Introduction of solvent causes the complexity of block copolymer self-assembly. Compared to self-assembly in bulk state, that solution has to account for the interaction between polymers and solvent. Despite the complex situation, the BCP self-assembly in aqueous solutions provides more potential in biomedical applications since water is a more bio-relevant solvent. Moreover, Diverse morphologies can be obtained by BCP self-assembly in solution.³⁴ More than 20 morphologies have been reported, such as spherical micelles, rods, bicontinuous structures, lamellae, vesicles, large compound micelles

(LCMs), large compound vesicles (LCVs), tubules, “onions”, “eggshells”, baroclinic tubules, pincushions, etc.³⁵

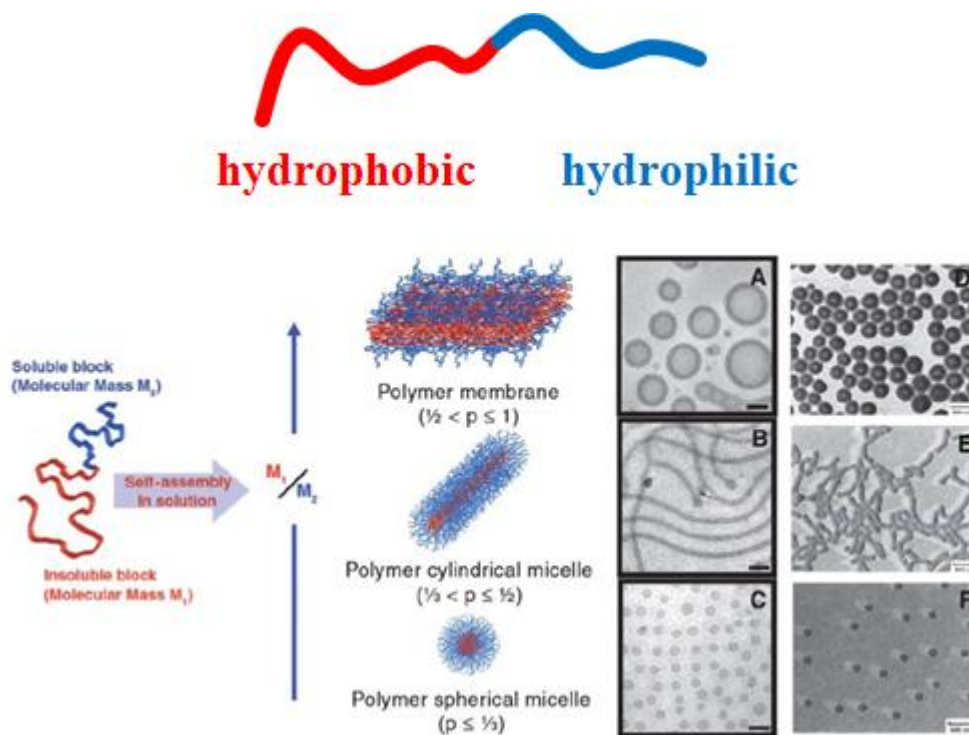


Figure 1.7. Block copolymer self-assembly in solution. (reprinted from ref [34] with permission from Elsevier)

1.3 Crystallization-Driven Self-Assembly

Investigations of block copolymer self-assembly in solvents were exclusively focused on block copolymers possessing amorphous core-forming blocks. Although BCP self-assembly has shown promising potential for many applications, efforts to expand its utility have suffered due to several limitations. Firstly, the formation of BCP micelles with diverse morphologies is quite challenging.³⁶ Even though 1D fibers or 2D micelles have significant advantages over spherical micelles, such as higher drug loading capacity, longer circulation time, and efficient accumulation, which are crucial factors in determining efficient drug carrier,³⁷ the self-assembly of amorphous core-containing block copolymers requires sophisticated material preparation procedure, for example, a narrow range of

polymer composition and self-assembly conditions. Second, length control and low dispersity of resultant micelles are pretty limited. The majority of impressive self-assemblies possessing amorphous core-forming blocks controlling micelle have an issue on control over micelles' dimension.³⁸

On the other hand, several interesting studies from the 1960s have reported block copolymers containing a crystallizable core-forming block that can form 2D micelles in selective solvents selective for the corona-forming blocks. BCP self-assembly that the crystallization of core-forming block plays a critical role in determining the morphology is referred to as crystallization-driven self-assembly (CDSA). Over the past two decades, CDSA of block copolymers with a crystallizable core-forming block in solution has been intensively studied to fabricate diverse morphologies from cylindrical micelles to 2D platelets. As a pioneer in this field, Manners and his coworkers have developed CDSA and living CDSA to construct various and well-controlled micelles. For example, poly(ferrocenyldimethylsilane) was utilized as a crystallizable core-forming block with various corona-forming blocks.³⁹⁻⁴¹ Not only ferrocenyl derivatives but also a broad spectrum of the crystallizable core-forming block has been used for CDSA, such as poly(L-lactic acid) (PLLA)⁴²⁻⁴⁴, polycaprolactone (PCL)⁴⁵⁻⁴⁷, poly(ethylene glycol) (PEG)^{48, 49}, polyethylene (PE)^{50, 51}, polythiophene (PHT)⁵² (**Figure 1.8**).

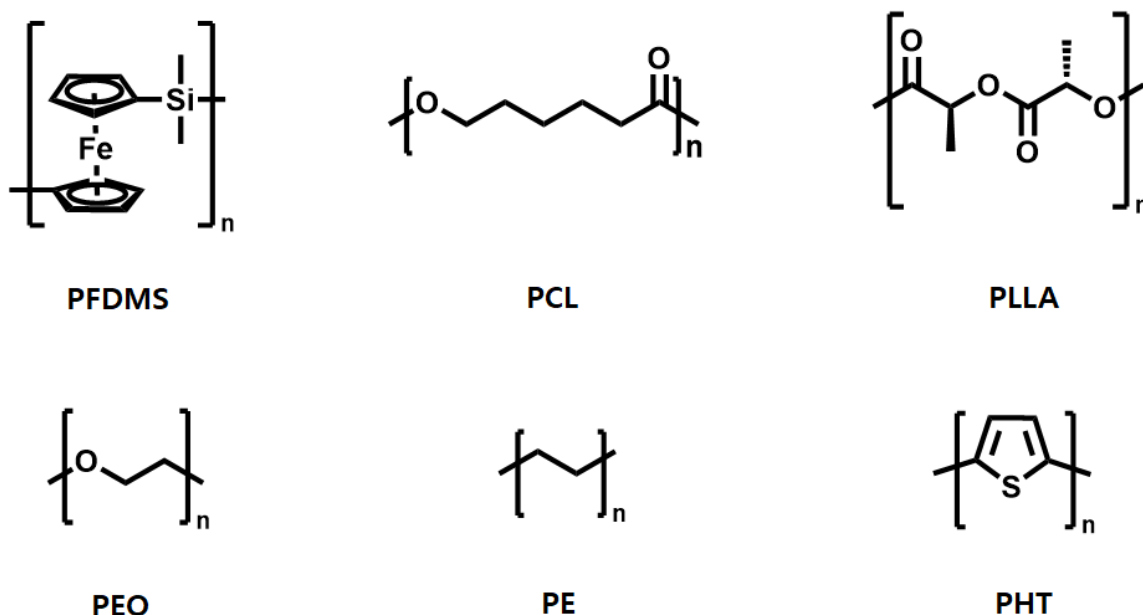


Figure 1.8. Representative structures of crystallizable polymers.

The formation of 1D and 2D micelles in CDSA undergoes two sept procedures. First, crystalline nuclei are formed during the precipitation step. The formation of nuclei is followed by subsequent epitaxial growth of unimers present in the polymer solution. The resulting micelles yield relatively largely dispersed size due to the difference in the rate of formation of nuclei. The rate of formation of nuclei would be expected to be slow compared to the rate of epitaxial growth of unimers (**Figure 1.9**). More precise control over size in resultant micelles can be accomplished by using seeded growth of unimers from preexisting nuclei present in the polymer solution.

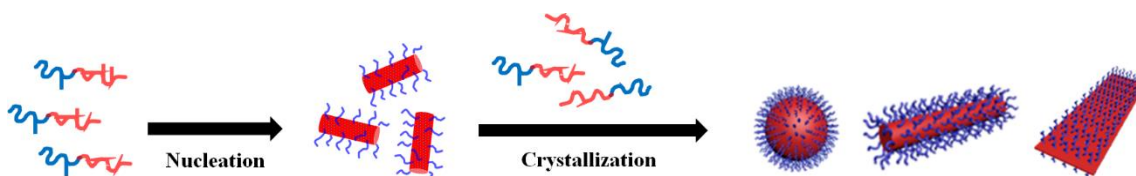


Figure 1.9. Illustration of crystallization-driven self-assembly of the block copolymer.

1.4 Polymer Mechanochemistry

The concept of polymer mechanochemistry can be traced back to the 1930s. Staudinger reported the molecular weight reduction of polyisoprene when subjected to mastication.⁵³ This phenomenon was further elucidated by Kauzmann and Eyring, which is attributed to the cleavage of the covalent bond in the polymer.⁵⁴ Mechanical deformation of material can limit the lifetime of material on both macroscopic and molecular levels.

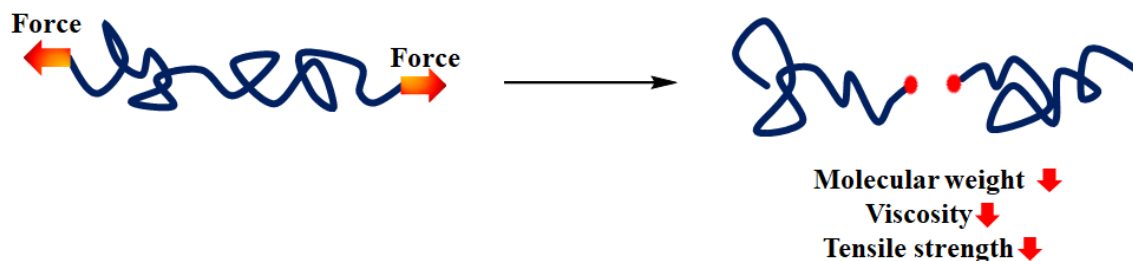


Figure 1.10. Illustration of polymer deformation under external force.

Polymer mechanochemistry refers to exploiting the mechanical force along with the polymer in order to induce chemical transduction. Polymer mechanochemistry takes advantage of the macromolecules to harness external forces and translate them into modulating chemical reactions. For example, the reactivity of small molecules can be affected by photochemical or high reaction temperatures. However, the high energies required for the reaction can alter the reaction pathway from desired ways to a variety of decomposition ways. In contrast, a mechanical force can offer opportunities to prevent the drawback from a chemical reaction of small molecules by lowering activation energy throughout the reaction. For example, Craig and Martinez demonstrate that mechanical activation of polymers containing *cis*- and *trans*-gDFCs showed thermodynamically disfavored isomerizations that yielded *cis*-gDFCs predominant polymers.⁵⁵ However,

thermolysis of the same starting materials resulted in most majority of *trans*-gDFC containing polymers.

Cycloreversion showed another limitation related to thermal activation of the chemical reaction. High temperatures are commonly required to promote this reaction, which can result in undesired decomposition.^{56, 57} In contrast, mechanical stimuli can accelerate the highly stable retrocyclization adduct otherwise difficult to achieve by thermal activation. For example, Bielawski et al. reported the mechanical cycloreversion of the 1,2,3-triazole moiety, which is a highly stable functional group.⁵⁸ The application of ultrasound to a triazole-containing poly(methyl acrylate) was proved to disassemble the adduct into their starting moieties, which are alkyne and azide functionalities.

Systematical installation of the mechanical responsive molecule into the polymer is a well-known methodology to produce stimuli-responsive polymers that result in desired outputs when exposed to chemical or physical input. The chain-like structure of polymers is suitable to accumulate mechanical energy onto the polymer backbone. Selective bond dissociation events can be modulated by the installation of the mechano-responsive small molecule into the polymer backbone. The concept of mechanical deformation of polymeric material had risen in destructive ways; however, rationalized design and systematic incorporation has shifted the concept toward productive ways.⁵⁹

Productive polymer mechanochemistry has emerged as a promising methodology for better material applications. While traditional polymer deformation induces the reduction of material physical and chemical properties, recent development in polymer mechanochemistry has proved that controlled polymer deformation brings advantages in

material applications. A good example is controlled catalyst activation by mechanical force.

1.5 Mechanophores

A mechanophore is any chemical molecule that contains mechanically weak bonds, which is a functional moiety that changes under external mechanical forces. Mechanochemical responses can vary from isomerization to specific bond-breaking events. Mechanophores are carefully designed to produce a predictable responsive result. The successful design of mechanophores needs the critical structural components that allow mechanically induced outputs. For example, most of the mechanophores possess a relatively weak chemical linkage, a strained ring structure, or an isomerizable bond that can show chain scission or conformational changes when force is applied to the target molecule. Therefore, molecules which fall into these criteria can be recognized as a mechanophore. A molecule that results in an undesirable or unpredictable response is not suitable for the development of a mechanophore.

The mechanophore can be classified into three classes based on their mechanochemical reactions when exposed to mechanical force, that is, bond cleavage (homolytic, heterolytic, or coordination bond scission),⁶⁰⁻⁶⁴ pericyclic reaction,⁶⁵⁻⁶⁷ and isomerization.⁶⁸⁻⁷⁰

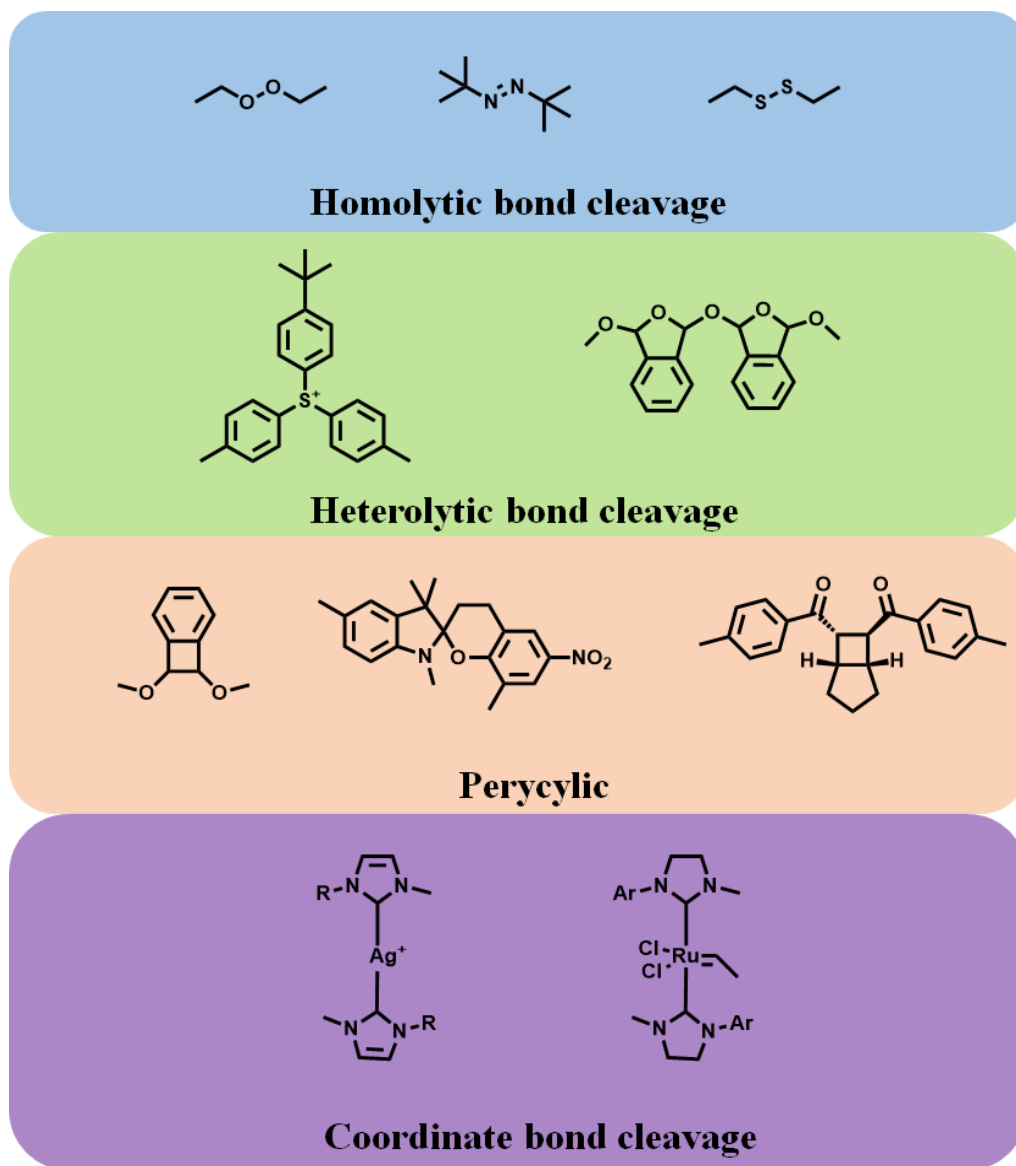


Figure 1.11. Representative structures of mechanophores.

One of the mechanochemical responses from mechanophore is the force-induced bond cleavage of relatively weak bonds.⁷¹ The bond cleavage is substantially affected by the bond dissociation energy (BDE). When force is applied onto the mechanophore, intrinsically weak bonds can undergo selective bond scission. For example, Encina and coworkers reported the selective bond scission of peroxide linkage, which is incorporated in the polymer backbone of polyvinylpyrrolidone. The BDE of peroxide is reported as ca.

35 kcal/mol.⁶⁰ The energy of the homolytic extrusion of nitrogen from the azo group is 24-30 kcal/mol.⁷² Ultrasound-induced site-specific cleavage of Azo-functionalized Poly(ethylene glycol) was reported by Moor and coworkers.⁷³ In contrast, strong bonds with high BDE exceeding 72 kcal/mol can also show site-specific bond cleavage. The mechanical activation is known to have an effect on bond weakening. When a strong bond is incorporated into the cyclic conformation, the ring strain can reduce the high BDE of the strong bonds, such as C-C, C-O, and C-N bonds. Three and four-membered, and bridged, and bicyclic rings, such as epoxide,⁷⁴ cyclobutane,⁶⁵ and spiropyran,⁷⁵ showed quite selective force-responsiveness while they possess high BDE. Generalized mechano-responses were shown in **Figure 1.12**.

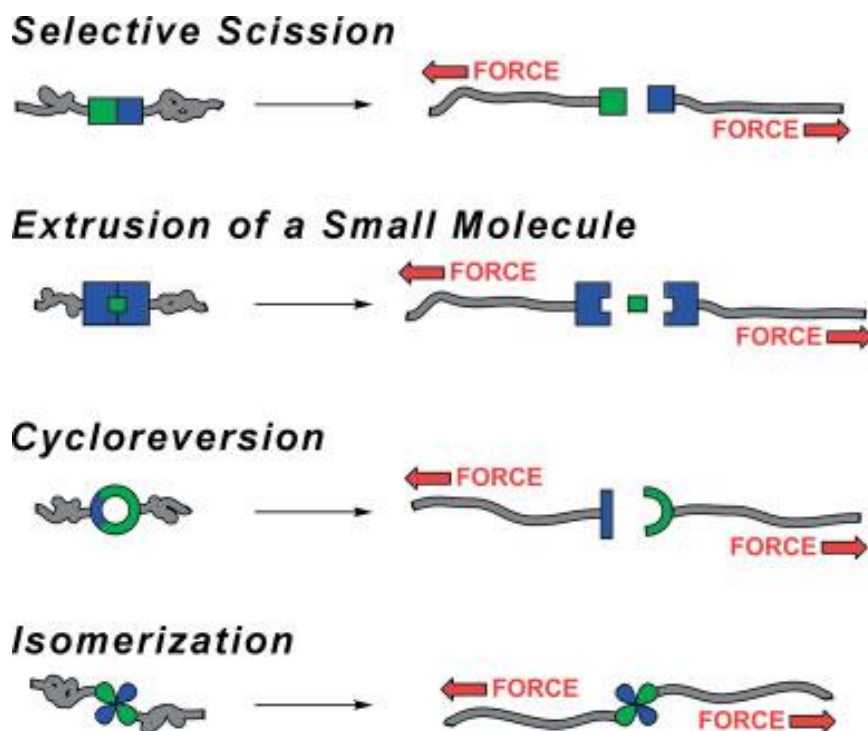


Figure 1.12. Representative modes of mechanical dissociation of mechanophores. (reprinted from ref [71] with permission from John Wiley and Sons)

Recently, metallocene mechanophore was proposed. Given the high bond dissociation energy (BDE) of metallocenes,⁷⁶⁻⁷⁸ metallocene was not considered as a

promising mechanophore. However, recent research has proven that metallocene-embedded polymers can be utilized as force-responsive materials under sonication.⁷⁹ Tang group further investigated the mechanical-susceptibility of ferrocene and ruthenocene.⁸⁰⁻⁸² Thus, the metallocene mechanophores have attracted increasing attention.

1.6 Polymerization Techniques

Ring-Opening Polymerization (ROP).

ROP is a very useful chain-growth polymerization method that has been frequently investigated.⁸³⁻⁸⁵ Strained ring containing a heteroatom, such as lactones, lactides, lactams, *N*-carboxy anhydrides, oxazolines, and siloxanes, are useful cyclic monomers that can undergo ROP polymerization.⁸⁶ The proposed polymerization mechanisms of ROP are typically classified into four types; anionic, cationic, organo-catalytic, and coordination-insertion. Biodegradable polymers, such as polylactic acid (PLA), polycaprolactone (PCL), poly(lactic-*co*-glycolic acid) obtained from the ROP are attractive materials because they are eco-friendly and biocompatible.⁸⁷ Metal catalysts, such as tin(II) bis(2-ethyl hexanoate) ($\text{Sn}(\text{Oct})_2$), aluminum alkoxides, and zinc salts, have been used for ROP. **Figure 1.13** shows a typical ROP of ϵ -caprolactone and representative examples of catalysts that can be used in ROP.



Ring-opening polymerization of ϵ -caprolactone

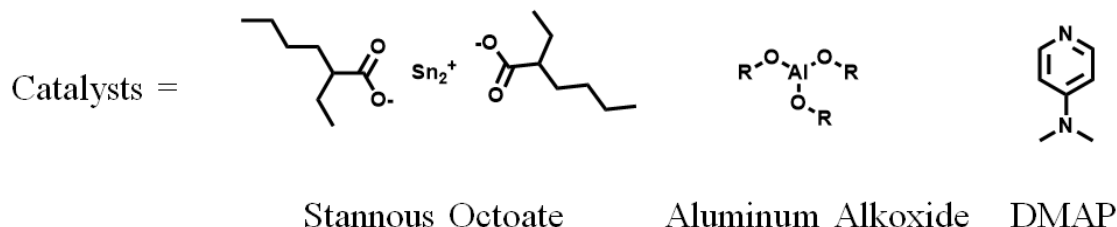


Figure 1.13. Typical ROP of ϵ -caprolactone and representative structures of catalysts used in ROP.

Reversible Addition-Fragmentation Chain-Transfer (RAFT) Polymerization.

RAFT polymerization is one of the controlled radical polymerization (CRP) methods that is frequently used for the preparation of precise polymers. This polymerization technique was first discovered in 1998.⁸⁸ RAFT polymerization is well-known for its improved compatibility toward various monomers compared to other controlled radical polymerization. RAFT involves a unique dithioester structure that is responsible for its polymerization behavior. The R-group should be suitable to stabilize a radical formed and reinitiate the growth of a new polymer. On the other hand, the Z-group can assist the stabilization of C=S bond and the intermediate radical in the equilibrium state. There are several types of RAFT agents, such as dithioester, trithioester, thiocarbamates, and xanthates.⁸⁹⁻⁹¹ The structure of R- and Z- group should be carefully designed to control the polymerization of a range of monomers. There are six steps involved in RAFT polymerization (**Figure 1.14**). Radical initiator, such as AIBN, is

decomposed to produce a free-radical source, resulting in two fragments ($I\bullet$) which react with a single monomer producing propagating polymeric radical ($P_1\bullet$). The propagating radical reacts with the RAFT agent to form a RAFT adduct radical to produce $R\bullet$ which can reinitiate new growing polymer fragments. Growing polymer fragments can share the present radical through a rapid interchange process. The chain growth can be accomplished by repeating these processes. The termination can occur through recombination and disproportionation. However, due to the structural stabilization of the radical, the termination and other side reactions can be suppressed. RAFT polymerization is also a well-understood method to prepare block copolymers due to their livingness. The RAFT agent is a dormant state after polymerization is finished. Thus, further incorporation of monomers is available through a successive polymerization process. The livingness of RAFT features predictable molecular weight and low dispersity, which is helpful for chain-end modification and macromolecular architecture.^{92, 93}

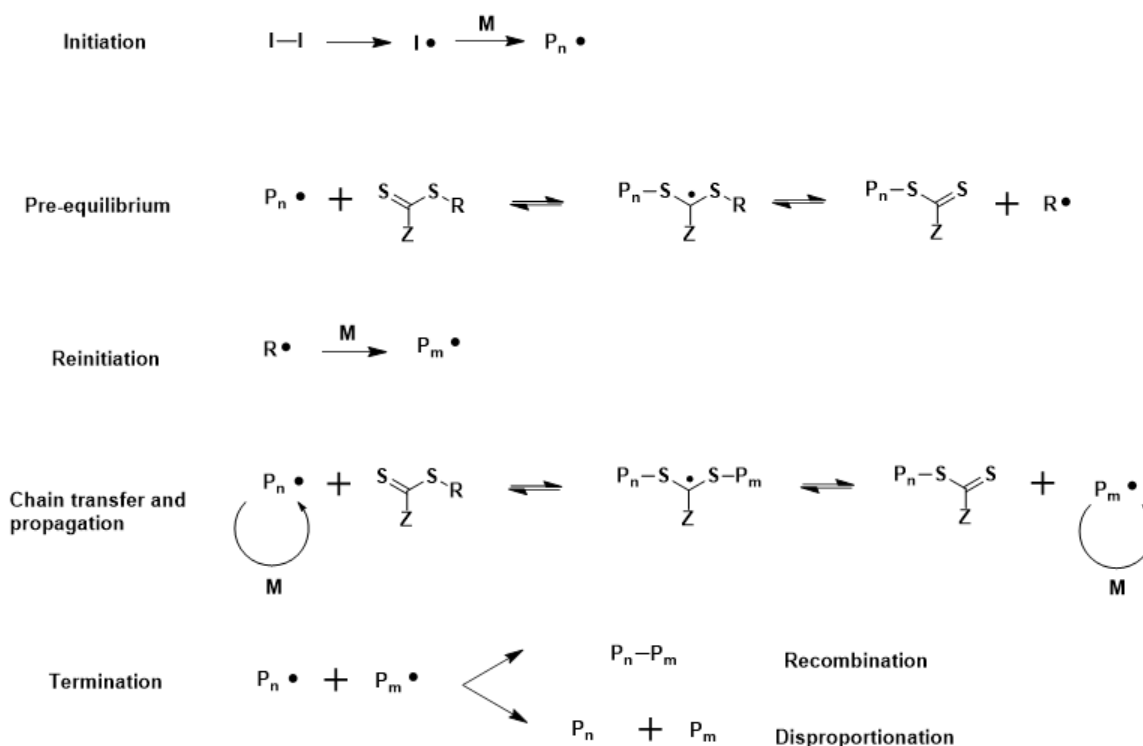


Figure 1.14. General mechanism of RAFT polymerization.

Ring-Opening Metathesis Polymerization (ROMP).

Ring-opening metathesis polymerization (ROMP) is a type of olefin metathesis chain-growth polymerization. ROMP is a well-known polymerization method of cyclic olefin monomers. The relief of ring strain in the cyclic olefin is the driving force of this polymerization. By contrast, a large ring-sized cyclic olefin also can be polymerized by increasing entropy of the system, which is denoted “Entropy-driven ring-opening metathesis polymerization” (ED-ROMP).⁹⁴ This technique is useful for the synthesis of linear polymers with high molecular weight and narrow molecular weight dispersity. In general, Grubbs’ catalysts are well-known for their high stability, functional group tolerance, fast initiation, and propagation rate.⁹⁵ Representative structures of Grubbs’ catalysts are shown in **Figure 1.15**.

ROMP undergoes a [2+2] cycloaddition of two alkenes via the formation of metallacyclobutane intermediate (**Figure 1.15**). A catalyst-mediated unsaturated carbon-carbon bond exchange occurs. The catalyst coordinates to the cyclic olefin, and a new olefin that is generated coordinates with the catalyst as the polymer chain grows. The metathesis of the unstrained olefinic bonds in the growing polymer chain known as backbiting and chain transfer can increase the dispersity of the polymers.

Norbornenes, cyclopentenes, and cyclooctenes are the most commonly used monomers for ROMP.⁹⁶ Besides, the sequential addition of different monomers can provide a method to prepare block copolymers.⁹⁷

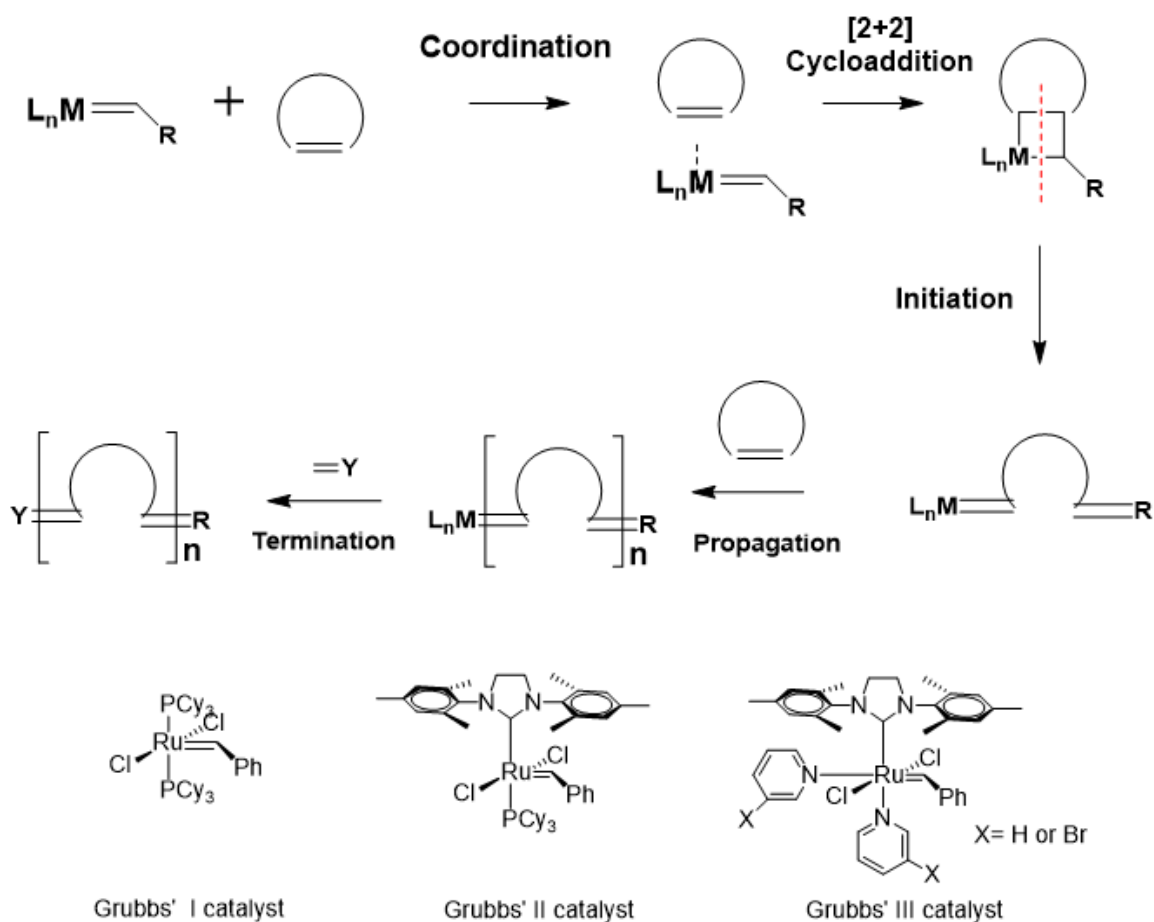


Figure 1.15. Mechanism of ROMP and structures of Grubbs' catalysts.

1.7 Research Objectives

This dissertation focused on two main research objectives. The first objective was to develop novel polymer materials produced from a combination of cationic metallo-polyelectrolytes and crystalline polymer for the construction of nano-objects via crystallization-driven self-assembly. Crystallizable polymer, PCL, is synthesized via ROP of ϵ -caprolactone. Further chemical modification of PCL affords macro-RAFT agent, which is a valuable macromolecule to produce block copolymers. Cobaltocenium monomer is introduced by RAFT polymerization for the various polymer composition. The prepared block copolymers show unique CDSA behaviors in the protic solvent. The formation of 2D micelles showed an unprecedented morphological transition based on their compositions. The resultant 2D micelles show improved stability under the increased ionic strength of the solution. The cationic characteristics and bioconjugation ability of micelles can be further utilized for biomedical applications.

The second objective of this dissertation is to develop new cationic metallocene mechanophores. In order to study the polymer mechanochemistry of cobaltocenium-containing polymers, a new design of cobaltocenium is required. The unique chemical structure of cobaltocenium can differentiate the force-responsiveness of metallocene mechanophore. The computational study can provide insight into the force-induced transduction of cobaltocenium mechanophore. For the improved incorporation of cobaltocenium, cyclic olefin moiety was introduced into the cobaltocenium structure. For the preparation of cobaltocenium cyclic olefin, an ally functional group was introduced with further chemical transformation to the cyclic form. The ROMP was used to incorporate the cobaltocenium moieties into the polymer backbone. The mechanical

susceptibility of cobaltocenium was examined by using ultra-sonication under a diluted system. The unique dissociative behavior of cobaltocenium was further confirmed by GPC and computational studies. This study of mechanochemistry of cationic metallocene mechanophore can further expand its possibility toward different types of cationic metallocene.

1.8 References

1. Abd-El-Aziz, A. S. Organometallic Polymers of the Transition Metals. *Macromol. Rapid Commun.* **2002**, *23*, 995-1031.
2. Abd-El-Aziz, A. S.; Strohm, E. A. Transition metal-containing macromolecules: En route to new functional materials. *Polymer* **2012**, *53*, 4879-4921.
3. Nguyen, P.; Gómez-Elipe, P.; Manners, I. Organometallic Polymers with Transition Metals in the Main Chain. *Chem. Rev.* **1999**, *99*, 1515-1548.
4. Manners, I. Polymers and the Periodic Table: Recent Developments in Inorganic Polymer Science. *Angew. Chem. Int. Ed.* **1996**, *35*, 1602-1621.
5. Stepnicka, P., *Ferrocenes: ligands, materials and biomolecules*. John Wiley & Sons: 2008.
6. Barlow, S.; O'Hare, D. Metal–Metal Interactions in Linked Metallocenes. *Chem. Rev.* **1997**, *97*, 637-670.
7. Kealy, T.; Pauson, P. A new type of organo-iron compound. *Nature* **1951**, *168*, 1039-1040.
8. Massey, J. A.; Winnik, M. A.; Manners, I.; Chan, V. Z. H.; Ostermann, J. M.; Enchelmaier, R.; Spatz, J. P.; Möller, M. Fabrication of Oriented Nanoscopic Ceramic Lines from Cylindrical Micelles of an Organometallic Polyferrocene Block Copolymer. *J. Am. Chem. Soc.* **2001**, *123*, 3147-3148.

9. Lu, J.; Chamberlin, D.; Rider, D. A.; Liu, M.; Manners, I.; Russell, T. P. Using a ferrocenylsilane-based block copolymer as a template to produce nanotextured Ag surfaces: uniformly enhanced surface enhanced Raman scattering active substrates. *Nanotechnology* **2006**, *17*, 5792.
10. Durkee, D. A.; Eitouni, H. B.; Gomez, E. D.; Ellsworth, M. W.; Bell, A. T.; Balsara, N. P. Catalysts from Self-Assembled Organometallic Block Copolymers. *Adv. Mater.* **2005**, *17*, 2003-2006.
11. Zhang, J.; Chen, Y. P.; Miller, K. P.; Ganewatta, M. S.; Bam, M.; Yan, Y.; Nagarkatti, M.; Decho, A. W.; Tang, C. Antimicrobial Metallopolymers and Their Bioconjugates with Conventional Antibiotics against Multidrug-Resistant Bacteria. *J. Am. Chem. Soc.* **2014**, *136*, 4873-4876.
12. Yan, Y.; Zhang, J.; Wilbon, P.; Qiao, Y.; Tang, C. Ring-Opening Metathesis Polymerization of 18-e Cobalt (I)-Containing Norbornene and Application as Heterogeneous Macromolecular Catalyst in Atom Transfer Radical Polymerization. *Macromol. Rapid Commun.* **2014**, *35*, 1840-1845.
13. Pageni, P.; Kabir, M. P.; Yang, P.; Tang, C. Binding of Cobaltocenium-Containing Polyelectrolytes with Anionic Probes. *J. Inorg. Organomet. Polym. Mater.* **2017**, *27*, 1100-1109.
14. Yang, P.; Bam, M.; Pageni, P.; Zhu, T.; Chen, Y. P.; Nagarkatti, M.; Decho, A. W.; Tang, C. Trio Act of Boronolactin with Antibiotic-Metal Complexed Macromolecules toward Broad-Spectrum Antimicrobial Efficacy. *ACS Infect. Dis.* **2017**, *3*, 845-853.
15. Thomi, L.; Schaefer, P.; Landfester, K.; Wurm, F. R. Stimulus-Responsive Release from Poly(ferrocenylsilane) Nanocontainers. *Macromolecules* **2016**, *49*, 105-109.
16. Cuadrado, I.; Casado, C. M.; Lobete, F.; Alonso, B.; González, B.; Losada, J.; Amador, U. Preparation and Redox Properties of Novel Polymerizable Pyrrole- and Allyl-Functionalized Cobaltocenium Monomers and Siloxane-Based Cobaltocenium Polymers. *Organometallics* **1999**, *18*, 4960-4969.

17. Noor, F.; Wüstholtz, A.; Kinscherf, R.; Metzler-Nolte, N. A Cobaltocenium–Peptide Bioconjugate Shows Enhanced Cellular Uptake and Directed Nuclear Delivery. *Angew. Chem. Int. Ed.* **2005**, *44*, 2429-2432.
18. Rogers, E. I.; Silvester, D. S.; Poole, D. L.; Aldous, L.; Hardacre, C.; Compton, R. G. Voltammetric Characterization of the Ferrocene|Ferrocenium and Cobaltocenium|Cobaltocene Redox Couples in RTILs. *J. Phys. Chem. C* **2008**, *112*, 2729-2735.
19. Zhang, J.; Yan, J.; Pageni, P.; Yan, Y.; Wirth, A.; Chen, Y.-P.; Qiao, Y.; Wang, Q.; Decho, A. W.; Tang, C. Anion-Responsive Metallopolymer Hydrogels for Healthcare Applications. *Sci. Rep.* **2015**, *5*, 11914.
20. Hadadpour, M.; Gwyther, J.; Manners, I.; Ragogna, P. J. Multifunctional Block Copolymer: Where Polymetallic and Polyelectrolyte Blocks Meet. *Chem. Mater.* **2015**, *27*, 3430-3440.
21. Lai, J. C.; Rounsfall, T.; Pittman Jr., C. U. Free-radical homopolymerization and copolymerization of vinylferrocene. *J. Polym. Sci., Part A-1: Polym. Chem.* **1971**, *9*, 651-662.
22. Arimoto, F.; Haven Jr, A. Derivatives of Dicyclopentadienyliron¹. *J. Am. Chem. Soc.* **1955**, *77*, 6295-6297.
23. Chandrasekhar, V.; Thirumoorthi, R. Coordination polymers containing ferrocene backbone. Synthesis, structure and electrochemistry. *Dalton. Trans.* **2010**, *39*, 2684-2691.
24. Knobloch, F.; Rauscher, W. Condensation polymers of ferrocene derivatives. *J. Polym. Sci.* **1961**, *54*, 651-656.
25. Gamble, A. S.; Patton, J. T.; Boncella, J. M. Acyclic diene metathesis polymerizations of ferrocene monomers. *Makromol. Chem. Rapid. Comm.* **1992**, *13*, 109-115.

26. Pittman Jr., C. U.; Ayers, O. E.; Suryanarayanan, B.; McManus, S. P.; Sheats, J. E. Organometallic polymers, 28 Condensation polymerization of cobalticinium salts. *Makromol. Chem.* **1974**, *175*, 1427-1437.
27. Manners, I. Poly (ferrocenylsilanes): novel organometallic plastics. *Chem. Commun.* **1999**, 857-865.
28. Tanabe, M.; Manners, I. Photolytic living anionic ring-opening polymerization (ROP) of silicon-bridged [1] ferrocenophanes via an iron-cyclopentadienyl bond cleavage mechanism. *J. Am. Chem. Soc.* **2004**, *126*, 11434-11435.
29. Ogasawara, M.; Nagano, T.; Hayashi, T. Metathesis Route to Bridged Metallocenes. *J. Am. Chem. Soc.* **2002**, *124*, 9068-9069.
30. Dragutan, I.; Dragutan, V.; Filip, P.; Simionescu, B. C.; Demonceau, A. ROMP Synthesis of Iron-Containing Organometallic Polymers. *Molecules* **2016**, *21*, 198.
31. Buretea, M. A.; Tilley, T. D. Poly (ferrocenylenevinylene) from ring-opening metathesis polymerization of ansa-(vinylene) ferrocene. *Organometallics* **1997**, *16*, 1507-1510.
32. Sha, Y.; Zhang, Y.; Zhu, T.; Tan, S.; Cha, Y.; Craig, S. L.; Tang, C. Ring-Closing Metathesis and Ring-Opening Metathesis Polymerization toward Main-Chain Ferrocene-Containing Polymers. *Macromolecules* **2018**, *51*, 9131-9139.
33. Cochran, E. W.; Garcia-Cervera, C. J.; Fredrickson, G. H. Stability of the gyroid phase in diblock copolymers at strong segregation. *Macromolecules* **2006**, *39*, 2449-2451.
34. Smart, T.; Lomas, H.; Massignani, M.; Flores-Merino, M. V.; Perez, L. R.; Battaglia, G. Block copolymer nanostructures. *Nano Today* **2008**, *3*, 38-46.
35. Mai, Y.; Eisenberg, A. Self-assembly of block copolymers. *Chem. Soc. Rev.* **2012**, *41*, 5969-5985.

36. Tritschler, U.; Pearce, S.; Gwyther, J.; Whittell, G. R.; Manners, I. 50th Anniversary Perspective: Functional Nanoparticles from the Solution Self-Assembly of Block Copolymers. *Macromolecules* **2017**, *50*, 3439-3463.
37. Truong, N. P.; Quinn, J. F.; Whittaker, M. R.; Davis, T. P. Polymeric filomicelles and nanoworms: two decades of synthesis and application. *Polym. Chem.* **2016**, *7*, 4295-4312.
38. MacFarlane, L.; Zhao, C.; Can, J.; Qiu, H.; Manners, I. Emerging Applications for Living Crystallization-Driven Self-Assembly. *Chem. Sci.* **2021**.
39. Massey, J.; Power, K. N.; Manners, I.; Winnik, M. A. Self-assembly of a novel organometallic– inorganic block copolymer in solution and the solid state: Nonintrusive observation of novel wormlike poly (ferrocenyldimethylsilane)-b-poly (dimethylsiloxane) micelles. *J. Am. Chem. Soc.* **1998**, *120*, 9533-9540.
40. Cao, L.; Manners, I.; Winnik, M. A. Influence of the Interplay of Crystallization and Chain Stretching on Micellar Morphologies: Solution Self-Assembly of Coil–Crystalline Poly (isoprene-block-ferrocenylsilane). *Macromolecules* **2002**, *35*, 8258-8260.
41. Song, S.; Zhou, H.; Hicks, G.; Rastogi, C. K.; Yu, Q.; Manners, I.; Winnik, M. A. Single-step self-assembly to uniform fiber-like core-crystalline block copolymer micelles. *Chem. Commun.* **2020**, *56*, 4595-4598.
42. Fu, J.; Luan, B.; Yu, X.; Cong, Y.; Li, J.; Pan, C.; Han, Y.; Yang, Y.; Li, B. Self-assembly of crystalline– coil diblock copolymer in solvents with varying selectivity: from spinodal-like aggregates to spheres, cylinders, and lamellae. *Macromolecules* **2004**, *37*, 976-986.
43. Yu, W.; Inam, M.; Jones, J. R.; Dove, A. P.; O'Reilly, R. K. Understanding the CDSA of poly (lactide) containing triblock copolymers. *Polym. Chem.* **2017**, *8*, 5504-5512.

44. Li, C.; Liu, R.; Xue, Q.; Huang, Y.; Su, Y.; Shen, Q.; Wang, D. Oil-in-Water Emulsion Templated and Crystallization-Driven Self-Assembly Formation of Poly (l-lactide)–Polyoxyethylene–Poly (l-lactide) Fibers. *Langmuir* **2017**, *33*, 13060-13067.
45. Zhang, Q.; Remsen, E. E.; Wooley, K. L. Shell cross-linked nanoparticles containing hydrolytically degradable, crystalline core domains. *J. Am. Chem. Soc.* **2000**, *122*, 3642-3651.
46. Du, Z.-X.; Xu, J.-T.; Fan, Z.-Q. Micellar Morphologies of Poly (ϵ -caprolactone)-b-poly (ethylene oxide) Block Copolymers in Water with a Crystalline Core. *Macromolecules* **2007**, *40*, 7633-7637.
47. Su, M.; Huang, H.; Ma, X.; Wang, Q.; Su, Z. Poly (2-vinylpyridine)-block-Poly (ϵ -caprolactone) Single Crystals in Micellar Solution. *Macromol. Rapid Commun.* **2013**, *34*, 1067-1071.
48. Mihut, A. M.; Chiche, A.; Drechsler, M.; Schmalz, H.; Di Cola, E.; Krausch, G.; Ballauff, M. Crystallization-induced switching of the morphology of poly (ethylene oxide)-block-polybutadiene micelles. *Soft Matter* **2009**, *5*, 208-213.
49. Mihut, A. M.; Drechsler, M.; Möller, M.; Ballauff, M. Sphere-to-rod transition of micelles formed by the semicrystalline polybutadiene-block-poly (ethylene oxide) block copolymer in a selective solvent. *Macromol. Rapid Commun.* **2010**, *31*, 449-453.
50. Schmalz, H.; Schmelz, J.; Drechsler, M.; Yuan, J.; Walther, A.; Schweimer, K.; Mihut, A. M. Thermo-reversible formation of wormlike micelles with a microphase-separated corona from a semicrystalline triblock terpolymer. *Macromolecules* **2008**, *41*, 3235-3242.
51. Schmelz, J.; Karg, M.; Hellweg, T.; Schmalz, H. General pathway toward crystalline-core micelles with tunable morphology and corona segregation. *ACS nano* **2011**, *5*, 9523-9534.

52. Kamps, A. C.; Fryd, M.; Park, S.-J. Hierarchical self-assembly of amphiphilic semiconducting polymers into isolated, bundled, and branched nanofibers. *ACS nano* **2012**, *6*, 2844-2852.
53. Staudinger, H.; Bondy, H. Isoprene and rubber. XIX. The molecular size of rubber and balata. *Rubber Chem. Technol.* **1930**, *3*, 519-521.
54. Kauzmann, W.; Eyring, H. The Viscous Flow of Large Molecules. *J. Am. Chem. Soc.* **1940**, *62*, 3113-3125.
55. Lenhardt, J. M.; Ong, M. T.; Choe, R.; Evenhuis, C. R.; Martinez, T. J.; Craig, S. L. Trapping a diradical transition state by mechanochemical polymer extension. *Science* **2010**, *329*, 1057-1060.
56. Herndon, W. C.; Grayson, C.; Manion, J. M. Retro-Diels-Alder reactions. III. Kinetics of the thermal decompositions of exo-and endo-dicyclopentadiene. *J. Org. Chem.* **1967**, *32*, 526-529.
57. Pool, B. R.; White, J. M. Structural Manifestations of the Retro Diels–Alder Reaction. *Org. Lett.* **2000**, *2*, 3505-3507.
58. Brantley, J. N.; Wiggins, K. M.; Bielawski, C. W. Unclicking the Click: Mechanically Facilitated 1,3-Dipolar Cycloreversions. *Science* **2011**, *333*, 1606-1609.
59. Li, J.; Nagamani, C.; Moore, J. S. Polymer Mechanochemistry: From Destructive to Productive. *Accounts. Chem. Res.* **2015**, *48*, 2181-2190.
60. Encina, M. V.; Lissi, E.; Sarasúa, M.; Gargallo, L.; Radic, D. Ultrasonic degradation of polyvinylpyrrolidone: Effect of peroxide linkages. *J. Polym. Sci. Polym. Lett. Ed.* **1980**, *18*, 757-760.
61. Berkowski, K. L.; Potisek, S. L.; Hickenboth, C. R.; Moore, J. S. Ultrasound-Induced Site-Specific Cleavage of Azo-Functionalized Poly(ethylene glycol). *Macromolecules* **2005**, *38*, 8975-8978.

62. Chen, Y.; Spiering, A.; Karthikeyan, S.; Peters, G. W.; Meijer, E.; Sijbesma, R. P. Mechanically induced chemiluminescence from polymers incorporating a 1, 2-dioxetane unit in the main chain. *Nat. Chem.* **2012**, *4*, 559.
63. Jakobs, R. T. M.; Sijbesma, R. P. Mechanical Activation of a Latent Olefin Metathesis Catalyst and Persistence of its Active Species in ROMP. *Organometallics* **2012**, *31*, 2476-2481.
64. Paulusse, J. M.; Sijbesma, R. P. Selectivity of mechanochemical chain scission in mixed palladium (II) and platinum (II) coordination polymers. *Chem. Commun.* **2008**, 4416-4418.
65. Kryger, M. J.; Ong, M. T.; Odom, S. A.; Sottos, N. R.; White, S. R.; Martinez, T. J.; Moore, J. S. Masked Cyanoacrylates Unveiled by Mechanical Force. *J. Am. Chem. Soc.* **2010**, *132*, 4558-4559.
66. Grady, M. E.; Beiermann, B. A.; Moore, J. S.; Sottos, N. R. Shockwave Loading of Mechanochemically Active Polymer Coatings. *Acs Appl. Mater. Interfaces* **2014**, *6*, 5350-5355.
67. Gossweiler, G. R.; Hewage, G. B.; Soriano, G.; Wang, Q.; Welshofer, G. W.; Zhao, X.; Craig, S. L. Mechanochemical activation of covalent bonds in polymers with full and repeatable macroscopic shape recovery. *ACS Macro Lett.* **2014**, *3*, 216-219.
68. Radiom, M.; Kong, P.; Maroni, P.; Schäfer, M.; Kilbinger, A. F. M.; Borkovec, M. Mechanically induced cis-to-trans isomerization of carbon-carbon double bonds using atomic force microscopy. *Phys. Chem. Chem. Phys.* **2016**, *18*, 31202-31210.
69. Huang, W.; Zhu, Z.; Wen, J.; Wang, X.; Qin, M.; Cao, Y.; Ma, H.; Wang, W. Single Molecule Study of Force-Induced Rotation of Carbon-Carbon Double Bonds in Polymers. *ACS Nano* **2017**, *11*, 194-203.
70. Surampudi, S. K.; Patel, H. R.; Nagarjuna, G.; Venkataraman, D. Mechanoisomerization of azobenzene. *Chem. Commun.* **2013**, *49*, 7519-7521.

71. Brantley, J. N.; Wiggins, K. M.; Bielawski, C. W. Polymer mechanochemistry: the design and study of mechanophores. *Polym. Int.* **2013**, *62*, 2-12.
72. Sun, C.-k.; Zhao, H.-m.; Fang, D.-C.; Li, Z.-h. Theoretical study on the thermal decomposition of azoisobutyronitrile. *J. Mol. Struct.-THEOCHEM* **2004**, *679*, 89-94.
73. Berkowski, K. L.; Potisek, S. L.; Hickenboth, C. R.; Moore, J. S. Ultrasound-induced site-specific cleavage of azo-functionalized poly (ethylene glycol). *Macromolecules* **2005**, *38*, 8975-8978.
74. Klukovich, H. M.; Kean, Z. S.; Ramirez, A. L. B.; Lenhardt, J. M.; Lin, J.; Hu, X.; Craig, S. L. Tension trapping of carbonyl ylides facilitated by a change in polymer backbone. *J. Am. Chem. Soc.* **2012**, *134*, 9577-9580.
75. Davis, D. A.; Hamilton, A.; Yang, J.; Cremer, L. D.; Van Gough, D.; Potisek, S. L.; Ong, M. T.; Braun, P. V.; Martínez, T. J.; White, S. R. Force-induced activation of covalent bonds in mechanoresponsive polymeric materials. *Nature* **2009**, *459*, 68-72.
76. Haaland, A. Molecular structure and bonding in the 3d metallocenes. *Accounts. Chem. Res.* **1979**, *12*, 415-422.
77. Musgrave, R. A.; Russell, A. D.; Hayward, D. W.; Whittell, G. R.; Lawrence, P. G.; Gates, P. J.; Green, J. C.; Manners, I. Main-chain metallopolymer at the static–dynamic boundary based on nickelocene. *Nat. Chem.* **2017**, *9*, 743.
78. Zhu, T.; Sha, Y.; Yan, J.; Pageni, P.; Rahman, M. A.; Yan, Y.; Tang, C. Metallo-polyelectrolytes as a class of ionic macromolecules for functional materials. *Nat. Commun.* **2018**, *9*, 1-15.
79. Di Giannantonio, M.; Ayer, M. A.; Verde-Sesto, E.; Lattuada, M.; Weder, C.; Fromm, K. M. Triggered Metal Ion Release and Oxidation: Ferrocene as a Mechanophore in Polymers. *Angew. Chem. Int. Ed.* **2018**, *57*, 11445-11450.
80. Sha, Y.; Zhang, Y.; Xu, E.; Wang, Z.; Zhu, T.; Craig, S. L.; Tang, C. Quantitative and Mechanistic Mechanochemistry in Ferrocene Dissociation. *ACS Macro Lett.* **2018**, *7*, 1174-1179.

81. Sha, Y.; Zhang, Y.; Xu, E.; McAlister, C. W.; Zhu, T.; Craig, Stephen L.; Tang, C. Generalizing metallocene mechanochemistry to ruthenocene mechanophores. *Chem. Sci.* **2019**, *10*, 4959-4965.
82. Zhang, Y.; Wang, Z.; Kouznetsova, T. B.; Sha, Y.; Xu, E.; Shannahan, L.; Fermen-Coker, M.; Lin, Y.; Tang, C.; Craig, S. L. Distal conformational locks on ferrocene mechanophores guide reaction pathways for increased mechanochemical reactivity. *Nat. Chem.* **2021**, *13*, 56-62.
83. Nuyken, O.; Pask, S. Ring-Opening Polymerization—An Introductory Review. *Polymers* **2013**, *5*, 361.
84. Sutar, A. K.; Maharana, T.; Dutta, S.; Chen, C.-T.; Lin, C.-C. Ring-opening polymerization by lithium catalysts: an overview. *Chem Soc Rev* **2010**, *39*, 1724-1746.
85. Albertsson, A.-C.; Varma, I. K. Recent Developments in Ring Opening Polymerization of Lactones for Biomedical Applications. *Biomacromolecules* **2003**, *4*, 1466-1486.
86. Odian, G. Ring-Opening Polymerization. *Principles of Polymerization, Fourth Edition* **2004**, 544-618.
87. Stridsberg, K. M.; Ryner, M.; Albertsson, A.-C., Controlled ring-opening polymerization: polymers with designed macromolecular architecture. In *Degradable aliphatic polyesters*, Springer: 2002; pp 41-65.
88. Chiefari, J.; Chong, Y.; Ercole, F.; Krstina, J.; Jeffery, J.; Le, T. P.; Mayadunne, R. T.; Meijs, G. F.; Moad, C. L.; Moad, G. Living free-radical polymerization by reversible addition– fragmentation chain transfer: the RAFT process. *Macromolecules* **1998**, *31*, 5559-5562.
89. Chong, Y.; Krstina, J.; Le, T. P.; Moad, G.; Postma, A.; Rizzardo, E.; Thang, S. H. Thiocarbonylthio compounds [sc (ph) s– r] in free radical polymerization with reversible addition-fragmentation chain transfer (raft polymerization). Role of the free-radical leaving group (r). *Macromolecules* **2003**, *36*, 2256-2272.

90. Keddie, D. J.; Moad, G.; Rizzardo, E.; Thang, S. H. RAFT agent design and synthesis. *Macromolecules* **2012**, *45*, 5321-5342.
91. Wood, M. R.; Duncalf, D. J.; Rannard, S. P.; Perrier, S. Selective one-pot synthesis of trithiocarbonates, xanthates, and dithiocarbamates for use in RAFT/MADIX living radical polymerizations. *Org. Lett.* **2006**, *8*, 553-556.
92. Convertine, A. J.; Sumerlin, B. S.; Thomas, D. B.; Lowe, A. B.; McCormick, C. L. Synthesis of block copolymers of 2-and 4-vinylpyridine by RAFT polymerization. *Macromolecules* **2003**, *36*, 4679-4681.
93. Moad, G.; Chong, Y.; Postma, A.; Rizzardo, E.; Thang, S. H. Advances in RAFT polymerization: the synthesis of polymers with defined end-groups. *Polymer* **2005**, *46*, 8458-8468.
94. Pearce, A. K.; Foster, J. C.; O'Reilly, R. K. Recent developments in entropy-driven ring-opening metathesis polymerization: Mechanistic considerations, unique functionality, and sequence control. *J. Polym. Sci. A Polym. Chem.* **2019**, *57*, 1621-1634.
95. Walsh, D. J.; Lau, S. H.; Hyatt, M. G.; Guironnet, D. Kinetic Study of Living Ring-Opening Metathesis Polymerization with Third-Generation Grubbs Catalysts. *J. Am. Chem. Soc.* **2017**, *139*, 13644-13647.
96. Sutthasupa, S.; Shiotsuki, M.; Sanda, F. Recent Advances in Ring-Opening Metathesis Polymerization, and Application to Synthesis of Functional Materials. *Polym J* **2010**, *42*, 905-915.
97. Ganewatta, M. S.; Ding, W.; Rahman, M. A.; Yuan, L.; Wang, Z.; Hamidi, N.; Robertson, M. L.; Tang, C. Biobased Plastics and Elastomers from Renewable Rosin via "Living" Ring-Opening Metathesis Polymerization. *Macromolecules* **2016**.

CHAPTER 2

CRYSTALLIZATION-DRIVEN SELF-ASSEMBLY OF METALLO-
POLYELECTROLYTE BLOCK COPOLYMERS WITH A
POLYCAPROLACTONE CORE-FORMING SEGMENT¹

¹ Cha, Y.; Jarrett-Wilkins, C.; Rahman, M. A.; Zhu, T.; Sha, Y.; Manners, I.; Tang, C. Crystallization-Driven Self-Assembly of Metallo-Polyelectrolyte Block Copolymers with a Polycaprolactone Core-Forming Segment. *ACS Macro Lett.* **2019**, 8, 835-840. Reproduced with permission of publisher. Copyright (2021) American Chemical Society.

2.1 Abstract

We report crystallization-driven self-assembly (CDSA) of metallo-polyelectrolyte block copolymers that contain cationic polycobaltocenium in the corona-forming block and crystallizable polycaprolactone (PCL) as the core-forming block. Dictated by electrostatic interactions originating from the cationic metalloblock and crystallization of the PCL, these amphiphilic block copolymers self-assembled into two dimensional platelet nanostructures in polar protic solvents. The 2D morphologies can be varied from elongated hexagons to diamonds, and their stability to fragmentation was found to be dependent on the ionic strength of the solution.

2.2 Introduction

Self-assembly of amphiphilic block copolymers is one of the most fascinating approaches to the creation of nanoscale micelles with core-corona architectures and a broad range of morphologies.¹⁻⁷ Unlike amorphous block copolymers, when placed in a selective solvent, block copolymers with a crystallizable core-forming block tend to form micelles with a low curvature of the core-corona interface. Most commonly either platelets or cylinders are formed, depending on the interplay between the crystallization of the core and interchain repulsion of corona. The central role of crystallization in the self-assembly process has given rise to the descriptor “Crystallization-Driven Self-Assembly (CDSA)”.⁸⁻

12

Metallopolymers, polymers containing metal centers in the main chain or pendant side chains, have also been featured in CDSA processes. The CDSA of poly(ferrocenyldimethylsilane) (PFS) to prepare a wide range of nanostructures that are spherical, cylindrical¹³⁻¹⁵ or platelet¹⁶⁻¹⁸ micelles has been extensively explored. To date,

most metallopolymer used for CDSA studies have been neutral. In contrast to neutral PFS, cationic cobaltocenium-containing polymers have several advantages, such as hydrophilicity, high chemical stability, and bioactivities.¹⁹⁻²⁷ As charged polyelectrolytes, cobaltocenium moieties have been utilized for solution self-assembly, including in one case for CDSA which gave platelets with a PFS core.²⁸ Recently, Qiu, Manners and coworkers reported the formation of chiral metallopolymer consisting of poly(cobaltoceniumethylene) with the assistance of *N*-acyl-amino-acid-derived anionic surfactants.²⁹ The Tang group have also reported the preparation and solution self-assembly of side-chain cobaltocenium-containing block copolymers in a mixture of acetone and chloroform that formed high-aspect-ratio nanotubular structures.³⁰

Polycaprolactone (PCL) is well known for biomedical applications because of its biocompatibility and biodegradability.³¹ PCL-containing block copolymers have been recently utilized for the CDSA process with the formation of spherical, cylindrical and lozenge-shaped morphologies.^{9, 32-37}

Herein we report the CDSA behavior of a metallo-polyelectrolyte block copolymer, polycaprolactone-*b*-poly(cobaltocenium amidoethyl methacrylate) (PCL-*b*-PCoAEMA). Driven by the crystallization of PCL and the electrostatic interactions within charged polycobaltocenium segments, this block copolymer can self-assemble into various two-dimensional platelet morphologies in selective solvents with PCL as the core block and cobaltocenium as the corona block.

2.3 Experimental

Materials

Cobaltocenium amidoethyl methacrylate hexafluorophosphate was synthesized according to a previously reported procedure.³⁸ ϵ -Caprolactone (98%) was purchased from Sigma Aldrich and distilled with calcium anhydride. Benzyl alcohol (98%, Sigma Aldrich) was distilled before use. Azobisisobutyronitrile (AIBN) was purchased from Sigma Aldrich and recrystallized in methanol. Copper iodide, propargyl alcohol, stannous octoate tetrabutylammonium chloride, 4-cyano-4-(phenylcarbonothioylthio)pentanoic acid and 4-(*N,N*-dimethylamino)pyridine were purchased from Sigma Aldrich and used as received without further purification unless it is mentioned.

Characterization

¹H-NMR spectra were recorded by a Bruker Avance III HD 300 using trimethylsilane as an internal standard. Molecular weight and molecular weight distribution of polymers were determined by gel permeation chromatography (GPC) with tetrahydrofuran (THF) as an eluent at a flow rate of 1 mL/min at 35 °C on a Waters GPC system equipped with a refractive index (RI) detector, and narrow dispersed polystyrene was used for calibration. GPC samples were prepared by dissolving the sample in THF with a concentration of 10.0 mg/mL and passing through microfilters with a pore size of 0.2 μ m. Crystallization temperature (T_c) and melting temperature (T_m) of polycaprolactone homopolymer were measured by using differential scanning calorimetry (DSC) conducted on a DSC 2000 instrument (TA Instruments). Samples were first heated from -30 to +200 °C at a rate of 10 °C/min. After cooling down to -30 °C at the same rate, the data were collected from the second heating and cooling scan. About 4 mg of sample was used for

the DSC test with nitrogen gas at a flow rate of 50 mL/min. Fourier transform infrared spectrometry (FTIR) spectra were taken from a PerkinElmer spectrum 100 FTIR spectrometer. Atomic force microscopy (AFM) was performed using a Multimode Nanoscope V system (Bruker, Santa Barbara, CA). Tapping mode AFM was used to map the topography by tapping the surface using an oscillating tip. Transmission Electron Microscopy (TEM) images were collected from JEOL 200CX transmission electron microscope with an acceleration voltage of 120 kV. The samples were prepared by drop-casting onto a copper grid and dried before measurement. The TEM images were further analyzed by ImageJ.

Synthesis of alkyne modified CTA

RAFT agent, 4-cyano-4-(phenylcarbo thioylthio) pentanoic acid (CPPA), was modified with propargyl alcohol via esterification. CPPA (0.5 g, 1.79 mmol), 4-dimethylaminopyridine (DMAP) (22 mg, 0.18 mmol) and propargyl alcohol (0.5 g, 0.89mmol) were placed into a round bottom flask, then added with 20 mL dry DCM and placed in an ice bath. 1-Ethyl-3-(3-dimethylaminopropyl)carbodiimide (EDC) (0.3 g, 1.93 mmol) was dissolved in dry DCM and added into the above reaction mixture dropwise. After addition of EDC, TEA (0.5 ml, 0.36 mmol) was added immediately. The reaction mixture was stirred for 24 hours. The reaction mixture was extracted by water three times. The organic layer was dried with anhydrous MgSO_4 and condensed by rotary evaporation. The product was purified by silica column chromatography using hexane and ethyl acetate (1:1) as eluents. The product was collected and dried under a vacuum. ^1H NMR (CDCl_3 , 300MHz, ppm): δ = 7.93 (d, 2H, *Ph*-), 7.48 (t, 1H, *Ph*-), 7.33 (t, 2H, *Ph*-), 4.66(s, 2H, - OCH_2CCH -), 2.75-2.36(m, 5H, - CH_2CH_2 -, - CCH), 1.87(s, 3H, - CH_3).

Synthesis of polycaprolactone homopolymer with –OH end group.

PCL was prepared by ring-opening polymerization of ϵ -caprolactone. The procedure was performed according to previous work.³⁹ Stannous octoate was used as a catalyst and benzyl alcohol was used as an initiator. ϵ -Caprolactone (3.0 g, 26.3 mmol), benzyl alcohol (90 mg, 0.12 mmol), and stannous octoate (50 mg, 0.12mmol) were placed in a 25 mL flame-dried round bottom flask. The mixture was dissolved in 5.0 mL toluene. The reaction solution was purged with nitrogen for 30 minutes, and placed into an oil bath preheated to 110 °C. The polymerization was proceeded for 3 hours and quenched by cooling the reaction mixture in an ice-water bath. The polymer was precipitated into cold methanol 3 times (2.41g, ca. 80% yield). The repeating unit of polymer was calculated to be 61 by ¹H-NMR analysis. *M_n* (GPC) = 6,500 g/mol, *D* = 1.25. ¹H-NMR (CDCl₃, ppm, 300 MHz): δ = 7.36 (br, 5H, *PhCH*₂O-), 5.13 (s, 2H, *PhCH*₂O-), 4.07 (t, 120H, -COOCH₂CH₂-), 3.66 (t, 2H, -CH₂CH₂OH), 2.32(t, 120H, -OCOCH₂CH₂-), 1.68-1.61 (m, 240H, -COOCH₂CH₂CH₂CH₂CH₂OH), 1.43-1.36 (m, 140H, -COOCH₂CH₂CH₂CH₂CH₂OH).

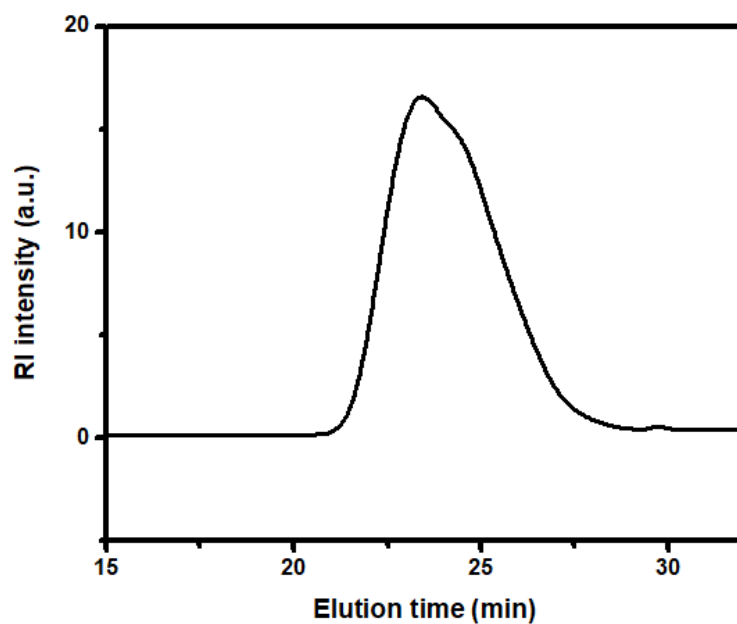


Figure 2.1. GPC trace of polycaprolactone homopolymer (M_n (GPC) = 6,500 g/mol, $D = 1.25$).

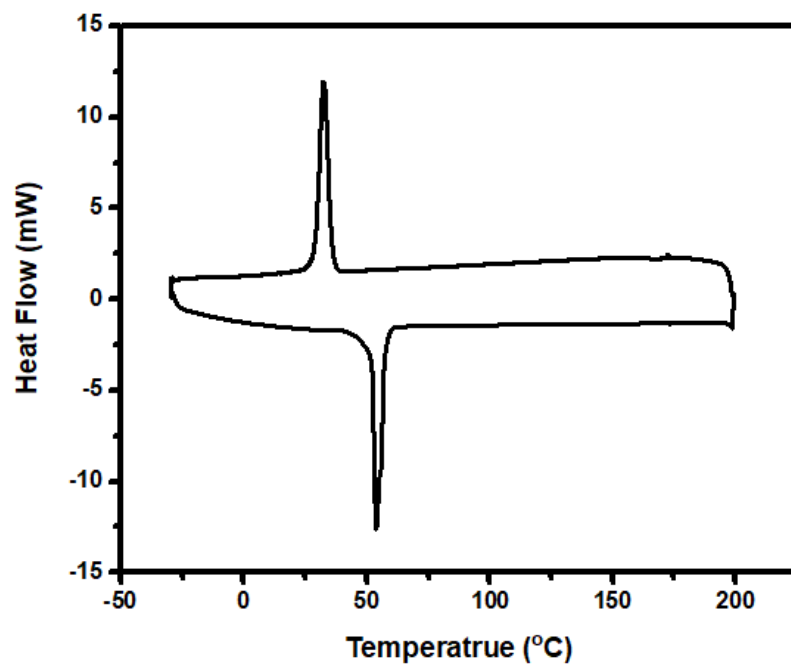


Figure 2.2. DSC curve of polycaprolactone homopolymer.

Modification of PCL-OH with azide.

The hydroxyl end group of PCL-OH was converted to azide via two-step modifications: tosylation and azide substitution. PCL-OH homopolymer (1.5 g, 0.25 mmol) was dissolved in 5 mL dichloromethane (DCM) and added by trimethylamine (0.35 ml, 2.54 mmol). The reaction solution was cooled in an ice bath. *p*-Toluenesulfonyl chloride (484 mg, 2.54 mmol) was dissolved in 5 mL DCM and added to the above reaction mixture dropwise. After 24 hours, the tosylated polymer was precipitated in cold methanol three times. PCL-OTs was converted to PCL-N₃ by reaction with sodium azide in dimethylformamide (DMF). PCL-OTs (1.04 g, 0.14 mmol) and sodium azide (650 mg, 10 mmol) were dissolved in dry DMF. The reaction proceeded at room temperature for 24 hours. The reaction mixture was extracted using DCM and brine three times to remove excess sodium azide. The organic layer was dried with anhydrous MgSO₄. The PCL-N₃ product was recovered by precipitation in cold methanol (1.1 g, 73% yield). Azide substitution was confirmed by IR spectrum. ¹H-NMR (CDCl₃, 300MHz, ppm): δ = 7.30 (br, 5H, *Ph*CH₂O-), 5.05 (s, 2H, *Ph*CH₂O-), 3.99 (t, 120H, -COOCH₂CH₂), 3.26 (t, 2H, CH₂CH₂N₃), 2.32 (t, 120H, -OCOCH₂CH₂-), 1.63-1.53 (m, 240H, -COOCH₂CH₂CH₂CH₂CH₂N₃), 1.36-1.29 (m, 140H, -COOCH₂CH₂CH₂CH₂CH₂N₃).

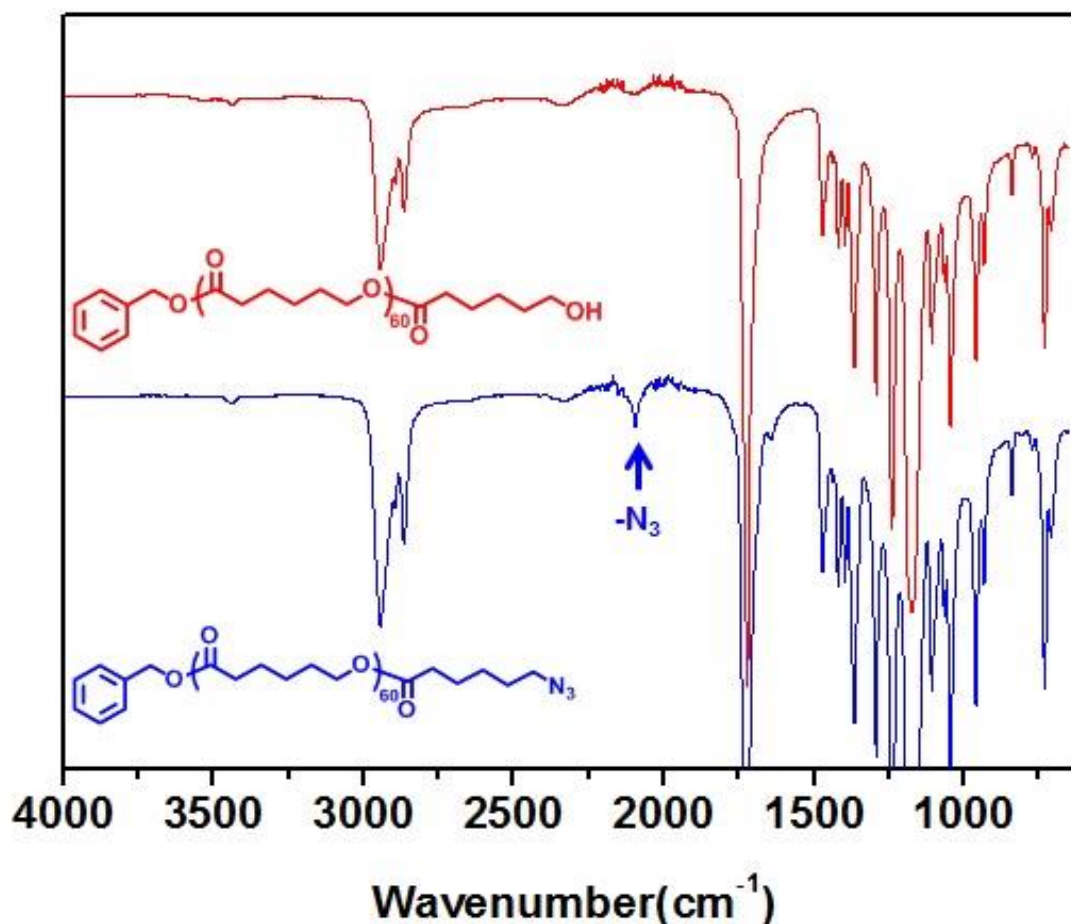


Figure 2.3. FT-IR spectra of PCL-OH (red) and PCL-N₃ (blue).

Synthesis of PCL Macro-CTA

Synthesis of PCL-RAFT agent was obtained by click reaction between PCL-N₃ and alkyne modified CPPA. Copper(I) iodide (0.8 mg, 4.2 μmol) and 1,8-diazabicyclo[5.4.0]undec-7-ene (DBU) (0.96 mg, 6.3 μmol) were dissolved in 3 ml dry tetrahydrofuran (THF). PCL-N₃ (0.3 g, 0.042 mmol) and alkyne modified CPPA (107 mg, 0.34 mmol) were dissolved in 10 mL dry THF and purged with nitrogen. A mixture of DBU and CuI was added to the above reaction mixture. The mixture was stirred for 24 hours and diluted with 10 ml DCM. The mixture was extracted with water to remove residual reagents. The product was recovered by precipitation in cold methanol and dried

under a vacuum. ^1H -NMR (CDCl_3 , 300MHz, ppm): δ = 7.81 (d, 2H, *Ph*-), 7.51 (m, 3H, *Ph*-, Triazole), 7.28 (m, 6H, *Ph*-), 5.19 (s, 2H, $-\text{CH}_2\text{Triazole}-$), 5.05 (s, 2H, $\text{PhCH}_2\text{O}-$), 4.01 (t, 120H, $-\text{COOCH}_2\text{CH}_2-$), 2.25 (t, 120H, $-\text{OCOCH}_2\text{CH}_2-$), 1.62-1.53 (m, 240H, $-\text{COOCH}_2\text{CH}_2\text{CH}_2\text{CH}_2\text{CH}_2-$), 1.36-1.29 (m, 120H, $-\text{COOCH}_2\text{CH}_2\text{CH}_2\text{CH}_2\text{CH}_2-$).

*Synthesis of PCL-*b*-PCoAEMAPF₆ block copolymer*

PCL-*b*-PCoAEMAPF₆ was synthesized through RAFT polymerization. PCL-RAFT macroinitiator (42 mg, 6 μmol), AIBN (0.3 mg, 1.8 μmol), and CoAEMAPF₆ were dissolved by 0.3 mL dry DMF in a Schlenk flask. The reaction mixture was purged with N_2 for 30min. The flask was placed into an oil bath preheated at 90°C. The conversion was monitored by ^1H NMR. Polymerization was quenched when the conversion reached about 50%. The polymers were precipitated in cold methanol to remove residual monomers. Yellow polymers were collected and dried in a vacuum. Yield: 100 mg, ^1H NMR ($\text{DMSO}-d_6$, 300MHz, ppm): 6.25 (br, 58H, *Cp ring*), 5.9 -5.8 (br, 142H, *Cp ring*) 4.01 (t, 120H, $-\text{OCH}_2\text{CH}_2-$), 2.25 (t, 122H, $-\text{OCO}-\text{CH}_2-$).

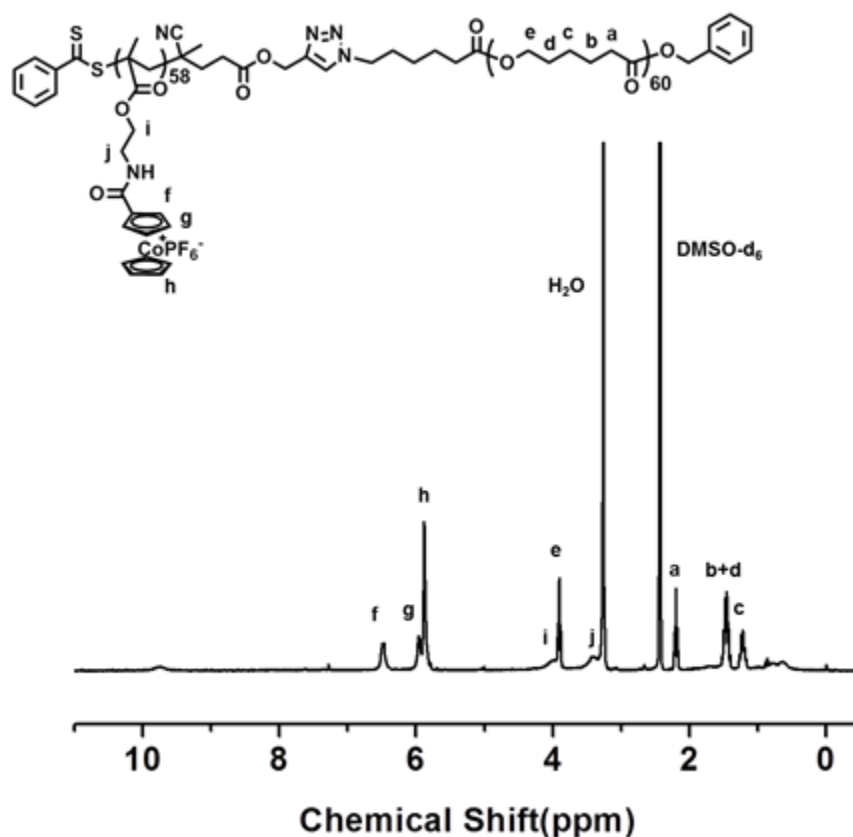


Figure 2.4. ^1H -NMR spectrum of PCL-*b*-PCoAEMAPF₆.

*Ion-exchange of PCL-*b*-PCoAEMAPF₆ block copolymer*

PCL-*b*-PCoAEMAPF₆ (100mg) was dissolved in 2mL acetonitrile (CAN). Tetrabutylammonium chloride (TBACl) (2.0 g) was dissolved in 10 mL ACN. The polymer solution was added to TBACl solution. The ion-exchanged polymers were precipitated out. The polymers were collected and washed by ACN three times. The polymers were collected and dried in a vacuum overnight.

Self-assembly of Cobaltocenium-containing block copolymers

PCL-*b*-PCoAEMA (2.0 mg) was dissolved in 4 mL distilled water and methanol respectively to make a concentration of 0.5 mg/mL. The polymer solutions were annealed at 40 °C for 1 hour. After 1 hour, the solutions were cooled down to room temperature slowly. The polymer solution was kept at room temperature for the designated time. TEM

samples were prepared by drop-casting of polymer solutions onto carbon-coated copper grids and dried overnight.

2.4 Results and Discussion

Preparation of cobaltocenium-containing block copolymers

The cobaltocenium-containing block copolymer was synthesized via sequential ring-opening polymerization (ROP) of caprolactone and reversible addition-fragmentation chain transfer (RAFT) polymerization of cobaltocenium amidoethyl methacrylate hexafluorophosphate (**Figure 2.5**). PCL was synthesized via ROP and the terminal hydroxyl group was further converted to azide group, which was then subject to a click-type cycloaddition reaction with an acetylene-containing chain transfer agent (CTA), yielding dithioester-capped PCL as macro-CTA. CoAEMA monomer was then introduced as the second block via RAFT using the above macro-CTA. The compositions of block copolymers can be adjusted by changing the feed ratios of monomer to macro-CTA and were established by $^1\text{H-NMR}$. The solubility of the cobaltocenium-containing block is largely dependent on its counterion. In order to increase the hydrophilicity of the corona-forming block, hexafluorophosphate counterion was exchanged for chloride by using tetrabutylammonium chloride, according to a previously reported procedure.⁴⁰

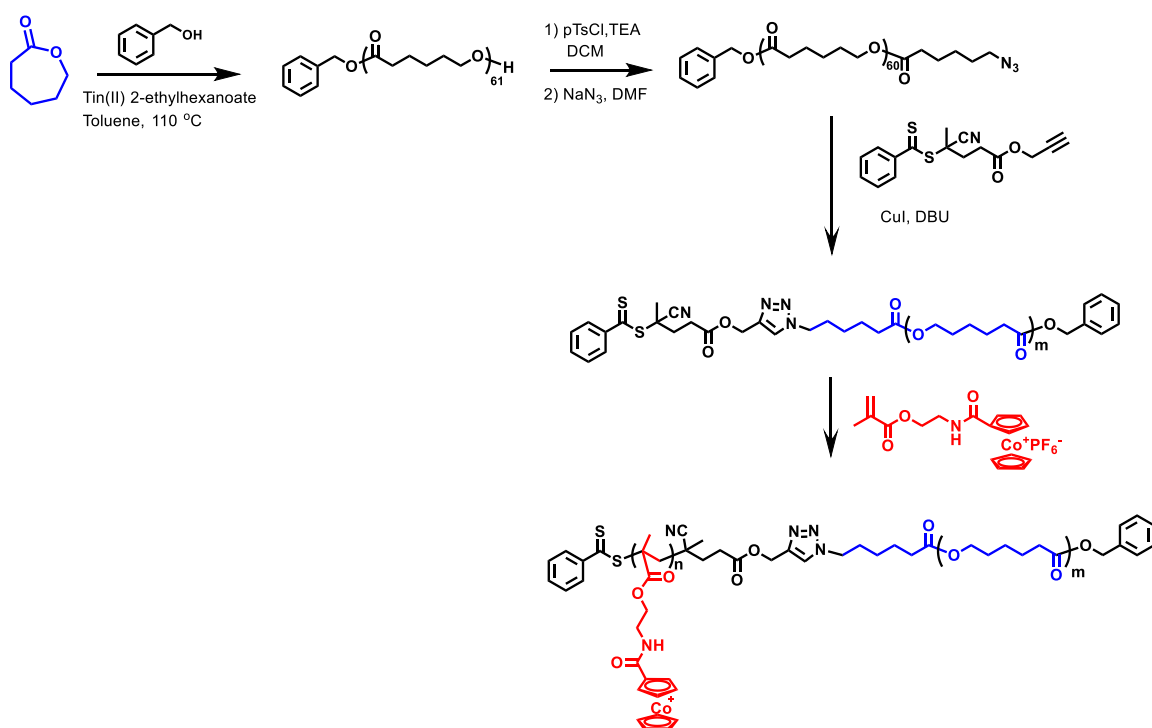


Figure 2.5. Synthesis of cobaltocenium-containing block copolymers.

CDSA in MeOH

First, we explored the self-assembly of the metallo-polyelectrolyte block copolymer with a short polycobaltocenium block (PCL₆₁-*b*-PCoAEMA₅₈). This block copolymer was dissolved in methanol with a concentration of 0.5 mg/mL, heated at 40 °C for 1 hour, and then slowly cooled to room temperature over 5 hours. Methanol was selected as the solvent because it is selective for the cobaltocenium block. The polymer solution was then aged at room temperature for one month and characterized by transmission electron microscopy (TEM) after solvent evaporation. TEM revealed the formation of platelets with a highly regular hexagonal shape and an average area of 19.6 μm^2 and a dispersity of A_w/A_n 1.24, where A_w is the weight-average area and A_n is the number-average area. (**Figure 2.6 and 2.7**). Selected area electron diffraction (SAED) from these hexagonal platelets showed that they possess a crystalline PCL core-forming

block (**Figure 2.6C**). The diffraction pattern is in accordance with those previously reported.^{35, 41, 42} Atomic force microscopy (AFM) clearly revealed that the hexagonal platelets have a thickness of ~10 nm. The linear zig-zag extended chain length of the PCL block is approximately 60 nm, which indicates the crystalline core contains chains that are folded ca. 6 times. Moreover, AFM analysis showed a distinct 1D region of elevation at the center (**Figure 2.6D**), which likely represents the location of a seed formed during the initial, self-nucleation stage of CDSA, which has been previously located in cases of seeded growth.^{18, 25}

The chemical composition of these 2D platelets was further characterized. Based on the chemical structure of block copolymer, 2D platelets are expected to be covered by cobaltocenium, which is more compatible with protic solvent. In order to prove this, we used TEM-EDX. As shown in **Figure 2.8**, scanning of the platelet surface showed the elemental cobalt, which is originated from cobaltocenium of the corona-forming block. Therefore, it is concluded that the resultant 2D platelets from PCL₆₁-*b*-PCoAEMA₅₈ are covered by cationic cobaltocenium blocks that can stabilize the 2D micelles.

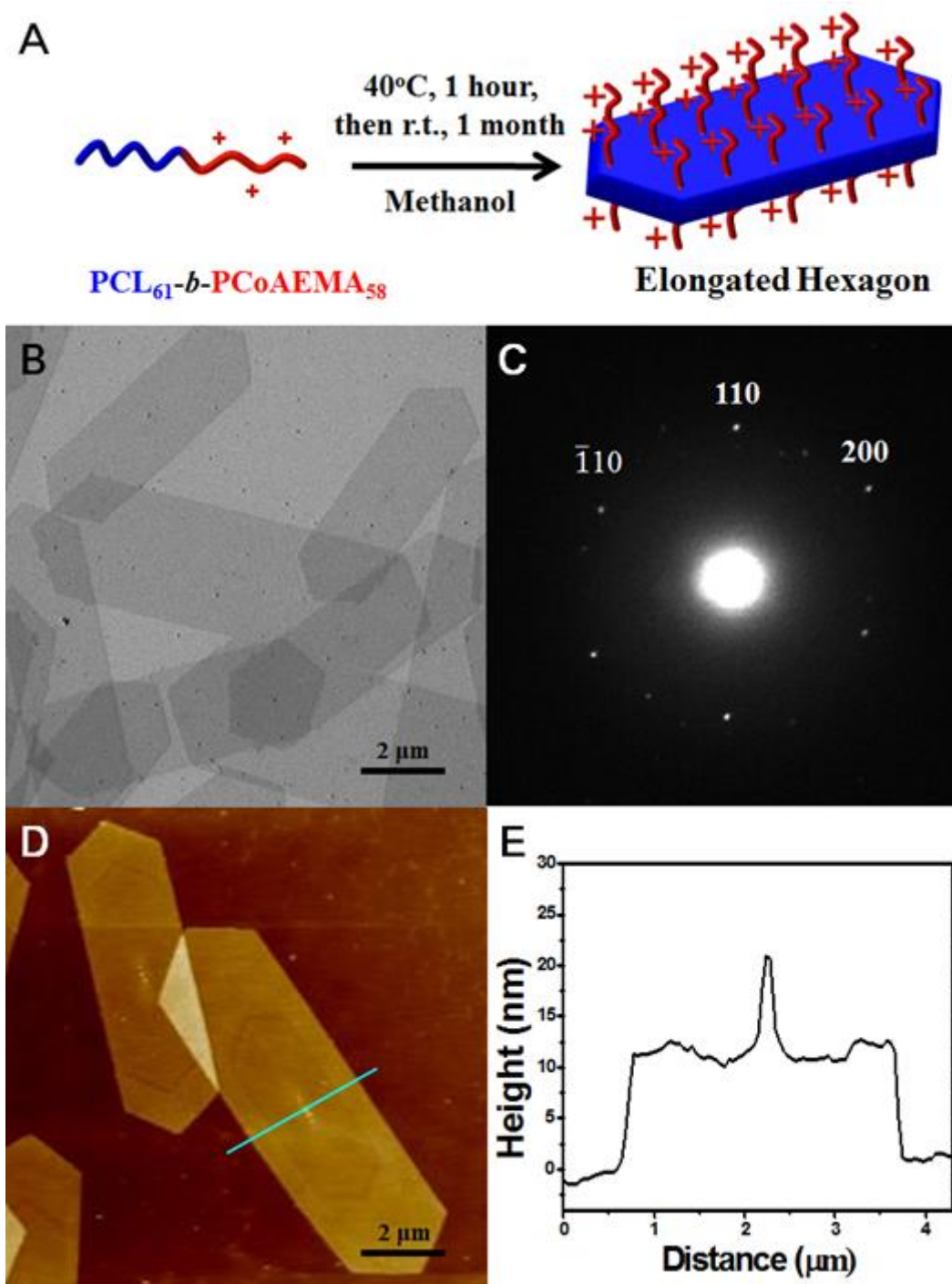


Figure 2.6. (A) Schematic illustration of the formation of 2D hexagonal platelets by CDSA of block copolymer $\text{PCL}_{61}\text{-}b\text{-PCoAEMA}_{58}$. (B) TEM micrograph of hexagonal platelets from $\text{PCL}_{61}\text{-}b\text{-PCoAEMA}_{58}$ obtained by heating the polymer solution in methanol at 40 °C for 1 h followed by cooling and aging at room temperature for 1 month. (C) TEM SAED of hexagonal platelets. (D) AFTM height image. (E) AFM height profile from image D.

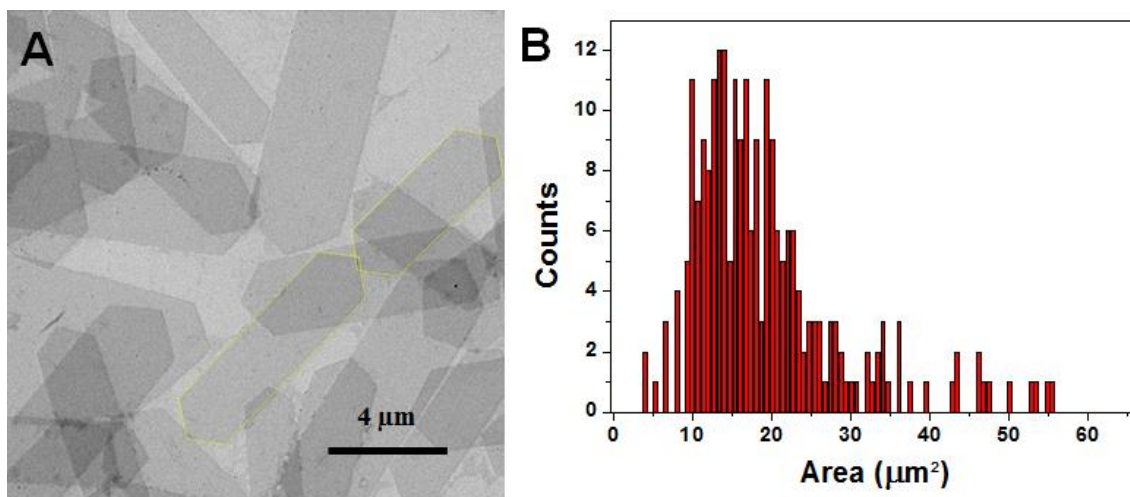


Figure 2.7. (A) Additional TEM micrograph of elongated hexagonal platelet of PCL₆₁-*b*-PCoAEMA₅₈ with a concentration of 0.5 mg/mL in methanol and annealing at 40 °C for 1 hour, followed by cooling to 25 °C and then aging for 1 month; and (B) area distribution (average area = 19.6 μm², area dispersity = 1.24).

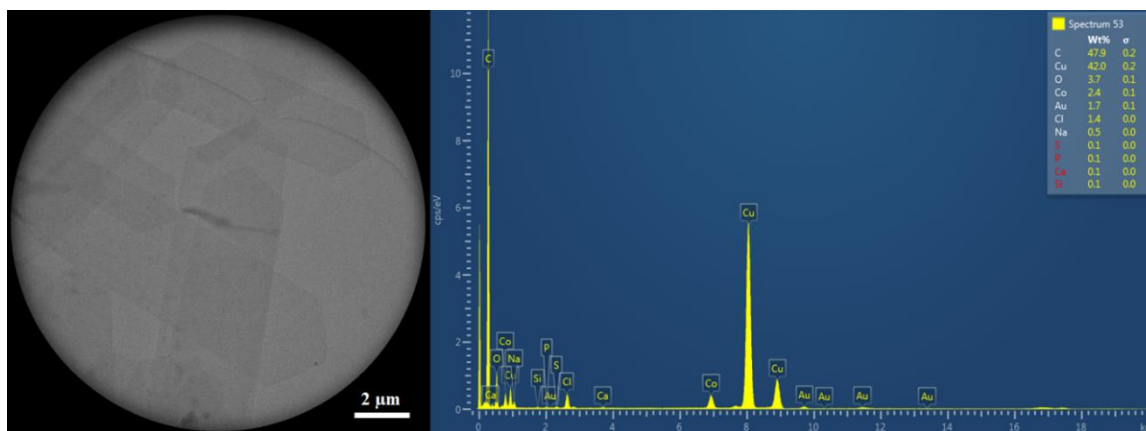


Figure 2.8. TEM-EDX analysis of hexagonal platelets.

To further explore the CDSA behavior of this block copolymer during the aging, ¹H NMR experiments were carried out in methanol-d₄. Before starting the CDSA process (i.e. prior to heating), the proton peaks of solvated PCL to poly(cobaltocenium) showed a ratio of ca. 1:1 between two segments in the as-prepared block copolymer (**Figure 2.4**). As the aging proceeded, the intensity of the proton peaks of PCL decreased, whereas the proton peaks of cyclopentadienyl ring of cobaltocenium maintained unchanged (**Figure 2.9**). After aging for 11 days, the peak ratio of PCL to cobaltocenium reached ~0.4:1. As

previously reported,⁴³ the protons at the α position of PCL are restricted and show a decreased intensity when the crystallization proceeds.

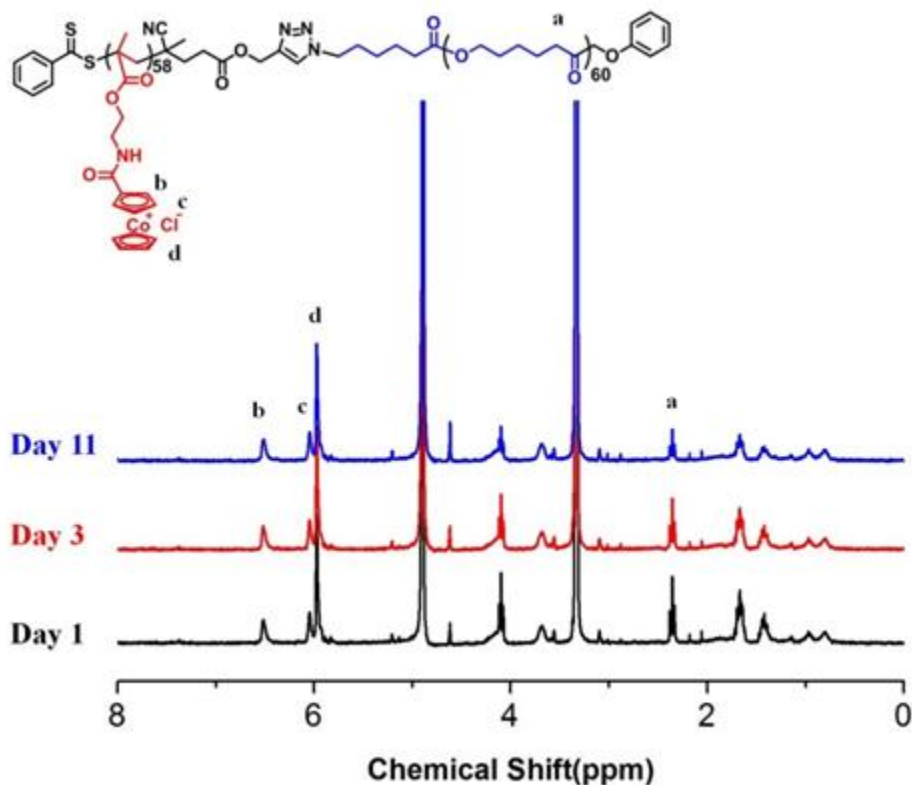


Figure 2. 9. Time dependent ^1H NMR spectra of $\text{PCL}_{61}\text{-}b\text{-PCoAEMA}_{58}$ in methanol- d_4 .

The time-dependent CDSA process was also monitored by TEM. As shown in **Figure 2.11A**, when $\text{PCL}_{61}\text{-}b\text{-PCoAEMA}_{58}$ was dissolved in methanol without heating, TEM image shows small crystallites, which could serve as seeds for subsequent CDSA. Afterward, the solution was subject to heating and aging as described above. After aging for 1 day, small elongated hexagonal platelets were formed (**Figure 2.11B**). With the increase of aging time, these hexagonal platelets grew larger (**Figure 2.11C-E**). The average area of hexagonal platelets after one-day aging was $1.68 \times 10^5 \text{ nm}^2$. It increased to $2.41 \times 10^5 \text{ nm}^2$ after 3 days and $2.92 \times 10^5 \text{ nm}^2$ after 11 days. The area dispersity was 1.09.

the aspect ratios (L_n/W_n , where L_n is the number-average length and W_n the number-average width) were similar, ca. 4.6, throughout the CDSA process.

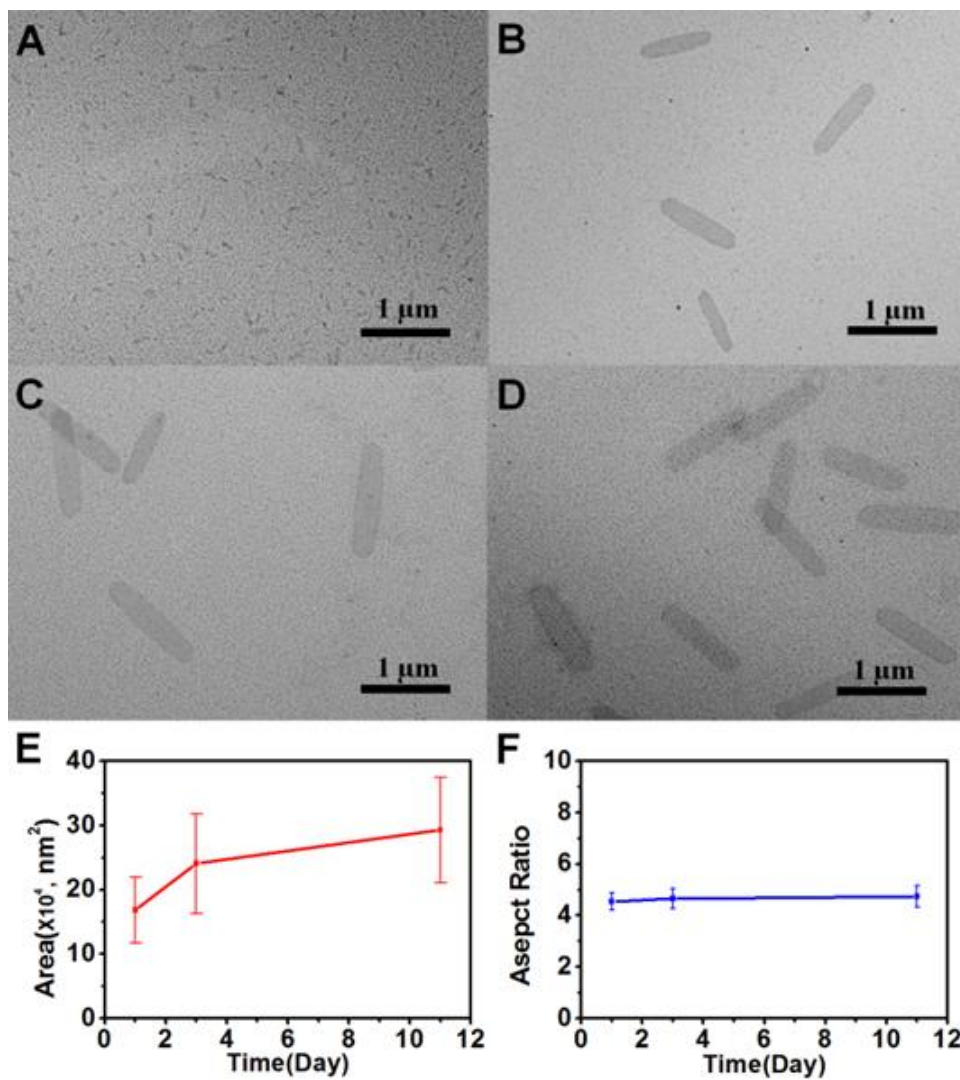


Figure 2.10. TEM micrographs of PCL₆₁-b-PCoAEMA₅₈ in methanol: (A) before heating; (B) aging for 1 day; (C) aging for 3 days; and (D) aging for 11 days. Plots of (E) area versus aging time and (F) aspect ratio versus aging time.

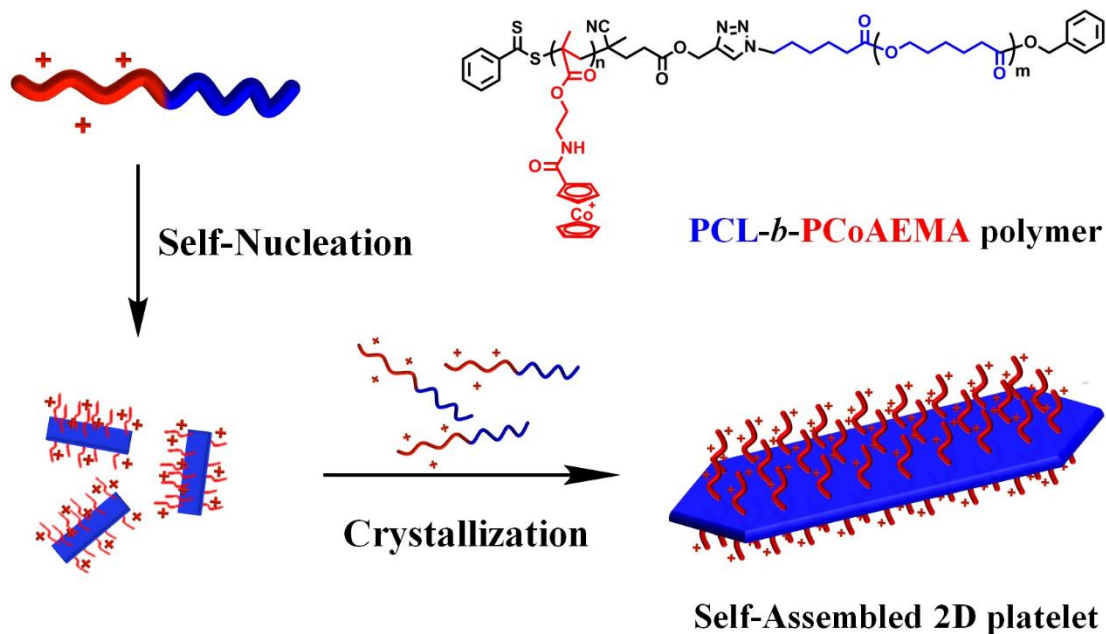


Figure 2.11. Illustration of CDSA of PCL-*b*-PCoAEMA block copolymer toward hexagonal platelet nanostructures.

Combined the results so far, the whole procedure of CDSA of PCL-*b*-PCoAEMA block copolymer proceeds that is similar to that of crystalline polymer (**Figure 2.11**). The block copolymer first forms small particles that can act as nuclei at the beginning of the procedure. Then, the rest of the unimers are attached to the nuclei, followed by the growth of micelles.

Effect of polymer composition on morphological transition

Next, we studied how the composition of block copolymers affected the CDSA process. We synthesized two block copolymers with a longer cobaltocenium block while keeping the degree of polymerization of the PCL block the same: PCL₆₁-*b*-PCoAEMA₂₄₄ and PCL₆₁-*b*-PCoAEMA₃₄₄. For amphiphilic block copolymers, an increased length of corona block can cause higher repulsion between chains, leading to larger interfacial curvature and thus resulting in morphological transformations.^{14, 44} We anticipated that the

longer corona of the cobaltocenium block would induce the morphological transition from 2D hexagonal platelets to 1D cylindrical or spherical morphologies. Self-assembly experiments were carried out using the same procedure as for PCL₆₁-*b*-PCoAEMA₅₈. However, TEM images showed that PCL₆₁-*b*-PCoAEMA₂₄₄ copolymer also produced hexagonal platelets which have an area dispersity of 1.05 with a larger width than that of PCL₆₁-*b*-PCoAEMA₅₈ (**Figures 2.12A and E**). PCL₆₁-*b*-PCoAEMA₃₄₄ showed the formation of diamond-shaped platelets with an area dispersity of 1.11 (**Figures 2.13A and E**) and lenticular shapes (**Figure 2.14**). Electron diffraction patterns of the wider hexagonal and diamond-shaped platelets revealed similar diffraction patterns to that of longer platelets (**Figures 2.12B and 2.13B**).

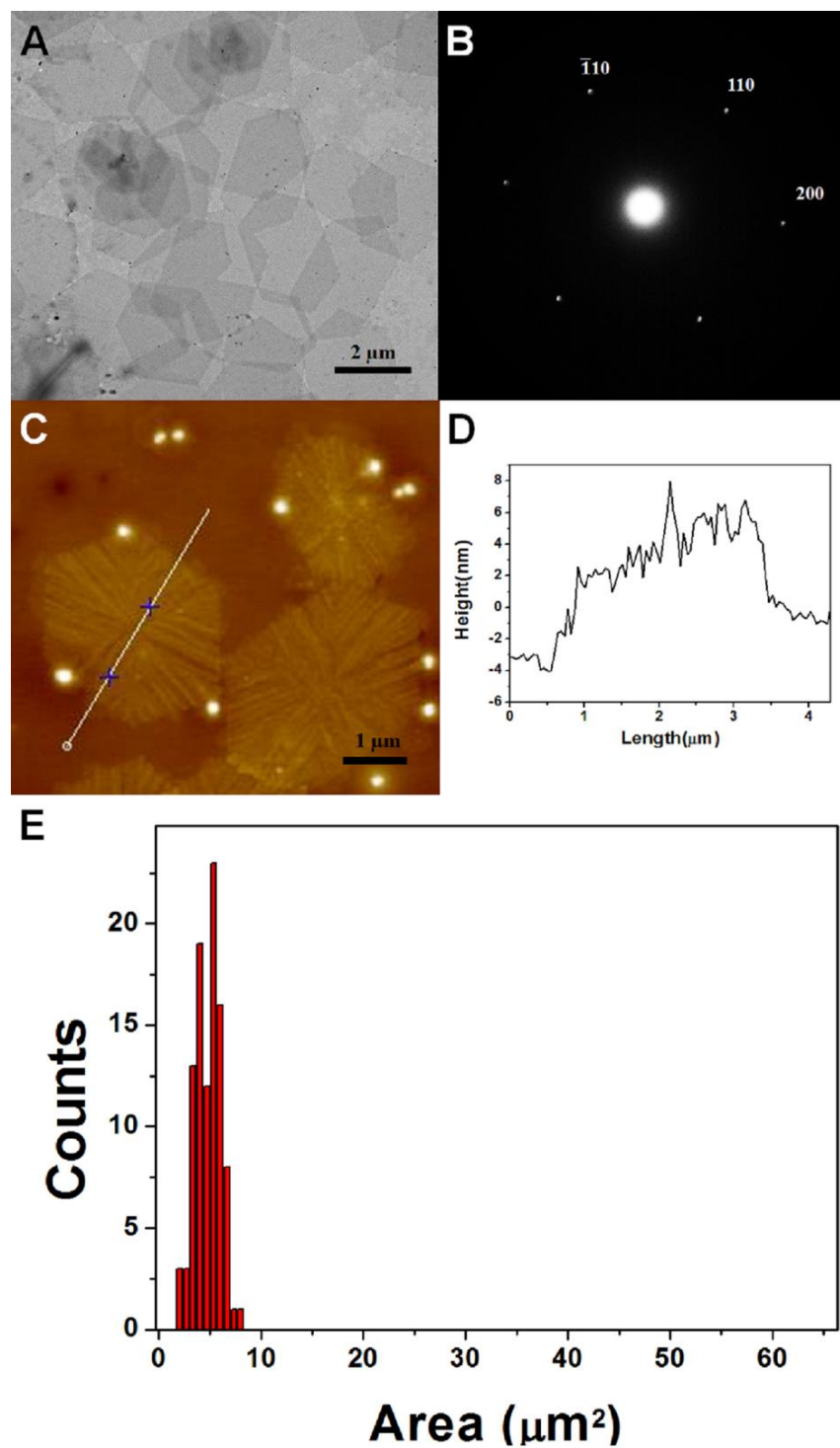


Figure 2.12. (A) TEM micrograph of wider hexagonal platelets obtained from PCL₆₁-*b*-PCoAEMA₂₄₄ in methanol (0.5 mg/mL) with heating at 40 °C for 1 hour, followed by cooling to 25 °C and then aging for 1 month; (B) Electron diffraction; (C) AFM height image; (D) AFM height profile from image C; and (E) area distribution (average area = 2.76 μm^2 , area dispersity = 1.05).

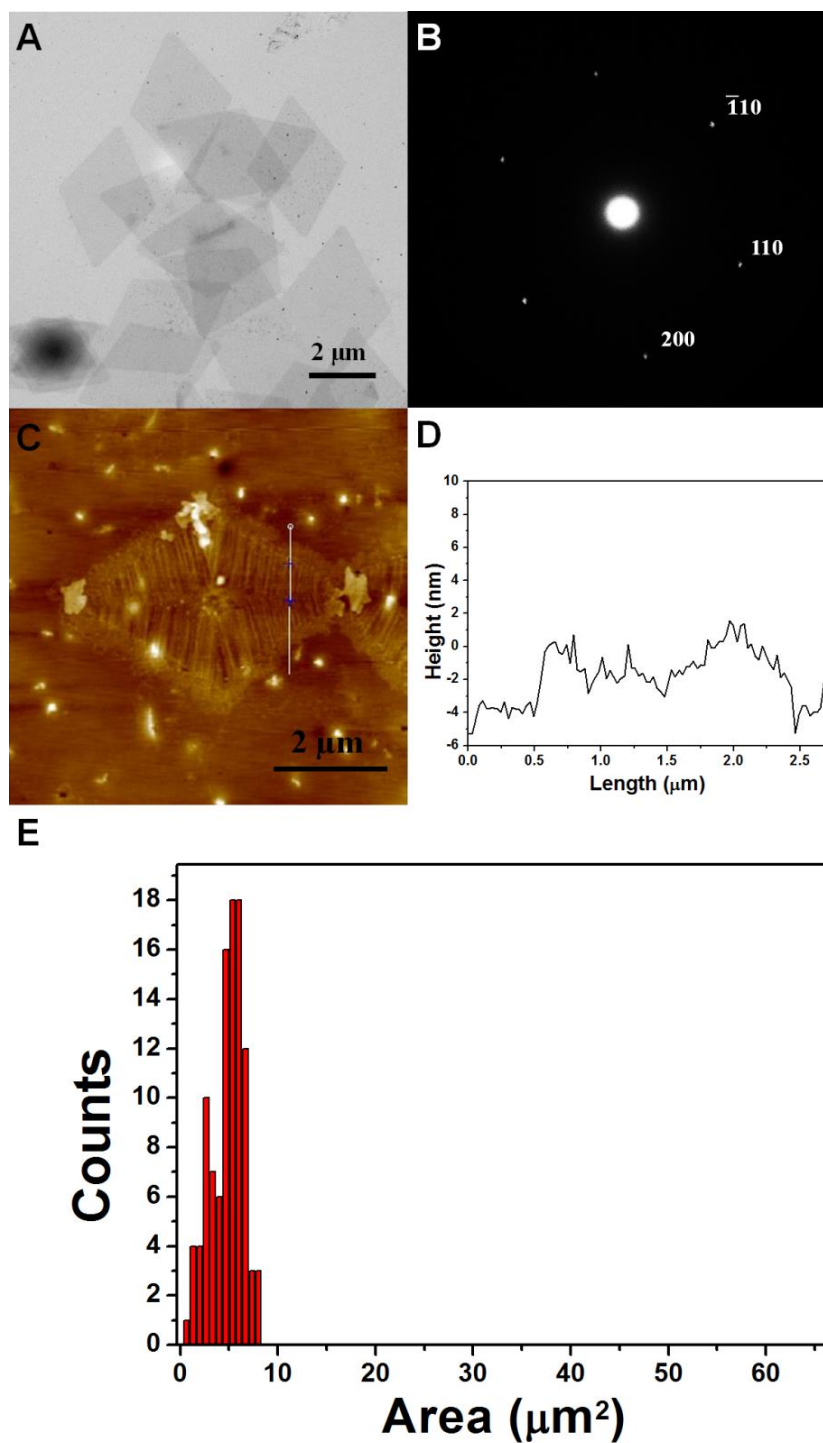


Figure 2.13. (A) TEM micrograph of diamond-shaped platelets of PCL₆₁-*b*-PCoAEMA₃₄₄ in methanol (0.5 mg/mL) with heating at 40 °C for 1 hour, followed by cooling to 25 °C and then aging for 1 month; (B) Electron diffraction; (C) AFM height image; (D) AFM height profile from image C; and (E) area distribution (average area = 3.37 μm², area dispersity = 1.11).

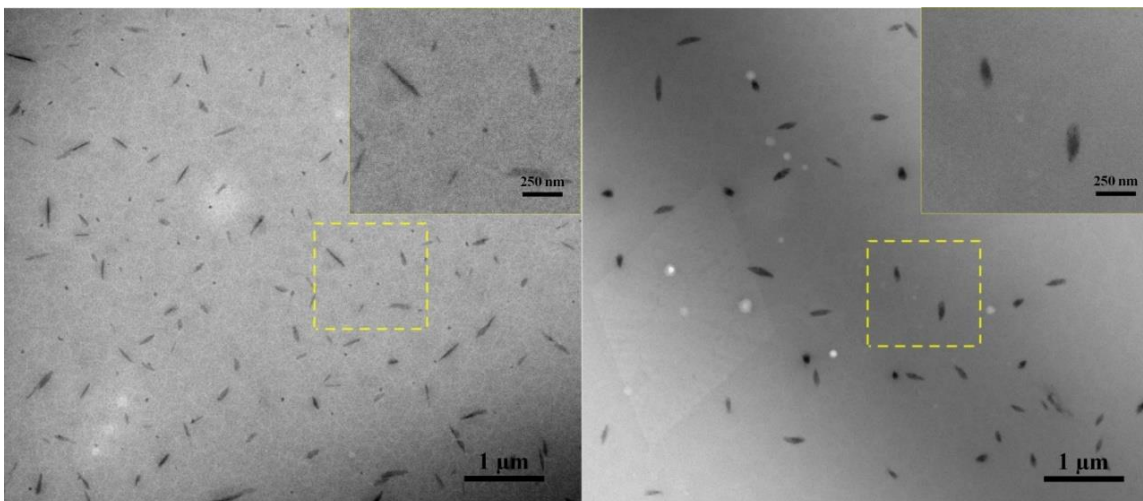


Figure 2.14. TEM micrographs of lenticular structures from PCL₆₁-*b*-PCoAEMA₃₄₄ in methanol (0.5 mg/mL) obtained by annealing at 40 °C for 1 hour, followed by cooling to 25 °C and then aging for 1 month. Insert: magnified areas from dashed yellow squares.

These 2D micelles share some common characteristics. We measured the angle of each platelet (depicted in the yellow line in **Figure 2.15C-E**). As shown in **Figure 2.15**, the angle at the end of the elongated hexagon is ca. 109°; the wider hexagons and the diamond platelets exhibit the same angles at ~109°. The corners of 2D platelets were superimposed on each other. To further characterize these 2D platelets, we measured the aspect ratios of each platelet. Elongated hexagons from PCL₆₁-*b*-PCoAEMA₅₈, wider hexagons from PCL₆₁-*b*-PCoAEMA₂₄₄ and diamond-shaped platelets from PCL₆₁-*b*-PCoAEMA₂₄₄ have the aspect ratios respectively at 3.3, 1.6 and 0.7. The relationship between aspect ratio and block ratio showed a linear relationship (**Figure 2.15F**). As the block ratio increased, the aspect ratio decreased. AFM images of wider hexagonal and diamond-shaped platelets show the reduced thickness, 6 nm, and 4 nm, respectively (**Figures 2.12D and 2.13D**), suggesting increased chain folding compared to the narrow hexagonal case with a thickness of ca. 10 nm in **Figure 2.6D and 2.6E**. We postulated that when the corona block is short, the growth of platelets is dominated by the preferred

unidirectional crystallization of the PCL block.⁴⁵ It is likely that with the increase in the spatial extent of the corona, the rate of longitudinal crystallization is reduced by the presence of the hairy cobaltocenium segment, forcing platelets to expand more uniformly in both longitudinal and lateral directions. The increase in chain folding detected would also help stabilize the resulting platelets by reducing inter-coronal steric interactions by lowering the areal brush density. It appears that for this system, this approach is favored over a reduction in the curvature of the core-corona interface to yield 1D fiber-like assemblies.

One of us reported diamond-shaped platelets from poly(L-lactide) homopolymers with a charged terminal phosphonium group.¹⁸ O'Reilly, Dove, and coworkers described well-defined diamond platelets from poly(*N*, *N*-dimethyl acrylamide)-*b*-P(L-lactide).⁴⁶ However, diamond platelets from a PCL-containing block copolymer have not yet been reported. It could be reasoned that the growth of 2D platelets is perpendicular to the axis of the long hexagonal platelet, as shown in **Figure 2.15D** (The dashed cartoon of the hexagon). Although the reason for this phenomenon is not clear, we hypothesized that the direction of growth is governed by the crystallization of the core-forming block. A 2D lamellar structure is accomplished by folding of the crystalline core block. The presence of a long corona block in a selective solvent can force more folding of PCL chains, as evidenced by the decrease of the thickness of platelets via AFM imaging.

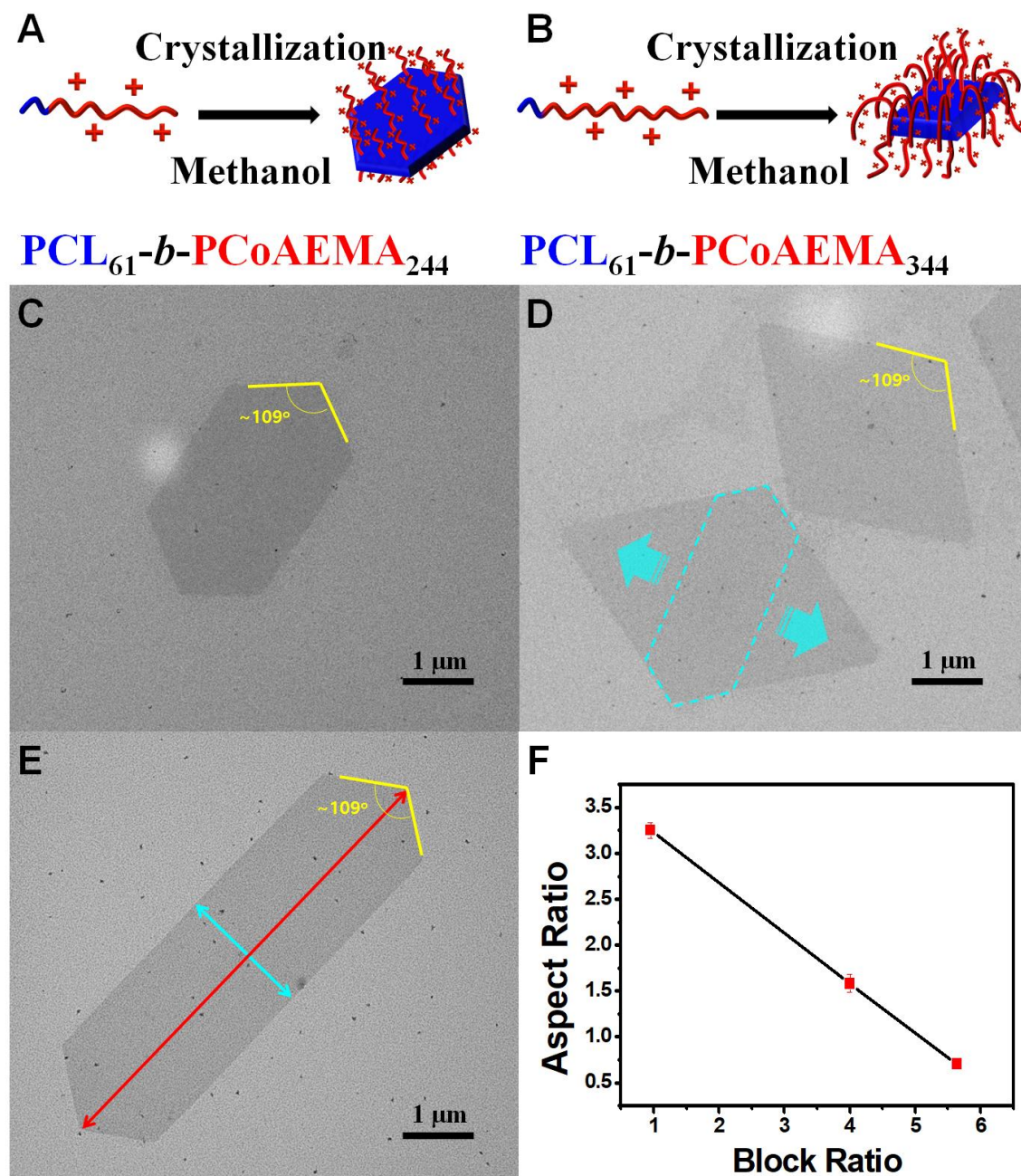


Figure 2.15. Schematic of (A, B) lower aspect ratio hexagonal platelet from $\text{PCL}_{61}\text{-}b\text{-PCoAEMA}_{244}$ and diamond-shaped platelet from $\text{PCL}_{61}\text{-}b\text{-PCoAEMA}_{344}$. TEM micrographs of platelets formed by (C) $\text{PCL}_{61}\text{-}b\text{-PCoAEMA}_{244}$ with an area dispersity of 1.05, (D) $\text{PCL}_{61}\text{-}b\text{-PCoAEMA}_{344}$ with an area dispersity of 1.11, and (E) $\text{PCL}_{61}\text{-}b\text{-PCoAEMA}_{58}$ in methanol and (F) plot of aspect ratio versus block ratio.

In order to further explore this phenomenon, we conducted additional experiments.

It was reported that blending of crystalline homopolymers with block copolymers could

accelerate the crystallization.³⁶ We prepared a homopolymer of PCL₃₈ and dissolved it in tetrahydrofuran at a concentration of 10 mg/mL. This solution was added to the diblock copolymer solution in methanol-based on a mass ratio of 1:1. The blended solution was heated at 40 °C and cooled to room temperature slowly over 5 hours. TEM characterization was carried out after aging for 1 week. TEM images revealed that the addition of homopolymer resulted in longer hexagonal platelets (**Figure 2.16**). Blending with PCL₆₁-*b*-PCoAEA₅₈ in methanol resulted in elongated hexagonal platelets with a higher aspect ratio at ~7.8. For the diblock copolymers that formed wider hexagonal and diamond-shaped platelets, they also showed long hexagonal platelets with higher aspect ratios at 6.67 and 6.52, respectively. Based on this observation, one might conclude that the increased crystallization rate of core-forming block induces the growth of 2D platelets along the longitudinal direction. The length of the corona-forming block plays an important role in the shape formation of 2D platelets and the direction of growth.

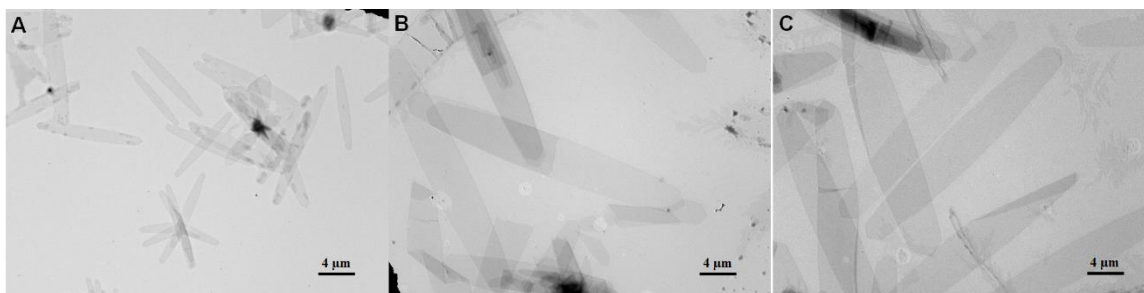


Figure 2.16. TEM micrographs of leaf-like platelet of (A) PCL₆₁-*b*-PCoAEMA₅₈; (B) PCL₆₁-*b*-PCoAEMA₂₄₄; and (C) PCL₆₁-*b*-PCoAEMA₃₄₄ in methanol (0.5 mg/mL), followed by addition of PCL₃₈ homopolymer in THF solution.

CDSA in the aqueous solution

Recent advances in self-assembly open a door for applications of micellar nanostructures in biomedical sciences. Chen and his coworkers showed that leaf-like 2D structures from poly(ethylene oxide)-*b*-polycaprolactone showed a selective permeability

to different cells.⁴⁷ DeSimone and his coworkers demonstrated that nanoparticles with higher aspect ratios showed faster cellular internalization.⁴⁸ However, few stable 1D micellar systems in water by the CDSA process have been reported. Manners and coworkers reported cylindrical micelles that can be dialyzed from DMF to water.⁴⁹ Living CDSA of PCL-containing triblock in aqueous media reported by O'Reilly, Dove, and coworkers.³² In terms of polyelectrolytes, cationic characteristics of the cobaltocenium block can play an important role on the colloidal stability of 2D structures in aqueous system. The salt responsiveness of quaternary ammonium-containing random copolymers has been previously described.⁵⁰ The increased ionic strength in aqueous solution can reduce the repulsive Coulomb interaction between cationic species.

In order to investigate the influence of electrostatic effects on the CDSA process, we changed the selective solvent from methanol to water, which would be expected to significantly enhance electrostatic repulsion between the cobaltocenium groups by increasing the solubility of the counterion. Following the same aging procedure, TEM analysis showed mainly the formation of small spherical micelles with a size of ~38 nm, consistent with 36.7 nm measured by Dynamic Light Scattering (**Figures 2.17**). This result suggests that the strong electrostatic repulsion of cationic cobaltocenium coronal segments in water induces maximum curvature of the core-corona interface to form spherical micelles where, as a result of the poorer quality of the solvent for PCL, rapid precipitation presumably leads to an amorphous core.

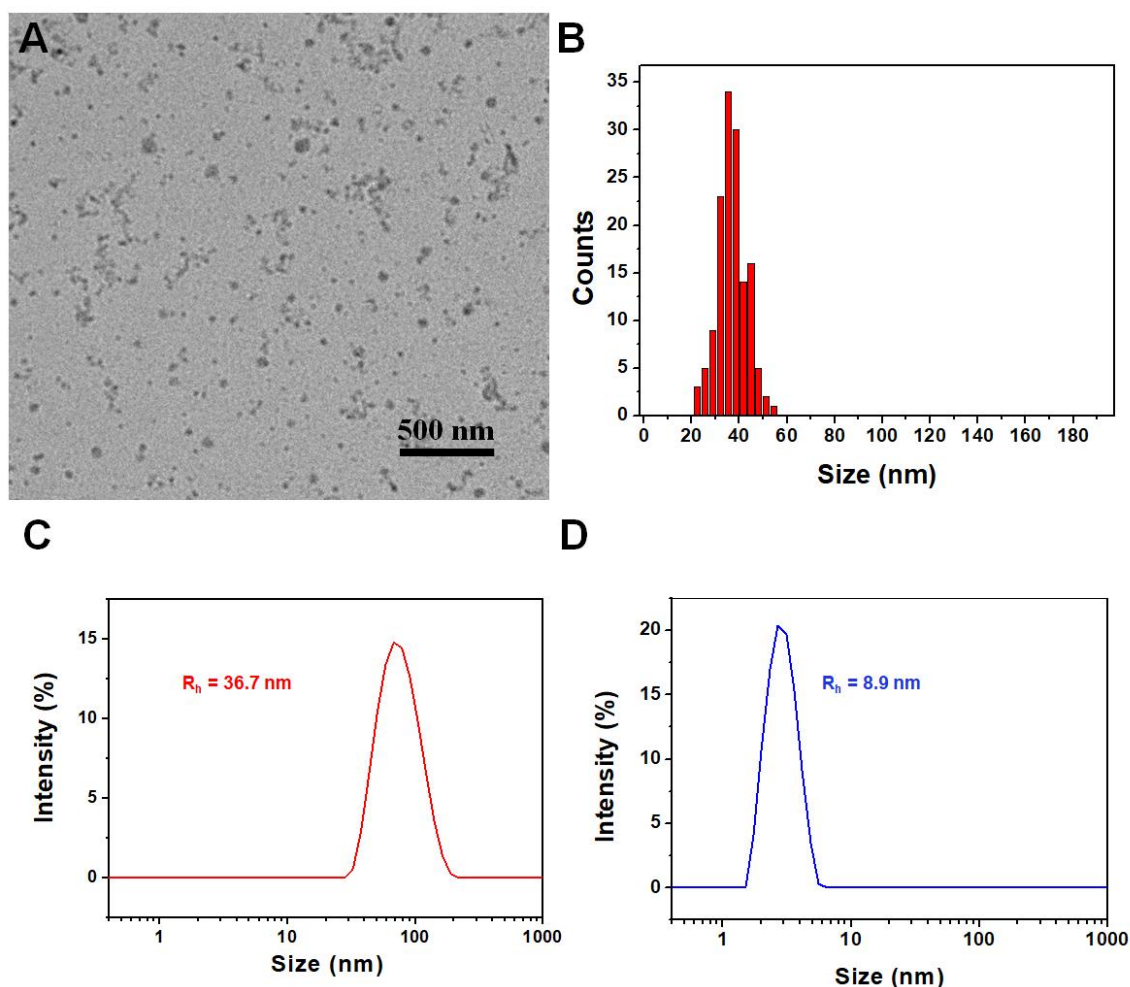


Figure 2.17. (A) TEM micrograph of sphere-shaped micelles of PCL₆₁-*b*-PCoAEMA₅₈ with a concentration of 0.5 mg/mL in water after annealing at 40 °C for 1 hour; (B) area distribution (average area = 19.6 μm^2 , area dispersity = 1.24); DLS profiles of spherical micelles from PCL₆₁-*b*-PCoAEMA₅₈: (C) in water (red, corresponds to the TEM micrograph in **Figure S7**, R_h = 36.7 nm); (D) unimers dissolved in DMF (blue, R_h = 8.9 nm) after annealing at 40 °C.

Ionic strength dependent stability of 2 D micelles

To provide further insight, we examined the effect of ionic strength on the formation of 2D platelets. Water was added to the solution of hexagonal platelets in methanol to give a volume ratio of methanol/water of 1/1. The hexagonal platelets were not stable and fragmented into smaller particles after 2 days (**Figure 2.18B**). However, when aqueous NaCl solution instead of pure water was added to the platelet micelle

solution in methanol (volume ratio = 1/1, the final concentration of sodium chloride was 1.0 M), the hexagonal platelets, which have an area dispersity of 1.08, were preserved (**Figure 2.18C**). A series of solutions with different ionic strengths were examined. The results indicated that an increase in ionic strength can screen repulsive interactions between the cationic cobaltocenium coronal chains and thus stabilize the platelets with respect to fragmentation.

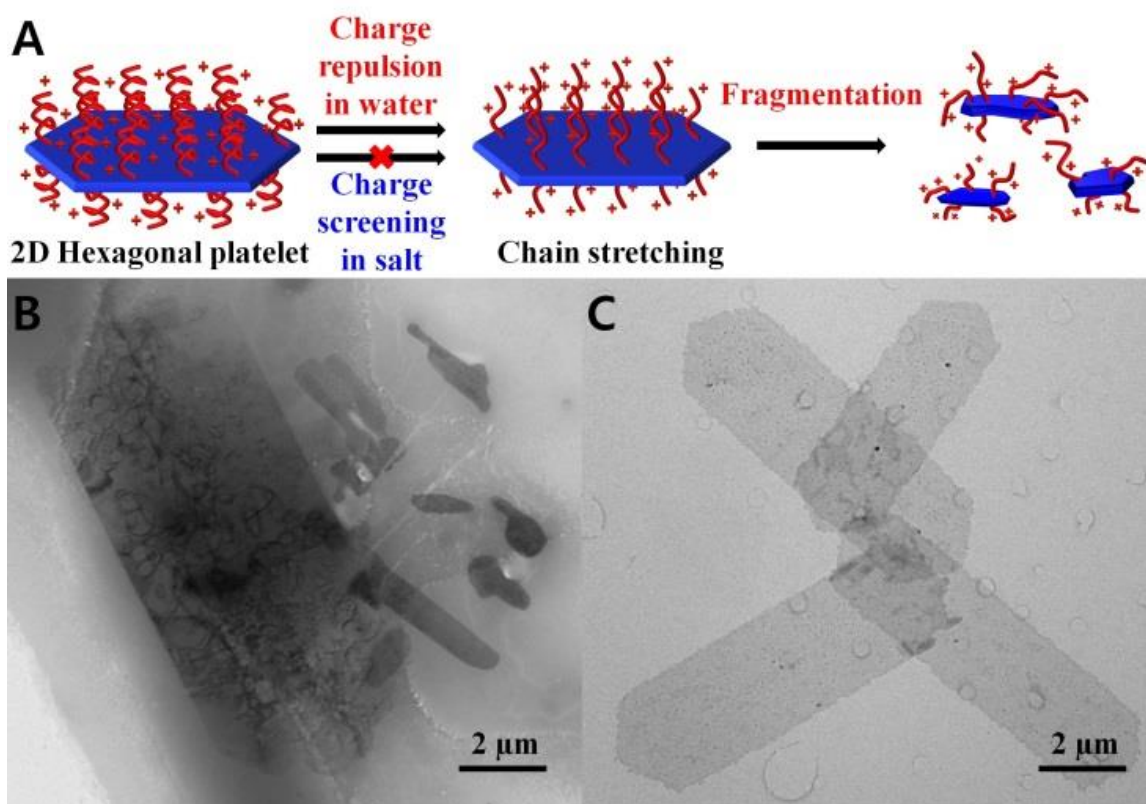


Figure 2.18. (A) Illustration of platelet fragmentation of $\text{PCL}_{61}\text{-}b\text{-PCoAEMA}_{58}$ caused by charge repulsion and preservation by charge screening in accordance with ionic strength; TEM micrographs: (B) fragmented hexagon by in methanol and water (v/v, 50/50), and (C) preserved hexagons by in methanol and 2.0 M NaCl aq. solution (v/v, 50/50).

2.5 Conclusion

In summary, cobaltocenium-containing metallo-polyelectrolyte block copolymers show some of unique crystallization-driven self-assembly behaviors in protic solvents that are selective for the polyelectrolyte block. The CDSA process resulted in exclusive 2D

platelet structures including narrow and wide hexagons and diamonds. Moreover, the interplay between electrostatics of corona and crystallization of core dictates the transformation of morphologies, especially when coupled with block copolymer compositions. The platelets exhibited ionic strength-dependent stability in aqueous solutions. Recent efforts have revealed that 2D sharp nanostructures can penetrate, cross, or mechanically wrap microbial cells. This feature, combined with the promising, previously reported biological behavior of cobaltocenium polymers, suggests that the 2D platelets described may open up new pathways toward biomedical applications.

2.6 References

1. Cui, H.; Chen, Z.; Zhong, S.; Wooley, K. L.; Pochan, D. J. Block copolymer assembly via kinetic control. *Science* **2007**, *317*, 647-50.
2. Discher, D. E.; Eisenberg, A. Polymer Vesicles. *Science* **2002**, *297*, 967-973.
3. Li, Z.; Kesselman, E.; Talmon, Y.; Hillmyer, M. A.; Lodge, T. P. Multicompartment Micelles from ABC Miktoarm Stars in Water. *Science* **2004**, *306*, 98-101.
4. Gröschel, A. H.; Walther, A.; Löbbling, T. I.; Schacher, F. H.; Schmalz, H.; Müller, A. H. Guided hierarchical co-assembly of soft patchy nanoparticles. *Nature* **2013**, *503*, 247-251.
5. Warren, N. J.; Armes, S. P. Polymerization-induced self-assembly of block copolymer nano-objects via RAFT aqueous dispersion polymerization. *J. Am. Chem. Soc.* **2014**, *136*, 10174-10185.
6. Rodriguez-Hernandez, J.; Chécot, F.; Gnanou, Y.; Lecommandoux, S. Toward 'smart' nano-objects by self-assembly of block copolymers in solution. *Prog. Polym. Sci.* **2005**, *30*, 691-724.

7. O'Reilly, R. K.; Hawker, C. J.; Wooley, K. L. Cross-linked block copolymer micelles: functional nanostructures of great potential and versatility. *Chem. Soc. Rev.* **2006**, *35*, 1068-1083.
8. Schöbel, J.; Karg, M.; Rosenbach, D.; Krauss, G.; Greiner, A.; Schmalz, H. Patchy Wormlike Micelles with Tailored Functionality by Crystallization-Driven Self-Assembly: A Versatile Platform for Mesostuctured Hybrid Materials. *Macromolecules* **2016**, *49*, 2761-2771.
9. Su, M.; Huang, H.; Ma, X.; Wang, Q.; Su, Z. Poly(2-vinylpyridine)-block -Poly(-caprolactone) single crystals in micellar solution. *Macromol. Rapid Commun.* **2013**, *34*, 1067-71.
10. Pitto-Barry, A.; Kirby, N.; Dove, A. P.; O'Reilly, R. K. Expanding the scope of the crystallization-driven self-assembly of polylactide-containing polymers. *Polym. Chem.* **2014**, *5*, 1427-1436.
11. Choi, I.; Yang, S.; Choi, T.-L. Preparing Semiconducting Nanoribbons with Tunable Length and Width via Crystallization-Driven Self-Assembly of a Simple Conjugated Homopolymer. *J. Am. Chem. Soc.* **2018**, *140*, 17218-17225.
12. Qiu, H.; Hudson, Z. M.; Winnik, M. A.; Manners, I. Micelle assembly. Multidimensional hierarchical self-assembly of amphiphilic cylindrical block comicelles. *Science* **2015**, *347*, 1329-32.
13. Wang, X.; Guerin, G.; Wang, H.; Wang, Y.; Manners, I.; Winnik, M. A. Cylindrical block copolymer micelles and co-micelles of controlled length and architecture. *Science* **2007**, *317*, 644-7.
14. Massey, J. A.; Temple, K.; Cao, L.; Rharbi, Y.; Raez, J.; Winnik, M. A.; Manners, I. Self-Assembly of Organometallic Block Copolymers: The Role of Crystallinity of the Core-Forming Polyferrocene Block in the Micellar Morphologies Formed by Poly(ferrocenylsilane-b-dimethylsiloxane) in Alkane Solvents. *J. Am. Chem. Soc.* **2000**, *122*, 11577-11584.

15. Gilroy, J. B.; Gadt, T.; Whittell, G. R.; Chabanne, L.; Mitchels, J. M.; Richardson, R. M.; Winnik, M. A.; Manners, I. Monodisperse cylindrical micelles by crystallization-driven living self-assembly. *Nat. Chem.* **2010**, *2*, 566-70.
16. Qiu, H.; Gao, Y.; Boott, C. E.; Gould, O. E.; Harniman, R. L.; Miles, M. J.; Webb, S. E.; Winnik, M. A.; Manners, I. Uniform patchy and hollow rectangular platelet micelles from crystallizable polymer blends. *Science* **2016**, *352*, 697-701.
17. Soto, A. P.; Gilroy, J. B.; Winnik, M. A.; Manners, I. Pointed-oval-shaped micelles from crystalline-coil block copolymers by crystallization-driven living self-assembly. *Angew. Chem. Int. Ed.* **2010**, *49*, 8220-3.
18. He, X.; Hsiao, M. S.; Boott, C. E.; Harniman, R. L.; Nazemi, A.; Li, X.; Winnik, M. A.; Manners, I. Two-dimensional assemblies from crystallizable homopolymers with charged termini. *Nat. Mater.* **2017**, *16*, 481-488.
19. Pageni, P.; Yang, P.; Bam, M.; Zhu, T.; Chen, Y. P.; Decho, A. W.; Nagarkatti, M.; Tang, C. Recyclable magnetic nanoparticles grafted with antimicrobial metallopolymer-antibiotic bioconjugates. *Biomaterials* **2018**, *178*, 363-372.
20. Zhang, J.; Chen, Y. P.; Miller, K. P.; Ganewatta, M. S.; Bam, M.; Yan, Y.; Nagarkatti, M.; Decho, A. W.; Tang, C. Antimicrobial metallopolymer and their bioconjugates with conventional antibiotics against multidrug-resistant bacteria. *J. Am. Chem. Soc.* **2014**, *136*, 4873-6.
21. Yang, P.; Bam, M.; Pageni, P.; Zhu, T.; Chen, Y. P.; Nagarkatti, M.; Decho, A. W.; Tang, C. Trio Act of Boronolactin with Antibiotic-Metal Complexed Macromolecules toward Broad-Spectrum Antimicrobial Efficacy. *ACS Infect. Dis.* **2017**, *3*, 845-853.
22. Engler, A. C.; Wiradharma, N.; Ong, Z. Y.; Coady, D. J.; Hedrick, J. L.; Yang, Y.-Y. Emerging trends in macromolecular antimicrobials to fight multi-drug-resistant infections. *Nano Today* **2012**, *7*, 201-222.
23. Qiu, H.; Gilroy, J. B.; Manners, I. DNA-induced chirality in water-soluble poly(cobaltoceniumethylene). *Chem. Commun.* **2013**, *49*, 42-4.

24. Fan, B.; Liu, L.; Li, J.-H.; Ke, X.-X.; Xu, J.-T.; Du, B.-Y.; Fan, Z.-Q. Crystallization-driven one-dimensional self-assembly of polyethylene-*b*-poly(tert-butylacrylate) diblock copolymers in DMF: effects of crystallization temperature and the corona-forming block. *Soft Matter* **2016**, *12*, 67-76.
25. Guerin, G.; Rupar, P. A.; Manners, I.; Winnik, M. A. Explosive dissolution and trapping of block copolymer seed crystallites. *Nat. Commun.* **2018**, *9*, 1-8.
26. Zhu, T.; Xu, S.; Rahman, A.; Dogdibegovic, E.; Yang, P.; Pageni, P.; Kabir, M. P.; Zhou, X. D.; Tang, C. Cationic Metallo-Polyelectrolytes for Robust Alkaline Anion-Exchange Membranes. *Angew. Chem. Int. Ed.* **2018**, *57*, 2388-2392.
27. Mayer, U. F.; Gilroy, J. B.; O'Hare, D.; Manners, I. Ring-opening polymerization of 19-electron [2]cobaltocenophanes: a route to high-molecular-weight, water-soluble polycobaltocenium polyelectrolytes. *J. Am. Chem. Soc.* **2009**, *131*, 10382-3.
28. Gilroy, J. B.; Patra, S. K.; Mitchels, J. M.; Winnik, M. A.; Manners, I. Main-Chain Heterobimetallic Block Copolymers: Synthesis and Self-Assembly of Polyferrocenylsilane-*b*-Poly(cobaltoceniummethylene). *Angew. Chem. Int. Ed.* **2011**, *50*, 5851-5855.
29. Musgrave, R. A.; Choi, P.; Harniman, R. L.; Richardson, R. M.; Shen, C.; Whittell, G. R.; Crassous, J.; Qiu, H.; Manners, I. Chiral Transmission to Cationic Polycobaltocenes over Multiple Length Scales Using Anionic Surfactants. *J. Am. Chem. Soc.* **2018**, *140*, 7222-7231.
30. Ren, L.; Hardy, C. G.; Tang, C. Synthesis and solution self-assembly of side-chain cobaltocenium-containing block copolymers. *J. Am. Chem. Soc.* **2010**, *132*, 8874-5.
31. Tian, H. Y.; Tang, Z. H.; Zhuang, X. L.; Chen, X. S.; Jing, X. B. Biodegradable synthetic polymers: Preparation, functionalization and biomedical application. *Prog. Polym. Sci.* **2012**, *37*, 237-280.

32. Arno, M. C.; Inam, M.; Coe, Z.; Cambridge, G.; Macdougall, L. J.; Keogh, R.; Dove, A. P.; O'Reilly, R. K. Precision Epitaxy for Aqueous 1D and 2D Poly(epsilon-caprolactone) Assemblies. *J. Am. Chem. Soc.* **2017**, *139*, 16980-16985.
33. Du, Z. X.; Xu, J. T.; Fan, Z. Q. Regulation of micellar morphology of PCL-b-PEO block copolymers by crystallization temperature. *Macromol. Rapid Commun.* **2008**, *29*, 467-471.
34. Glavas, L.; Olsen, P.; Odelius, K.; Albertsson, A. C. Achieving micelle control through core crystallinity. *Biomacromolecules* **2013**, *14*, 4150-6.
35. He, W. N.; Xu, J. T.; Du, B. Y.; Fan, Z. Q.; Wang, X. S. Inorganic-Salt-Induced Morphological Transformation of Semicrystalline Micelles of PCL-b-PEO Block Copolymer in Aqueous Solution. *Macromol. Chem. Phys.* **2010**, *211*, 1909-1916.
36. Rizis, G.; van de Ven, T. G.; Eisenberg, A. "Raft" formation by two-dimensional self-assembly of block copolymer rod micelles in aqueous solution. *Angew. Chem. Int. Ed.* **2014**, *53*, 9000-3.
37. Wang, J.; Lu, Y.; Chen, Y. Fabrication of 2D surface-functional polymer platelets via crystallization-driven self-assembly of poly(epsilon-caprolactone)-contained block copolymers. *Polymer* **2019**, *160*, 196-203.
38. Zhang, J.; Yan, J.; Pageni, P.; Yan, Y.; Wirth, A.; Chen, Y.-P.; Qiao, Y.; Wang, Q.; Decho, A. W.; Tang, C. Anion-responsive metallopolymer hydrogels for healthcare applications. *Sci. Rep.* **2015**, *5*, 1-10.
39. Möller, M.; Kånge, R.; Hedrick, J. Sn (OTf) ₂ and Sc (OTf) ₃: efficient and versatile catalysts for the controlled polymerization of lactones. *J. Polym. Sci. A Polym. Chem.* **2000**, *38*, 2067-2074.
40. Zhang, J.; Yan, Y.; Chance, M. W.; Chen, J.; Hayat, J.; Ma, S.; Tang, C. Charged metallopolymer as universal precursors for versatile cobalt materials. *Angew. Chem. Int. Ed.* **2013**, *52*, 13387-91.

41. Bittiger, H.; Marchessault, R. H.; Niegisch, W. D. Crystal structure of poly- ϵ -caprolactone. *Acta Crystallographica Section B Structural Crystallography and Crystal Chemistry* **1970**, *26*, 1923-1927.
42. Ganda, S.; Dulle, M.; Drechsler, M.; Forster, B.; Forster, S.; Stenzel, M. H. Two-Dimensional Self-Assembled Structures of Highly Ordered Bioactive Crystalline-Based Block Copolymers. *Macromolecules* **2017**, *50*, 8544-8553.
43. Tanaka, H.; Nishi, T. Study of crystallization process of polymer from melt by a real-time pulsed NMR measurement. *J. Chem. Phys.* **1986**, *85*, 6197-6209.
44. Cao, L.; Manners, I.; Winnik, M. A. Influence of the Interplay of Crystallization and Chain Stretching on Micellar Morphologies: Solution Self-Assembly of Coil-Crystalline Poly(isoprene-block-ferrocenylsilane). *Macromolecules* **2002**, *35*, 8258-8260.
45. Gast, A. P.; Vinson, P. K.; Cogan-Farinas, K. A. An intriguing morphology in crystallizable block copolymers. *Macromolecules* **1993**, *26*, 1774-1776.
46. Inam, M.; Cambridge, G.; Pitto-Barry, A.; Laker, Z. P. L.; Wilson, N. R.; Mathers, R. T.; Dove, A. P.; O'Reilly, R. K. 1D vs. 2D shape selectivity in the crystallization-driven self-assembly of polylactide block copolymers. *Chem. Sci.* **2017**, *8*, 4223-4230.
47. Zhu, W.; Peng, B.; Wang, J.; Zhang, K.; Liu, L.; Chen, Y. Bamboo leaf-like micro-nano sheets self-assembled by block copolymers as wafers for cells. *Macromol. Biosci.* **2014**, *14*, 1764-70.
48. Gratton, S. E.; Ropp, P. A.; Pohlhaus, P. D.; Luft, J. C.; Madden, V. J.; Napier, M. E.; DeSimone, J. M. The effect of particle design on cellular internalization pathways. *Proc. Natl. Acad. Sci. U. S. A.* **2008**, *105*, 11613-8.
49. Nazemi, A.; Boott, C. E.; Lunn, D. J.; Gwyther, J.; Hayward, D. W.; Richardson, R. M.; Winnik, M. A.; Manners, I. Monodisperse Cylindrical Micelles and Block Comicelles of Controlled Length in Aqueous Media. *J. Am. Chem. Soc.* **2016**, *138*, 4484-93.

50. Yao, K.; Chen, Y.; Zhang, J.; Bunyard, C.; Tang, C. Cationic salt-responsive bottle-brush polymers. *Macromol. Rapid Commun.* **2013**, *34*, 645-51.

CHAPTER 3

PREPARATION OF [3]- AND [4]-ANSA-COBALTOCENIUM
HEXAFLUOROPHOSPHATE AND THEIR APPLICATION IN RING-
OPENING METATHESIS POLYMERIZATION FOR MAIN-CHAIN
COBALTOCENIUM-CONTAINING POLYMERS

3.1 Abstract

We report the synthesis of diallyl cobaltocenium and *ansa*-cobaltocenium hexafluorophosphate. The diallyl cobaltocenium shows an isomerization behavior. Isomerization of the terminal alkene induces the formation of internal alkene, which is a more thermodynamically stable structure. Ring-closing metathesis (RCM) of isomers results in two cyclic cobaltocenium monomers with different ring sizes guided by the ring strain energy: [3]- and [4]-*ansa*-cobaltocenium. These *ansa*-cobaltocenium monomers are successfully subject to ring-opening metathesis polymerization (ROMP), leading to main-chain polymers with controlled molecular weight.

3.2 Introduction

Metallopolymers, polymers containing organometallic moieties at the side chain or main-chain, have attracted intensive interests owing to their various applications in electronics, catalyst, nanomaterial, biomedicine, and sensor.¹⁻⁷

Metallopolymers can be categorized based on topologies: linear, cyclic, hyperbranched, and dendritic.⁸⁻¹² Among the structures of metallopolymers, polymers with metallocene at the side-chain have been widely studied due to accessible and scalable preparation.^{13, 14} Likewise, main-chain metallocene-containing polymers also have attracted considerable attention due to selective stimuli-responsiveness,¹⁵⁻¹⁷ construction of conjugation structure.¹⁸⁻²⁰

Earlier the incorporation of organometallic moieties into polymer backbone have been achieved via polycondensation of difunctional metallocenes by step-growth approach. However, several limitations, such as highly pure monomer, exact stoichiometry, high

reaction temperature, and unexpected side reactions, made it difficult to get high molecular weight.²¹ Alternatively, the discovery of ring-opening polymerization of strained metallocenophanes has opened up a methodology to prepare high molecular weight of main-chain metallocene polymers.²² More recently, Manners and coworkers have intensively investigated the preparation of main-chain ferrocene-containing polymers by ring opening polymerization (ROP).^{7, 23-25} Polymerization of strained metallocenophane enables to get the higher molecular weight of polymers. Many other strategies have been utilized to make main-chain metallocopolymers.²⁶

Strained metallocenophane has been gained great attentions their useful structures for the preparation of high molecular weight of main-chain metallocene polymers. Mostly, ferrocene is the center of investigation. Their stimulus-responsive and crystalline characteristics have been utilized in several applications.²⁷⁻³⁰ However, cationic metallocene has scarcely developed in main-chain metallocene polymers.³¹⁻³³ Cobaltocenium, isoelectronic to 18-e ferrocene, has some of unique properties. In contrast to neutral ferrocene, cobaltocenium has a positive charge by oxidation of 19-e cobaltocene. The air-stable and water-soluble cobaltocenium provides new possibilities for applications. As a class of cationic polyelectrolytes, cobaltocenium-containing polymers show potential in energy storage, self-assembly, and antimicrobial applications.³⁴⁻³⁸ For the cobaltocenium-containing polymers, side-chain cobaltocenium polymers have been intensively investigated due to the accessible synthetic method and polymerization techniques. However, main-chain cobaltocenium-containing polymers are rarely reported because of the synthetic challenges in the monomer synthesis and polymerization. The first main-chain cobaltocenium containing polymers were prepared by Ito and Kenjo in 1968 as

an ion-exchanger.³⁹ Sheats et al. reported the main-chain cobaltocenium polymers by condensation polymerization and transesterification.^{40, 41} However, the resulting polymers by the aforementioned methods actually revealed to be oligomers with very low degree of polymerization (DP = 3-6). Manners and coworkers also reported the main-chain cobaltocenium polymers prepared by ring-opening polymerization of ansa-cobaltocenophane followed by oxidation of polymers.³¹ They showed the formation of a higher molecular weight of cationic polyelectrolytes ($M_w = \sim 55,000$ g/mol).

Recently, ring-opening metathesis polymerization has risen as an attractive method to prepare main-chain metallocopolymers. Although, ferrocene and ruthenocene have been achieved with the main-chain topology by ROMP,⁴²⁻⁴⁴ main-chain cobaltocenium-containing polymers by ROMP have not been reported. In the case of 18-e cobaltocenium, the cationic charge of the molecule makes it difficult to be utilized in ROP. ROMP has good monomer and solvent tolerance and control over the polymerization. Therefore, the synthesis of cyclic cobaltocenium monomer can be an alternative method for the preparation of main-chain cobaltocenium-containing polymers by ROMP.

Herein we report the synthesis of cyclic cobaltocenium monomers via ring-closing metathesis (RCM) from allyl-substituted cobaltocenium. Interestingly, the diallyl cobaltocenium showed a thermal isomerization behavior. RCM of the isomers resulted in two different cyclized cobaltocenium monomers: [3]-*ansa* cobaltocenium and [4]-*ansa* cobaltocenium hexafluorophosphate. Furthermore, the cyclic cobaltocenium olefins were successfully copolymerized with cyclooctene derivatives through ROMP using Grubbs III catalyst.

3.3 Experimental

Materials

Dicyclopentadiene, allyl bromide, lithium diisopropyl amide (LDA), sodium hexafluorophosphate, ethyl vinyl ether (EVE), sodium hydride (60% dispersion in mineral oil), sodium (sticks stored in mineral oil), Grubbs catalyst 2nd and 3rd generation were purchased from Sigma-Aldrich and used as received without further purification. Cobalt(II) bromide was purchased from Beantown Chemical. Methanol, dichloromethane, tetrahydrofuran, and acetone were purchased from VWR. Chloroform-*d*, acetone-*d*₆, dimethyl sulfoxide (DMSO)-*d*₆ were purchased from Cambridge Isotope Laboratories. 1,2-epoxy-5-cyclooctene, 5-hydroxy-1-cyclooctene and 5-methoxy-1-cyclooctene were synthesized and characterized according to our previous report.

Characterization

¹H NMR (300 MHz) and ¹³C NMR (75 MHz) spectra were recorded on a Bruker Avance III HD 300 spectrometer using Acetone-*d*₆, DMSO-*d*₆, and CDCl₃ as solvents. The chemical shifts are reported with respect to CHCl₃/CDCl₃ ($\delta(^1\text{H}) = 7.26$ ppm, $\delta(^{13}\text{C}) = 77.0$ ppm). EI mass spectra were collected Waters Micromass Q-Tof mass spectrometer, and the ionization source was positive ion electrospray. Gel permeation chromatography (GPC) was performed in tetrahydrofuran (THF) at a flow rate of 1.0 mL/min at 35 °C on a Waters-GPC system equipped with a refractive index (RI) detector, and narrow dispersed PS was employed for molecular weight calibration. UV-Vis spectra were recorded on a Shimadzu UV-2450 spectrophotometer using chloroform as a solvent with a scan range of 200 nm to 600 nm.

Synthesis of allylic cyclopentadiene

Cyclopentadiene was obtained by cracking of dicyclopentadiene at 150°C. The freshly prepared cyclopentadiene (6.99 g, 105.8 mmol) was added into the r.b.f. containing sodium (2.4g, 105 mmol) and 200 mL of dry tetrahydrofuran by dropwise addition. The reaction solution was refluxed at 80°C overnight. Allyl bromide (15.0 g, 111 mmol) was diluted with dry THF and added into the reaction mixture by dropwise addition. The reaction mixture was stirred overnight and quenched by sat. NH_4Cl solution. The solvent was removed by a rotary evaporator. The liquid residue was dissolved in ether and extracted with sat. NaHCO_3 , DI water, and sat. NaCl solution. The organic layer was dried by anhydrous MgSO_4 , and solvent was removed. 9.5 g of dark orange oil was obtained. Further purification was carried out by fractional vacuum distillation (75 mmHg). 3.7 g of golden liquid was obtained as a product with 29% yield. $^1\text{H NMR}$ (300 MHz, CDCl_3): δ = 6.51-5.97 (m, **Cp**, 3H), 5.85 (m, $-\text{CH}=\text{CH}_2$, 1H), 4.97 (m, $-\text{CH}=\text{CH}_2$, 2H), 3.09 (d, $-\text{CH}_2-$, 2H), 2.88 (d, $-\text{CH}_2-$, 2H).

Synthesis of 1,1'-(diallyl) cobaltocenium and 1-(allyl),1'-(1-propene-1-yl) cobaltocenium hexfluorophosphate

The solution of 2.4 g (22.6 mmol) allyl cyclopentadiene was dissolved in 100 mL THF and cooled down to -78 °C. 11.3 mL (22.6 mmol) 2.0M lithium diisopropyl amide solution in hexane and ethylbenzene was added. The reaction mixture was stirred at -78 °C for 2 h. Then 3.36 g (11.3 mmol) CoBr_2 was added. The reaction mixture was warmed to room temperature and stirred overnight. The solvent was removed by rotavap and dissolved in 90 mL of hot water, resulting in a dark brown solution. The aqueous solution was air-bubbled for 4 h to oxidize the neutral cobaltocene to cobaltocenium bromide. Then, the

aqueous solution was boiled with activated charcoal for 30 min. The solution was filtered through celite and washed with water. An orange-colored solution was gathered. The orange color solution was added by 4.30 g (22.6 mmol) NaPF₆ and extracted with DCM for ion-exchange with PF₆⁻. The organic layer was dried with anhydrous MgSO₄. The solvent was removed in vacuo, affording dark red oil (2.80 g, 59 % yield) as a mixture of 1,1'-(diallyl) cobaltocenium and 1-(allyl),1'-(1-propene-1-yl) cobaltocenium hexfluorophosphate. ¹H NMR (300 MHz, acetone-*d*₆): δ = 6.69 (m, -CH=CH-, 0.5H), 6.31 (m, -CH=CH-, 0.5H), 6.06 (m, -CH=CH₂, 2.5H), 5.85-5.64 (m, *Cp*, 12H), 3.36 (d, -CH₂-, 4H), 3.24 (d, -CH₂-, 1H), 1.88 (d, -CH₃, 1.5H). ¹³C NMR (75MHz, acetone-*d*₆): δ = 134.22 (CH=CH₂), 117.59 (CH=CH₂), 106.83, 84.21, 84.01 (*Cp*), 31.45 (CH₂). MS(ESI) m/z calculated for C₁₆H₁₈Co⁺(M⁺) 269.25, found 269.

Synthesis of 1,1'-(diallyl) cobaltocenium, 1-(allyl),1'-(1-propene-1-yl) cobaltocenium, and 1,1'-(di-1-propene-1-yl) cobaltocenium hexfluorophosphate

The synthesis of three isomers was carried out by analogous procedure to the previous one. 1.0 (9.3 mmol) allyl bromide was charged into a round bottom flask filled with 50 mL THF. The solution was cooled down to -78 °C, then 4.6 mL (9.3 mmol) of 2.0 M LDA solution was added in a dropwise manner. The reaction mixture was stirred for 2 h, followed by the addition of 1.02 g (4.6 mmol) CoBr₂. The solution was warmed to room temperature and stirred overnight. Solvent removed in vacuo. The residue was dissolved in water, followed by oxidation for 4 h. The aqueous solution was filtered through celite, then stirred at 50 °C for 1 h. The solution was added by 1.74 g (9.2 mmol) NaPF₆ and extracted with DCM. The organic layer was dried with MgSO₄, dried under vacuum. 0.92 g (48 % yield) dark red oil was obtained in a mixture of three isomers. ¹H NMR (300 MHz, acetone-

d6): δ = 6.71-6.64 (m, $-\text{CH}=\text{CH}-$, 3H), 6.54-6.46 (m, $-\text{CH}=\text{CH}-$, 3H), 6.34-6.26 (m, $-\text{CH}=\text{CH}_2$, 3H), 5.85-5.64 (m, *Cp*, 43H), 3.36 (d, $-\text{CH}_2-$, 4H). 3.24 (d, $-\text{CH}_2-$, 6H), 1.88 (d, $-\text{CH}_3$, 19H). ^{13}C NMR (75MHz, acetone-*d6*): δ = 136.39, 136.16, 134.48, 134.31 ($\text{CH}=\text{CH}_2$), 120.44, 119.69, 117.58, 117.54 ($\text{CH}=\text{CH}_2$), 106.79, 106.16, 103.72, 84.33, 84.26, 84.22, 84.04, 84.01, 81.09, 80.61 (*Cp*), 31.43, 30.79 (CH_2), 16.42, 16.24 (CH_3). MS(ESI) *m/z* calculated for $\text{C}_{16}\text{H}_{18}\text{Co}^+(\text{M}^+)$ 269.25, found 269.

Synthesis of cyclic cobaltocenium monomer olefins

Mixture of 1,1'-(diallyl) cobaltocenium and 1-(allyl),1'-(1-propene-1-yl) cobaltocenium hexafluorophosphate (300mg, 0.7 mmol) was dissolved in anhydrous DCM. Grubbs II catalyst (28 mg, 0.033 mmol) was added, and the resulting solution was refluxed at 50°C for 2 h. Several drops of EVE were added to the solution to quench the reaction. The solvent was removed, and the product was purified by column chromatography using basic aluminum oxide. At first, DCM was used as an eluent to remove the catalyst, and then acetone was used to obtain the product. The organic solution was collected and dried by vacuum. The dark yellowish solid was obtained. The crude product was dissolved in 0.5 mL of acetone and precipitated in ether. 274 mg of yellow solid was obtained in 95% yield. ^1H NMR (300 MHz, acetone-*d6*): δ = 6.42 (m, $-\text{CH}=\text{CH}-$, 0.4H), 6.30 (m, $-\text{CH}=\text{CH}-$, 2H), 6.18 (m, $-\text{CH}=\text{CH}$, 0.4H), 5.85-5.72 (m, *Cp*, 12H), 3.36 (d, $-\text{CH}_2-$, 4H). 3.24 (d, $-\text{CH}_2-$, 0.8H). ^{13}C NMR (75MHz, acetone-*d6*): δ = 130.11 ($\text{CH}=\text{CH}_2$), 115.10 ($\text{CH}=\text{CH}$), 107.50, 85.80, 85.61, 85.29, 84.26, 83.69 (*Cp*), 22.05 (CH_2). MS(ESI) *m/z* calculated for $\text{C}_{14}\text{H}_{14}\text{Co}^+(\text{M}^+)$ 241.04, found 241, and calculated for $\text{C}_{13}\text{H}_{12}\text{Co}^+(\text{M}^+)$ 227.03, found 227.

Synthesis of P1

Cyclic cobaltocenium monomers (33.8 mg, 0.087 mmol) and 1,2-epoxy-5-cyclooctene (173 mg, 1.39 mmol) were dissolved in 1.0 ml DCM (1.5 M) and degassed. Grubbs III catalyst (1.0 mg, 1.4 μ mol) was dissolved in 0.1 mL DCM and added to initiate the polymerization at room temperature. After the reaction was conducted for 3 h, several drops of EVE were added to quench the polymerization. The polymer was precipitated in cold methanol three times and dried under a vacuum. The orange solid was obtained (101 mg, 49 % yield).

Synthesis of P2

Cyclic cobaltocenium monomers (30.0 mg, 0.077 mmol) and 5-hydroxy-1-cyclooctene (209 mg, 1.65 mmol) were dissolved in 1 mL DCM (1.5 M) and degassed. Grubbs III catalyst (1.7 mg, 1.7 μ mol) was added for the initiation. After 3 h, EVE was added to quench the reaction. The polymer was precipitated in cold methanol three times. Yellow solid was obtained (193 mg, 80 % yield).

Synthesis of P3

cobaltocenium monomers (30.0 mg, 0.077 mmol) and 5-methoxy-1-cyclooctene (200 mg, 1.426 mmol) were dissolved in 1 mL DCM (1.5 M) and degassed. Grubbs III catalyst (1.1 mg, 1.5 μ mol) was added for the initiation. After 3 h, EVE was added to quench the reaction. The polymer was precipitated in cold methanol three times. Yellow solid was obtained (164 mg, 71% yield).

DFT calculation for the ring strain

Molecular geometry optimization of substituted cobaltocenium and their ring-closed derivatives was carried out by using Q-chem 4.3.⁴⁵ B97-D functional was employed to describe the structures of cobaltocenium. The def2-svp basis sets for C, H, F, and P atoms and the more extensive def2-tzvp basis set for Co.⁴⁶ The calculation was carried out in the gas state. The simulation takes advantage of the energy difference between reactants and products (**Figure 3.1**). The optimized energy of each molecule was used to calculate the ΔE using the equation below.

$$\Delta E = (E_{cyclic} + E_{gas}) - E_{open}$$

The E_{cyclic} indicates the optimized energy of cyclic cobaltocenium; E_{gas} indicates the optimized energy of ethylene; E_{open} indicates the optimized energy of di-olefin cobaltocenium.

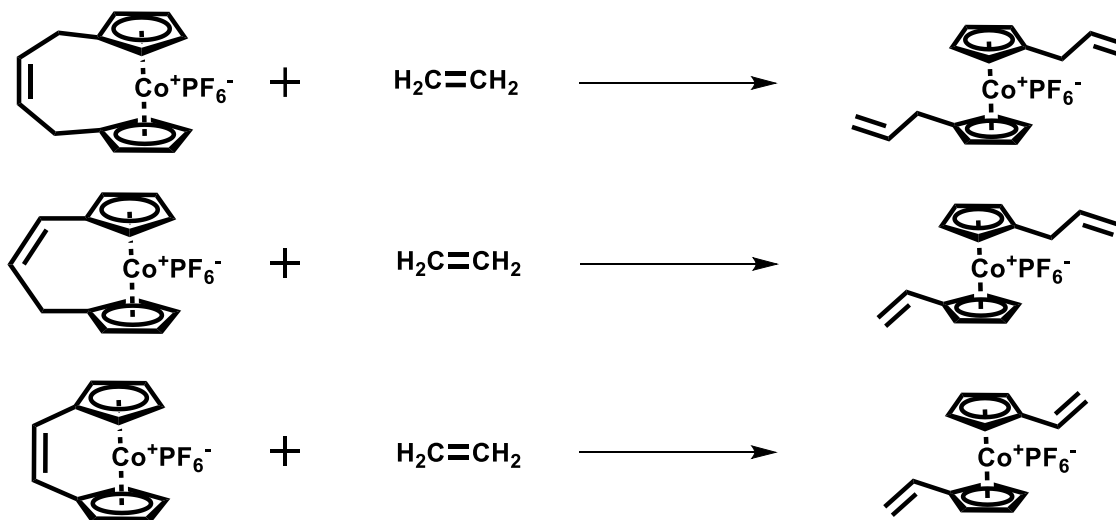


Figure 3.1. The reaction of cyclic cobaltoceniums with gas molecules.

3.4 Results and Discussion

Several literatures have reported the synthesis of cyclic cobaltocene or cobaltocenium salt.⁴⁷⁻⁵² However, further polymerization of cyclic cobaltocene or cobaltocenium salt has been rarely studied.^{31, 32} For ROMP, unsaturated carbon-bridge is an important functional linkage for the design of cyclic metallocene monomers. For example, 1,1'-(1,3-butadienylene)ferrocene was successfully polymerized via ROMP.⁴⁴ In order to introduce an unsaturated bridge onto cobaltocenium, the substitution of cobaltocenium is a key hurdle to overcome. Synthesis of substituted cobaltocenium can be performed mainly in three ways: “flytrap” reaction between the bridged dicyclopentadienide and cobalto(II) dihalide,⁴⁹ direct substitution of cobaltocenium,⁵³ and modification of cyclopentadiene (Cp). Modification of Cp has advantages over the former methods: better scalability, and better reaction selectivity. Therefore, we started the modification of Cp with functional olefin group, then synthesized disubstituted cobaltocenium. Our group previously reported the synthetic methods for the multi-substituted cobaltocenium from substituted Cp derivatives.³⁴ Building on prior research, we introduced allyl group onto Cp by nucleophilic addition. The allyl cyclopentadiene was treated with lithium diisopropylamide (LDA) to make allylcyclopentadienyl ligand followed by addition of CoBr₂, oxidation, and ion-exchange with hexafluorophosphate, resulting in 1,1'-diallyl cobaltocenium hexafluorophosphate (**Figure 3.2**). The diallyl substituted cobaltocenium is an effective precursor for the preparation of 1,1'-bridged cobaltocenium by RCM. Hayashi and coworkers reported the synthesis of bridged metallocenes, which contains Fe(II), Ru(II), Zr(IV), and Hf(IV) as metal centers. 1,1'-diallylmetallocenes were used to prepare the cyclized metallocene by RCM.⁵⁴

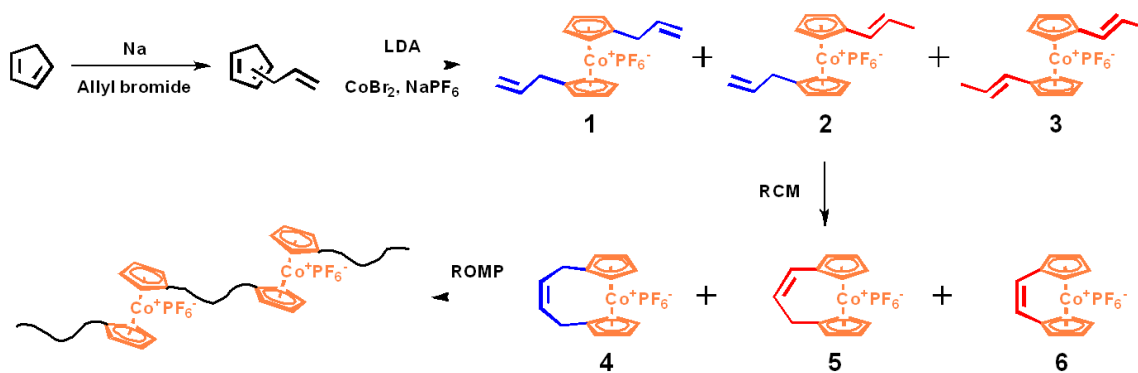


Figure 3.2. Synthesis of diallyl cobaltocenium hexafluorophosphate, cyclic cobaltocenium monomer via RCM, and main-chain cobaltocenium-containing polymers via ROMP.

Initially, it was surprising to observe that the reaction between allyl Cp and CoBr₂ afforded two inseparable isomers: 1,1'-diallyl cobaltocenium **1** and 1-allyl-1'-(1-propenyl) cobaltocenium **2** with a ratio of 6.4:3.6 based on ¹H NMR (**Figure 3.3**). The mass analysis showed that only one corresponding mass value, 269 for C₁₆H₁₈Co⁺, was observed. The ratio was calculated based on the integration of 3.25 and 3.37, which correspond to -CH₂- of allyl moiety of each isomer, respectively. It is noted that ~ 1.8 ppm is assigned to a terminal -CH₃ of the isomerized allyl group in cobaltocenium. The isomers were further characterized by 2D COSY ¹H NMR (**Figure 1B**). We ascribed this isomerization to the heat during the work-up step of the reaction. After reaction between allyl Cp and CoBr₂, reaction residue was dissolved in hot water and followed by oxidation. The isomerization of terminal alkenes to internal alkenes is thermodynamically favorable. Applied heat would facilitate the formation of a more stable internal alkene.

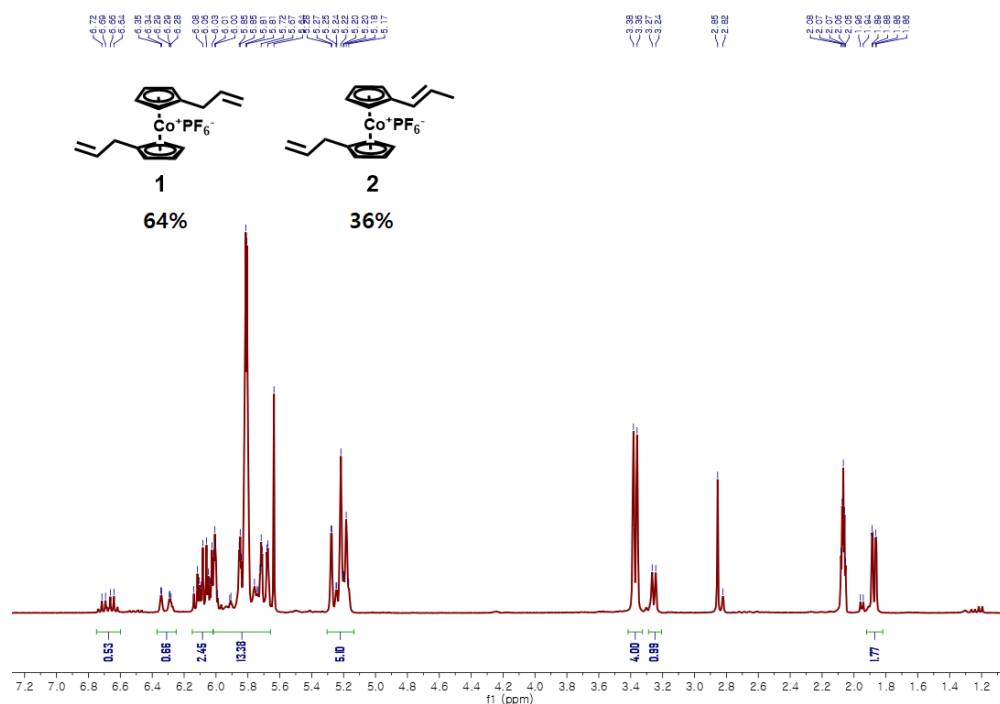


Figure 3.3. ^1H -NMR spectrum of mixture (6.4:3.6 ratio) of 1,1'-diallyl cobaltocenium **1** and 1-allyl-1'-(1-propen-1-yl) cobaltocenium hexafluorophosphate **2**.

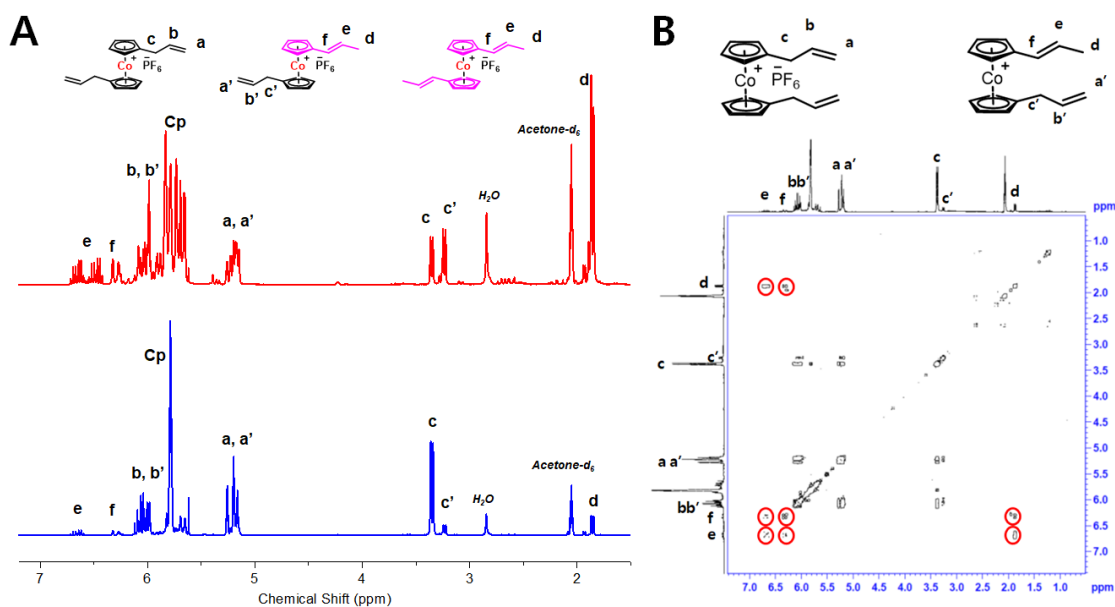


Figure 3.4. (A) ^1H NMR spectra of mixtures of compound **1** and **2** with 8.0:2.0 ratio (bottom blue) and the mixture of compound **1**, **2**, and **3** with 1.7:5.0:3.3 ratio (top red); (B) 2D COSY ^1H NMR of compound **1** and **2** with 8.0:2.0 ratio

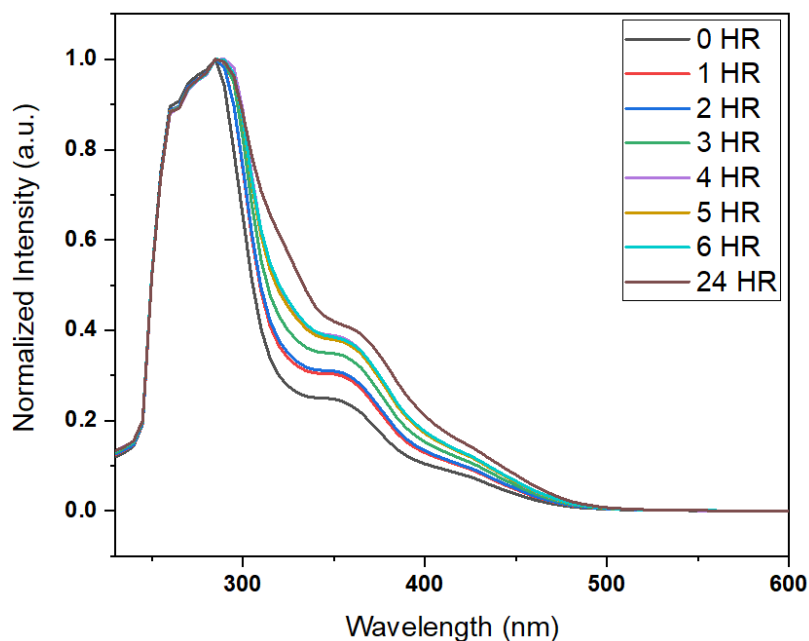


Figure 3.5. UV-vis absorption spectra of the isomerized cobaltocenium.

As the isomerization of terminal alkenes to internal alkenes can be assisted by heat,⁵⁵ we tested the effect of the temperature for the aqueous solution, which contains 1,1'-diallyl cobaltocenium bromide, from room temperature to 4 °C and 50 °C. When stirred at 4 °C, the isomerization was slightly suppressed, showing a decreased portion of internal alkene (**Figure 3.4A**). The isomer ratio was changed from 6.4:3.6 to 8.0:2.0. We attributed this result to the effect of conjugation, which can more stabilize the internal alkene. The resulting internal alkene can form π -conjugation with Cp, which can more stabilize the internal alkene. On the other hand, the increase of temperature to 50 °C afforded three isomers: 1,1'-diallyl cobaltocenium **1**; 1-allyl-1'-(1-propenyl) cobaltocenium **2**; 1,1'-(di(1-propenyl)) cobaltocenium **3** (**Figure 3.4A**). The isomer ratio was changed to 1.7:5.0:3.3, which correspond to compounds **1**, **2**, and **3**, respectively. When heating from 4 °C to 50 °C, the portion of more thermodynamically stable isomers increased from 20% to 70%.

Moreover, allyl moieties were both isomerized. By using UV spectroscopy, we confirmed that heating resulted in the formation of more internal double bonds, which induced the increase of absorption intensity at 360 nm (**Figure 3.5**). We assigned this absorption at a higher wavelength is due to the increased conjugation of π -bond.

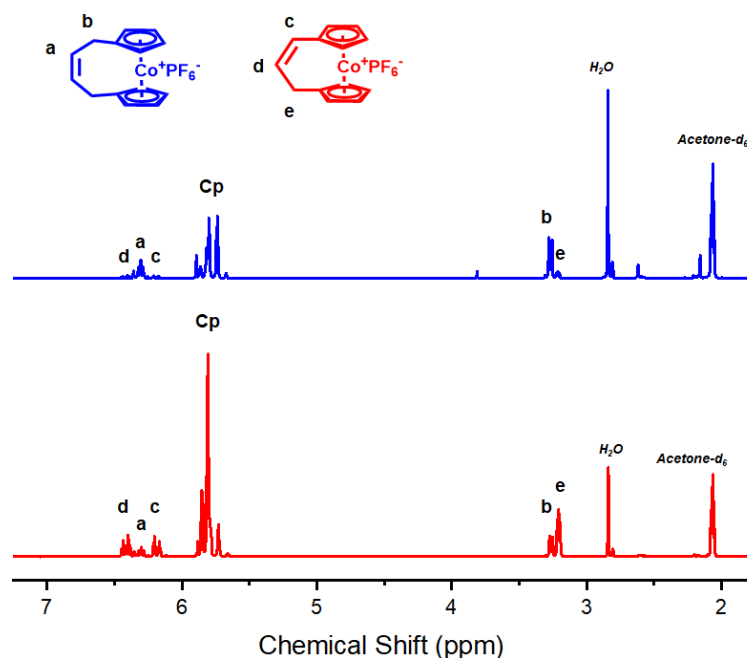


Figure 3.6. ¹H NMR spectra of mixtures of compounds **4** and **5** with 7.0:3.0 ratio (top blue) and 2.2:7.8 ratio (bottom red).

We expected that cyclic cobaltocenium olefins could be utilized as a potential building block for ROMP.^{28, 42, 44} The isomerization was further verified by RCM of the di-substituted cobaltocenium compounds with ruthenium catalyst. We hypothesized that all isomers would undergo RCM, which could form cyclic cobaltocenium monomers with different ring sizes. First, the mixture of compounds **1** and **2** (8.0: 2.0) was subjected to RCM. It was found that the resulting cyclic cobaltocenium olefins have two different *ansa*-cobaltocenium hexafluorophosphate: 1,1'-(2-buten-1,4-diyl) cobaltocenium **4**, 1,1'-(1-propen-1,3-diyl) cobaltocenium **5**. Prior to RCM, the mass analysis did not show the

difference between both isomers. However, post-RCM products showed two different molecular mass, 241 and 227, which correspond to cyclic monomers **4** and **5**. ^1H NMR revealed that the resulting cyclized cobaltocenium has a 7.0:3.0 ratio, originated from the 8:2 ratio of **1** and **2**. The increased portion of compound **5** might be attributed to the conjugation of double bond of compound **5** that can stabilize the system. Next, the cobaltocenium isomers which contains compound **1**, **2**, and **3** with the ratio of 1.7:5.0:3.3 were reacted with Grubbs II catalyst for the preparation of three different cyclic cobaltocenium. All isomers were expected to form different ring-size of cyclic monomers. Interestingly, the result showed that only **4** and **5** were obtained, but not **6** (**Figure 2**). We ascribed that this result may be due to the higher ring strain of hypothetical **6**. The smaller ring size induces a highly tilted structure of cobaltocenium, leading to high ring strain, which was ascribed to the successful synthesis of monomer **6**.

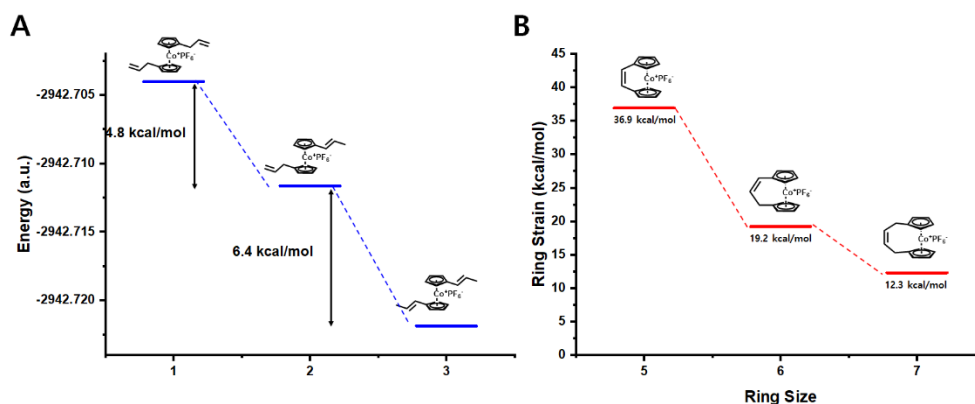


Figure 3.7. (A) Optimized energy of **1**, **2**, and **3**; (B) Ring strain energy of **4**, **5**, and **6**.

We further carried out atomistic computation to compare the ring strain of three cyclic cobaltocenium monomers. The ring strain can be assessed by calculating their ring-opening energy (negative value of ring strain) using the density functional theory (DFT).⁵⁶ In comparison, the ring strain of cyclic ferrocene olefin was also evaluated using a similar

method.⁴² As shown Figure 3A, compound **3** has the lowest energy, 11.2 kcal/mol lower than **1**. The ring strain of cyclic monomers was calculated based the reaction between cyclic cobaltocenium olefins and an ethylene molecule, producing corresponding ring-opened structures (Scheme S1). It was shown that the ring strain of monomer **6** is three times higher than that of **4** (Figure 3B). The ring strains of seven-membered (**4**) and six-membered (**5**) cyclic cobaltocenium are comparable. It should be noted that this estimation is semi-quantitative.

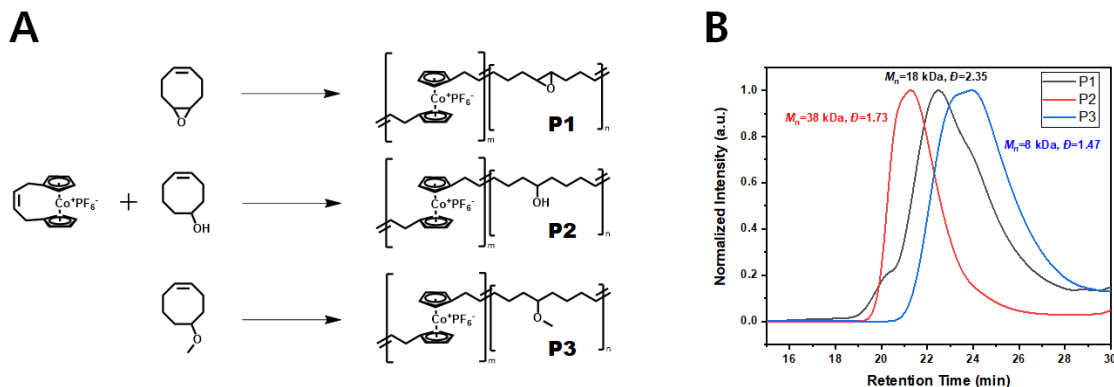


Figure 3.8. (A) Synthesis of ROMP for main-chain cobaltocenium-containing polymers; (B) GPC trace of copolymers.

Cyclic olefins of ferrocene and ruthenocene have been reported as precursors for preparing polymers.^{28, 42, 57-59} The synthesis of main-chain cobaltocenium-containing polymers via ROMP has not reported. We first performed the synthesis of main-chain cobaltocenium-containing homopolymers by ROMP using cyclic cobaltocenium monomers. However, homopolymerization of cyclic cobaltocenium olefin monomers was unsuccessful. This result might be attributed to the less reactivity of cyclic cobaltocenium or the poor solubility of resulting polymers in the polymerization medium. As studied earlier,^{17, 20} some modification of cyclic cobaltocenium monomer might be helpful to improve the solubility of resulting polymers and obtain high molecular weight. We next

tested copolymerization with cyclooctene derivatives, which have been used to prepare other main-chain metallopolymer via ROMP.^{29, 43} Cyclooctene derivatives have comparable ring strain to that of compound **4** and are versatile to further functionalization.⁶⁰ The copolymerization was carried out between 1,2-epoxy-5-cyclooctene, 5-hydroxy-1-cyclooctene, and 5-methoxy-1-cyclooctene by ROMP with ratio of [monomer]:[cat.] = 1000:1 (**Figure 4A**). It revealed that cyclic cobaltocenium monomers were successfully incorporated in the main-chain polymers. The incorporation of cobaltocenium into the polymer backbone was confirmed by ¹H NMR and ¹⁹F NMR (**Figure 5**). The labeling ratio, actually inserted portion, was calculated by comparison of the characteristic cobaltocenium peaks (Cp= 5.4~5.7 ppm, -CH₂- = 3.2 ppm) and other characteristic peaks from cyclooctene derivatives. The results are summarized in **Table 1**. Molecular weight was determined by gel permeation chromatography (GPC) with THF as an eluent (**Figure 4B**). As shown in **Table 1**, the molecular weight (*M_n*) of **P3** was relatively lower than **P1** and **P2**. Due to the electrostatic binding between the cobaltocenium moieties and GPC column, it is hard to calibrate the peak signal from more cobaltocenium labeled polymer **P3**. The incorporation of cobaltocenium in the main chain shows different efficiency. In the case of 1,2-epoxy-5-cyclooctene and 5-hydroxy-1-cyclooctene, the labeling ratio was lower than 5-methoxy-1-cyclooctene.

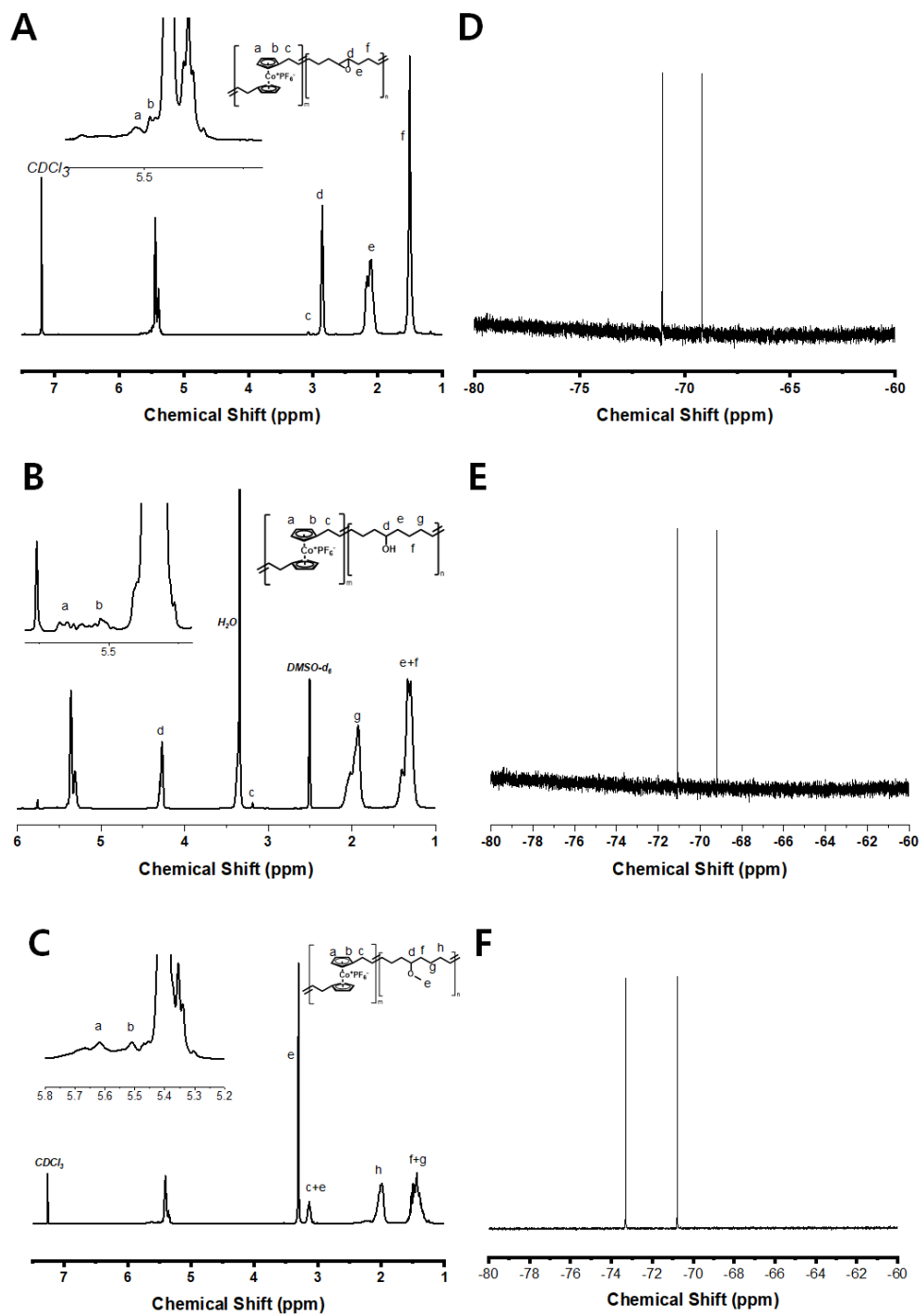


Figure 3.9. ^1H NMR spectra of (A) P1, (B) P2, and (C) P3; ^{19}F NMR spectra of (D) P1, (E) P2, and (F) P3.

Table 1. Results of ROMP for main-chain cobaltocenium-containing polymers.

Polymers	Feed ratio	Labeling ratio	M_n	\bar{D}
P1	5.9%	1.9%	17,600	2.35
P2	4.4%	1.3%	38,300	1.73
P3	5.9%	5.2%	8,700	1.47

3.5 Conclusion

In summary, we successfully synthesized 1,1'-dially cobaltocenium. The diallyl cobaltocenium showed isomerization behavior, affording three isomers. The isomerization was sensitive to temperature. RCM of these isomers afforded cyclic cobaltocenium with two different ring sizes. dictated by the ring strain energy. ROMP was utilized for making main-chain cobaltocenium-containing copolymers from cyclic cobaltocenium and cyclooctene derivatives.

3.6 References

1. Kumar, A.; Bawa, S.; Ganorkar, K.; Ghosh, S. K.; Bandyopadhyay, A. Syntheses, characterization, multi-acid fluorescence sensing and electroluminescence properties of Cr(ii)-based metallopolymer. *Polym. Chem.* **2020**, *11*, 6579-6590.
2. Wang, Y.; Astruc, D.; Abd-El-Aziz, A. S. Metallopolymer for advanced sustainable applications. *Chem. Soc. Rev.* **2019**, *48*, 558-636.
3. Yan, Y.; Zhang, J.; Wilbon, P.; Qiao, Y.; Tang, C. Ring-Opening Metathesis Polymerization of 18-e Cobalt(I)-Containing Norbornene and Application as

Heterogeneous Macromolecular Catalyst in Atom Transfer Radical Polymerization. *Macromol. Rapid Commun.* **2014**, *35*, 1840-1845.

4. Katz, T. J.; Sudhakar, A.; Teasley, M. F.; Gilbert, A. M.; Geiger, W. E.; Robben, M. P.; Wuensch, M.; Ward, M. D. Synthesis and properties of optically active helical metallocene oligomers. *J. Am. Chem. Soc.* **1993**, *115*, 3182-3198.
5. Karayilan, M.; Brezinski, W. P.; Clary, K. E.; Lichtenberger, D. L.; Glass, R. S.; Pyun, J. Catalytic Metallopolymers from [2Fe-2S] Clusters: Artificial Metalloenzymes for Hydrogen Production. *Angew. Chem. Int. Ed.* **2019**, *58*, 7537-7550.
6. Whittell, G. R.; Hager, M. D.; Schubert, U. S.; Manners, I. Functional soft materials from metallopolymers and metallosupramolecular polymers. *Nat. Mater.* **2011**, *10*, 176-188.
7. Manners, I. Polyferrocenylsilanes: metallopolymers for electronic and photonic applications. *J. Opt. A: Pure Appl. Opt.* **2002**, *4*, S221-S223.
8. Alkan, A.; Wurm, F. R. Water-Soluble Metallocene-Containing Polymers. *Macromol. Rapid Commun.* **2016**, *37*, 1482-1493.
9. Abd-El-Aziz, A. S.; Bernardin, S. Synthesis and reactivity of arenes coordinated to cyclopentadienyliron cations. *Coordin. Chem. Rev.* **2000**, *203*, 219-267.
10. Yan, Y.; Pageni, P.; Kabir, M. P.; Tang, C. Metallocenium Chemistry and Its Emerging Impact on Synthetic Macromolecular Chemistry. *Synlett* **2016**, *27*, 984-1005.
11. Astruc, D.; Ornelas, C.; Ruiz, J. Metallocenyl Dendrimers and Their Applications in Molecular Electronics, Sensing, and Catalysis. *Accounts. Chem. Res.* **2008**, *41*, 841-856.
12. Herbert, D. E.; Gilroy, J. B.; Chan, W. Y.; Chabanne, L.; Staubitz, A.; Lough, A. J.; Manners, I. Redox-Active Metallomacrocycles and Cyclic Metallopolymers: Photocontrolled Ring-Opening Oligomerization and Polymerization of Silicon-Bridged [1]Ferrocenophanes Using Substitutionally-Labile Lewis Bases as Initiators. *J. Am. Chem. Soc.* **2009**, *131*, 14958-14968.

13. Hardy, C. G.; Ren, L.; Zhang, J.; Tang, C. Side-Chain Metallocene-Containing Polymers by Living and Controlled Polymerizations. *Israel J. Chem.* **2012**, *52*, 230-245.
14. Gu, H.; Ciganda, R.; Gatard, S.; Lu, F.; Zhao, P.; Ruiz, J.; Astruc, D. On metallocene-containing macromolecules and their applications. *J. Organomet. Chem.* **2016**, *813*, 95-102.
15. Shultz, G. V.; Berryman, O. B.; Zakharov, L. N.; Tyler, D. R. Preparation of photodegradable oligomers containing metal–metal bonds using ADMET. *J. Inorg. Organomet. Polym. Mater.* **2008**, *18*, 149-154.
16. Tyler, D. R. Photochemically degradable polymers containing metal–metal bonds along their backbones. *Coordin. Chem. Rev.* **2003**, *246*, 291-303.
17. Masson, G.; Lough, A. J.; Manners, I. Soluble poly (ferrocenylenevinylene) with t-butyl substituents on the cyclopentadienyl ligands via ring-opening metathesis polymerization. *Macromolecules* **2008**, *41*, 539-547.
18. Southard, G. E.; Curtis, M. D. Poly (3, 3 '-dihexyl-4, 4 '-dimethyl-1, 1 '-ferrocenylene-1, 4-phenylene) and Poly (3, 3 '-dihexyl-4, 4 '-dimethyl-1, 1 '-ferrocenylene-2, 5-thienylene). *Organometallics* **1997**, *16*, 5618-5620.
19. Gao, X.; Deng, L.; Hu, J.; Zhang, H. Ferrocene-containing conjugated oligomers synthesized by acyclic diene metathesis polymerization. *Polymers* **2019**, *11*, 1334.
20. Heo, R. W.; Somoza, F. B.; Lee, T. R. Soluble conjugated polymers that contain ferrocenylene units in the backbone. *J. Am. Chem. Soc.* **1998**, *120*, 1621-1622.
21. Nguyen, P.; Gómez-Elipé, P.; Manners, I. Organometallic polymers with transition metals in the main chain. *Chem. Rev.* **1999**, *99*, 1515-1548.
22. Brandt, P. F.; Rauchfuss, T. B. Polyferrocenylene persulfides. *J. Am. Chem. Soc.* **1992**, *114*, 1926-1927.

23. Herbert, D. E.; Mayer, U. F.; Manners, I. Strained Metallocenophanes and Related Organometallic Rings Containing π -Hydrocarbon Ligands and Transition-Metal Centers. *Angew. Chem. Int. Ed.* **2007**, *46*, 5060-5081.
24. Finckh, W.; Tang, B. Z.; Foucher, D. A.; Zamble, D. B.; Ziembinski, R.; Lough, A.; Manners, I. The polymerization behavior of [1]- and [2] ferrocenophanes containing silicon atoms in the bridge: comparison of the molecular structure of the strained, polymerizable cyclic ferrocenylsilane $\text{Fe}(\eta^5\text{-C}_5\text{H}_4)_2(\text{SiMe}_2)$ with that of the cyclic ferrocenyldisilane $\text{Fe}(\eta^5\text{-C}_5\text{H}_4)_2(\text{SiMe}_2)_2$. *Organometallics* **1993**, *12*, 823-829.
25. Zechel, D. L.; Hultsch, K. C.; Rulkens, R.; Balaishis, D.; Ni, Y.; Pudelski, J. K.; Lough, A. J.; Manners, I.; Foucher, D. A. Thermal and Transition-Metal-Catalyzed Ring-Opening Polymerization (ROP) of [1]Silaferrocenophanes with Chlorine Substituents at Silicon: A Route to Tunable Poly(ferrocenylsilanes). *Organometallics* **1996**, *15*, 1972-1978.
26. Williams, K. A.; Boydston, A. J.; Bielawski, C. W. Main-chain organometallic polymers: synthetic strategies, applications, and perspectives. *Chem. Soc. Rev.* **2007**, *36*, 729-744.
27. Di Giannantonio, M.; Ayer, M. A.; Verde-Sesto, E.; Lattuada, M.; Weder, C.; Fromm, K. M. Triggered metal ion release and oxidation: ferrocene as a mechanophore in polymers. *Angew. Chem. Int. Ed.* **2018**, *57*, 11445-11450.
28. Sha, Y.; Rahman, M. A.; Zhu, T.; Cha, Y.; McAlister, C. W.; Tang, C. ROMPI-CDSA: ring-opening metathesis polymerization-induced crystallization-driven self-assembly of metallo-block copolymers. *Chem. Sci.* **2019**, *10*, 9782-9787.
29. Sha, Y.; Zhang, Y.; Xu, E.; Wang, Z.; Zhu, T.; Craig, S. L.; Tang, C. Quantitative and Mechanistic Mechanochemistry in Ferrocene Dissociation. *ACS Macro Lett.* **2018**, *7*, 1174-1179.
30. Hsiao, M.-S.; Yusoff, S. F. M.; Winnik, M. A.; Manners, I. Crystallization-driven self-assembly of block copolymers with a short crystallizable core-forming segment:

controlling micelle morphology through the influence of molar mass and solvent selectivity. *Macromolecules* **2014**, *47*, 2361-2372.

31. Mayer, U. F. J.; Gilroy, J. B.; O'Hare, D.; Manners, I. Ring-Opening Polymerization of 19-Electron [2]Cobaltocenophanes: A Route to High-Molecular-Weight, Water-Soluble Polycobaltocenium Polyelectrolytes. *J. Am. Chem. Soc.* **2009**, *131*, 10382-10383.
32. Musgrave, R. A.; Choi, P.; Harniman, R. L.; Richardson, R. M.; Shen, C.; Whittell, G. R.; Crassous, J.; Qiu, H.; Manners, I. Chiral Transmission to Cationic Polycobaltocenes over Multiple Length Scales Using Anionic Surfactants. *J. Am. Chem. Soc.* **2018**, *140*, 7222-7231.
33. Qiu, H.; Gilroy, J. B.; Manners, I. DNA-induced chirality in water-soluble poly(cobaltoceniumethylene). *Chem. Commun.* **2013**, *49*, 42-44.
34. Zhu, T.; Xu, S.; Rahman, A.; Dogdibegovic, E.; Yang, P.; Pageni, P.; Kabir, M. P.; Zhou, X.-d.; Tang, C. Cationic Metallo-Polyelectrolytes for Robust Alkaline Anion-Exchange Membranes. *Angew. Chem. Int. Ed.* **2018**, *57*, 2388-2392.
35. Zhang, J.; Chen, Y. P.; Miller, K. P.; Ganewatta, M. S.; Bam, M.; Yan, Y.; Nagarkatti, M.; Decho, A. W.; Tang, C. Antimicrobial Metallopolymers and Their Bioconjugates with Conventional Antibiotics against Multidrug-Resistant Bacteria. *J. Am. Chem. Soc.* **2014**, *136*, 4873-4876.
36. Zhu, T.; Sha, Y.; Yan, J.; Pageni, P.; Rahman, M. A.; Yan, Y.; Tang, C. Metallo-polyelectrolytes as a class of ionic macromolecules for functional materials. *Nat. Commun.* **2018**, *9*, 4329.
37. Noor, F.; Wüstholtz, A.; Kinscherf, R.; Metzler-Nolte, N. A Cobaltocenium–Peptide Bioconjugate Shows Enhanced Cellular Uptake and Directed Nuclear Delivery. *Angew. Chem. Int. Ed.* **2005**, *44*, 2429-2432.

38. Cha, Y.; Jarrett-Wilkins, C.; Rahman, M. A.; Zhu, T.; Sha, Y.; Manners, I.; Tang, C. Crystallization-Driven Self-Assembly of Metallo-Polyelectrolyte Block Copolymers with a Polycaprolactone Core-Forming Segment. *ACS Macro Lett.* **2019**, *8*, 835-840.
39. Takuji, I.; Tadao, K. A New Anion Exchanger Containing Cobalticinium Cation. *B. Chem. Soc. Jpn.* **1968**, *41*, 614-619.
40. Pittman Jr., C. U.; Ayers, O. E.; Suryanarayanan, B.; McManus, S. P.; Sheats, J. E. Organometallic polymers, 28 Condensation polymerization of cobalticinium salts. *Makromol. Chem.* **1974**, *175*, 1427-1437.
41. Carraher Jr., C. E.; Peterson, G. F.; Sheats, J. E.; Kirsch, T. Production of organometallic polymers by interfacial technique, 33.. Synthesis of oligomeric cobalticinium containing dialkylstannanediyl polyesters. *Makromol. Chem.* **1974**, *175*, 3089-3096.
42. Sha, Y.; Zhang, Y.; Zhu, T.; Tan, S.; Cha, Y.; Craig, S. L.; Tang, C. Ring-Closing Metathesis and Ring-Opening Metathesis Polymerization toward Main-Chain Ferrocene-Containing Polymers. *Macromolecules* **2018**, *51*, 9131-9139.
43. Sha, Y.; Zhang, Y.; Xu, E.; McAlister, C. W.; Zhu, T.; Craig, Stephen L.; Tang, C. Generalizing metallocene mechanochemistry to ruthenocene mechanophores. *Chem. Sci.* **2019**, *10*, 4959-4965.
44. Stanton, C. E.; Lee, T. R.; Grubbs, R. H.; Lewis, N. S.; Pudelski, J. K.; Callstrom, M. R.; Erickson, M. S.; McLaughlin, M. L. Routes to Conjugated Polymers with Ferrocenes in Their Backbones: Synthesis and Characterization of Poly(ferrocenylenedivinylene) and Poly(ferrocenylenebutenylene). *Macromolecules* **1995**, *28*, 8713-8721.
45. Shao, Y.; Gan, Z.; Epifanovsky, E.; Gilbert, A. T. B.; Wormit, M.; Kussmann, J.; Lange, A. W.; Behn, A.; Deng, J.; Feng, X.; Ghosh, D.; Goldey, M.; Horn, P. R.; Jacobson, L. D.; Kaliman, I.; Khaliullin, R. Z.; Kuś, T.; Landau, A.; Liu, J.; Proynov, E. I.; Rhee, Y. M.; Richard, R. M.; Rohrdanz, M. A.; Steele, R. P.; Sundstrom, E. J.; Woodcock, H. L.; Zimmerman, P. M.; Zuev, D.; Albrecht, B.; Alguire, E.; Austin, B.;

Beran, G. J. O.; Bernard, Y. A.; Berquist, E.; Brandhorst, K.; Bravaya, K. B.; Brown, S. T.; Casanova, D.; Chang, C.-M.; Chen, Y.; Chien, S. H.; Closser, K. D.; Crittenden, D. L.; Diedenhofen, M.; DiStasio, R. A.; Do, H.; Dutoi, A. D.; Edgar, R. G.; Fatehi, S.; Fusti-Molnar, L.; Ghysels, A.; Golubeva-Zadorozhnaya, A.; Gomes, J.; Hanson-Heine, M. W. D.; Harbach, P. H. P.; Hauser, A. W.; Hohenstein, E. G.; Holden, Z. C.; Jagau, T.-C.; Ji, H.; Kaduk, B.; Khistyayev, K.; Kim, J.; Kim, J.; King, R. A.; Klunzinger, P.; Kosenkov, D.; Kowalczyk, T.; Krauter, C. M.; Lao, K. U.; Laurent, A. D.; Lawler, K. V.; Levchenko, S. V.; Lin, C. Y.; Liu, F.; Livshits, E.; Lochan, R. C.; Luenser, A.; Manohar, P.; Manzer, S. F.; Mao, S.-P.; Mardirossian, N.; Marenich, A. V.; Maurer, S. A.; Mayhall, N. J.; Neuscamman, E.; Oana, C. M.; Olivares-Amaya, R.; O'Neill, D. P.; Parkhill, J. A.; Perrine, T. M.; Peverati, R.; Prociuk, A.; Rehn, D. R.; Rosta, E.; Russ, N. J.; Sharada, S. M.; Sharma, S.; Small, D. W.; Sodt, A.; Stein, T.; Stück, D.; Su, Y.-C.; Thom, A. J. W.; Tsuchimochi, T.; Vanovschi, V.; Vogt, L.; Vydrov, O.; Wang, T.; Watson, M. A.; Wenzel, J.; White, A.; Williams, C. F.; Yang, J.; Yeganeh, S.; Yost, S. R.; You, Z.-Q.; Zhang, I. Y.; Zhang, X.; Zhao, Y.; Brooks, B. R.; Chan, G. K. L.; Chipman, D. M.; Cramer, C. J.; Goddard, W. A.; Gordon, M. S.; Hehre, W. J.; Klamt, A.; Schaefer, H. F.; Schmidt, M. W.; Sherrill, C. D.; Truhlar, D. G.; Warshel, A.; Xu, X.; Aspuru-Guzik, A.; Baer, R.; Bell, A. T.; Besley, N. A.; Chai, J.-D.; Dreuw, A.; Dunietz, B. D.; Furlani, T. R.; Gwaltney, S. R.; Hsu, C.-P.; Jung, Y.; Kong, J.; Lambrecht, D. S.; Liang, W.; Ochsenfeld, C.; Rassolov, V. A.; Slipchenko, L. V.; Subotnik, J. E.; Van Voorhis, T.; Herbert, J. M.; Krylov, A. I.; Gill, P. M. W.; Head-Gordon, M. Advances in molecular quantum chemistry contained in the Q-Chem 4 program package. *Mol. Phys.* **2015**, *113*, 184-215.

46. Pritchard, B. P.; Altarawy, D.; Didier, B.; Gibson, T. D.; Windus, T. L. New Basis Set Exchange: An Open, Up-to-Date Resource for the Molecular Sciences Community. *J. Chem. Inf. Model.* **2019**, *59*, 4814-4820.
47. Fox, S.; Dunne, John P.; Tacke, M.; Schmitz, D.; Dronskowski, R. Synthesis and Structural Characterisation of a Novel Chiral ansa-Cobaltocenium Hexafluorophosphate. *Eur. J. Inorg. Chem.* **2002**, *2002*, 3039-3046.

48. Pagels, N.; Prosenc, M. H.; Heck, J. An ansa-Cobaltocene with a Naphthalene Handle: Synthesis and Spectroscopic and Structural Characterization. *Organometallics* **2011**, *30*, 1968-1974.
49. Drewitt, M. J.; Barlow, S.; O'Hare, D.; Nelson, J. M.; Nguyen, P.; Manners, I. The first [2]cobaltocenophane and [2]metallocenophanium salts. *Chem. Commun.* **1996**, 2153-2154.
50. Mayer, U. F. J.; Charmant, J. P. H.; Rae, J.; Manners, I. Synthesis and Structures of Strained, Neutral [d7] and Cationic [d6] Hydrocarbon-Bridged [n]Cobaltocenophanes (n = 2, 3). *Organometallics* **2008**, *27*, 1524-1533.
51. Braunschweig, H.; Breher, F.; Kaupp, M.; Gross, M.; Kupfer, T.; Nied, D.; Radacki, K.; Schinzel, S. Synthesis, Crystal Structure, EPR and DFT Studies, and Redox Properties of [2]Tetramethyldisilacobaltocenophane. *Organometallics* **2008**, *27*, 6427-6433.
52. Ransom, P.; Ashley, A.; Thompson, A.; O'Hare, D. Synthesis, structure and characterisation of rac and meso-ansa-bridged permethylindenyl cobalt complexes. *J. Organomet. Chem.* **2009**, *694*, 1059-1068.
53. Vanicek, S.; Kopacka, H.; Wurst, K.; Müller, T.; Schottenberger, H.; Bildstein, B. Chemoselective, Practical Synthesis of Cobaltocenium Carboxylic Acid Hexafluorophosphate. *Organometallics* **2014**, *33*, 1152-1156.
54. Ogasawara, M.; Nagano, T.; Hayashi, T. Metathesis Route to Bridged Metallocenes. *J. Am. Chem. Soc.* **2002**, *124*, 9068-9069.
55. Hubert, A.; Reimlinger, H. The Isomerization of Olefins Part II. Thermal and Catalytic Isomerization of Olefins using Acids, Metals, Metal Complexes, or Boron Compounds as Catalysts. *Synthesis* **1970**, *1970*, 405-430.
56. You, W.; Hugar, K. M.; Coates, G. W. Synthesis of Alkaline Anion Exchange Membranes with Chemically Stable Imidazolium Cations: Unexpected Cross-Linked

Macrocycles from Ring-Fused ROMP Monomers. *Macromolecules* **2018**, *51*, 3212-3218.

57. Dragutan, I.; Dragutan, V.; Filip, P.; Simionescu, B. C.; Demonceau, A. ROMP Synthesis of Iron-Containing Organometallic Polymers. *Molecules* **2016**, *21*, 198.
58. Buretea, M. A.; Tilley, T. D. Poly(ferrocenylenevinylene) from Ring-Opening Metathesis Polymerization of ansa-(Vinylene)ferrocene. *Organometallics* **1997**, *16*, 1507-1510.
59. Heo, R. W.; Park, J.-S.; Goodson, J. T.; Claudio, G. C.; Takenaga, M.; Albright, T. A.; Randall Lee, T. ROMP of t-butyl-substituted ferrocenophanes affords soluble conjugated polymers that contain ferrocene moieties in the backbone. *Tetrahedron* **2004**, *60*, 7225-7235.
60. Martinez, H.; Ren, N.; Matta, M. E.; Hillmyer, M. A. Ring-opening metathesis polymerization of 8-membered cyclic olefins. *Polym. Chem.* **2014**, *5*, 3507-3532.

CHAPTER 4

MECHANOCHEMISTRY OF CATIONIC METALLOCENE

MECHANOPORE

4.1 Abstract

Recent research on the mechanochemistry of metallocene mechanophore has provided a new concept of force-responsiveness of thermally and chemically stable organometallic compounds. This led us to explore the omnipresence of mechanical lability on metallocene mechanochemistry. In this work, we report the mechanochemistry of main-chain cobaltocenium-containing polymers. We find that the cobaltocenium, isoelectronic to ferrocene, showed the selective dissociation by external force even though it has higher bond dissociation energy (BDE). Unlike the mechanical scission of neutral metallocene, the hexafluorophosphate, a counterion to cobaltocenium, played a vital role in the dissociation mechanism. Moreover, the dissociation of cobaltocenium showed a unique post chain scission process, resulting in the increased molecular weight by back complexation between cobalt cation and cyclopentadienyl ligand.

4.2 Introduction

A mechanophore, a mechanically labile building block, is the most critical component for mechano-responsive polymers. Mechanical degradation of polymers causes the reduction in molecular weight, viscosity, and mechanical strength. The recent surging of novel mechanophores has enabled new opportunities to open up mechanochemistry.¹ Several types of mechanophores have been investigated, including color change,²⁻⁵ catalysis,⁶⁻¹⁰ small molecule release,¹¹⁻¹³ and self-strengthening.¹⁴⁻¹⁶

Typically, the design of mechano-responsive material mainly focused on introducing selectively weak chemical bonds with a low bond dissociation energy (BDE), such as peroxide,¹⁷ diazo,¹⁸ disulfide,¹⁹ C-S²⁰. However, mechanophores are not just

restricted weak bonds. Significantly strong bonds, such as C-C, C-N, and C-O, are also studied for mechanophore when coupled with ring-strained structures.²¹⁻²³

Recently, the mechanochemistry of metallocene-containing polymers has been explored.²⁴⁻²⁷ Neutral metallocenes (*e.g.*, ferrocene and ruthenocene) have emerged as a new type of mechanophores despite their thermodynamically and chemically inert characteristics with the high BDE of the metal-cyclopentadienyl (Cp) bond. However, we together with others have demonstrated that metallocenes are mechanically labile at the main chain of a polymer under acoustic waves.

Cobaltocenium, an isoelectronic molecule to neutral ferrocene, represents a type of charged metallocene (or metallocenium) with superior thermal and chemical stability.^{28, 29} The BDE of Co-Cp is reported to be comparable to that of ferrocene,³⁰⁻³² while the charged nature and the pairing of counterion also provide cobaltocenium with some of unique properties that have been used for various applications, ranging from biomedical to membranes.³³⁻³⁹ However, the knowledge of neutral metallocenes as mechanophore could not be directly translated into cationic metallocenium due to two fundamental challenges: (1) The presence of counterion could complete the chain scission of the metal center and Cp; (2) the synthesis of main-chain metallocenium polymers. The former should consider how the counterion interacts with intermediates of chain scission; while the latter could exclude many functional groups (*e.g.*, ester) that destabilize metallocenium, but have negligible impact on neutral metallocenes. Nevertheless, the success of mechanochemistry of neutral metallocenes has alluded us to explore cobaltocenium as a possible mechanophore and its mechanism of chain scission.

Herein we report the design, synthesis and mechanochemistry of main-chain cobaltocenium-containing polymers. The cobaltocenium is integrated into a polyethylene-like backbone with the aid of metathesis chemistry. Acoustic sonication was employed to explore the mechanochemistry coupled with mechanistic trapping of scission intermediates. The results indicate that cobaltocenium possesses some unique mechano-responsive behaviors, different from neutral metallocenes. The chain scission mechanism was further illustrated by computational methods.

4.3 Experimental

Materials

Cobalt bromide (99%), lithium diisopropyl amide (2.0 M in hexane, THF, ethylbenzene, 99%), 4-bromo-1-butene (99%), 1-ethyl-3-(3-dimethylaminopropyl) carbodiimide (EDC, 99%), trimethylamine (99%), azobisisobutyronitrile (AIBN, 99%), 4-cyano-4-(phenylcarbonothioylthio)pentanoic acid (CPPA), ethyl vinyl ether (EVE, 99%), 3-bromo-1-propanol (98%), methylmethacrylate (98%), Grubbs II, Grubbs III catalysts (98%) were purchased from Sigma-Aldrich and used as received. 5-methoxy cyclooctene, ethynyl cobaltocenium hexafluorophosphate, ester-linked cobaltocenium PMA were synthesized according to previous report.^{25, 40, 41} All solvents were dried and freshly distilled before use.

Characterization

¹H NMR, ¹³C NMR, and ¹⁹F NMR spectra were recorded by Bruker Avance III HD 300 spectrometer using CDCl₃ or acetone-d₆ as solvents. EI mass spectra were collected Waters Micromass Q-Tof mass spectrometer, and the ionization source was positive ion

electrospray. Gel permeation chromatography (GPC) was performed in the tetrahydrofuran (THF) at a flow rate of 1.0 mL/min at 35 °C on a Waters-GPC system equipped with a refractive index (RI) detector, and narrow dispersed PS was employed for molecular weight calibration. UV-Vis spectra were recorded on a Shimadzu UV-2450 spectrophotometer using DCM as a solvent.

Sonication Test

Sonication experiment was conducted by Vibra cell Model VCX500 sonicator at 20 kHz with a 13 mm titanium probe purchased from Sonics & Materials. Sonication was carried out by using 2.5 mg/mL monomer/polymer solutions in DCM in a 20 mL suslik vessel immersed in an ice bath. The solution was degassed by N₂ for 15 min before sonication. The solution was exposed to N₂ throughout the sonication process. Pulsed ultrasound was produced at a power of 8.7 W/cm² with a 13 mm replaceable titanium tip from Sonics and Materials. The parameters of sonication were set with a 50 % duty cycle (1s on and 1s off) and output control at 6. The samples were taken at a designated time for further analysis.

DFT calculation details

The stretched structure evolution of the cobaltocenium model compound was studied by using Q-Chem 4.3 package.⁴² 1,1'-diethyl cobaltocenium hexafluorophosphate was used as a model structure, as shown in **Figure 4.1**, to illustrate the stretching of the polymer chain. B97-D functional was employed to describe the conformational evolution of cobaltocenium mechanophore. We use def2-tzvp basis set for Co, F and def2-svp basis set for C, O, F, and H atoms.⁴³ In order to mimic the stretching of the polymer, the end-to-

end distance of the model structure was gradually increased; meanwhile, all other geometries were fully relaxed. To calculate each step's potential energy, the end-to-end distance of the target molecule was fixed, then potential and geometry were optimized. The relaxation of stress was performed by removing the fixed end-to-end distance of the model compound. The energy and geometry were optimized. The distance between cobalt and P atom of PF_6^- was measured by using I-Qmol.

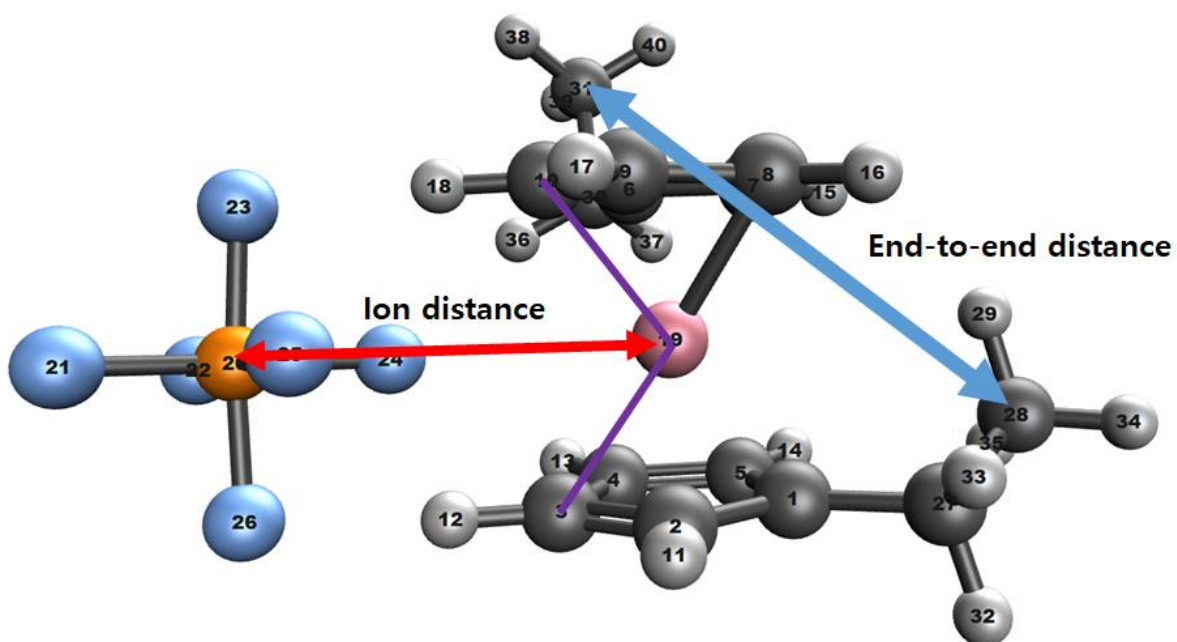


Figure 4.1. The structure of model cobaltocenium compound.

Synthesis of azide-modified chain transfer agent

3-azidopropanol was prepared according to the previous report.⁴⁴ 3-azidopropanol (199 mg, 1.96 mmol), 4-cyano-4-(phenylcarbonothioylthio)pentanoic acid (CPPA) (500mg, 1.8 mmol), DMAP (33 mg, 0.27 mmol) was placed in a N_2 purged round bottom flask. EDC hydrochloride (414 mg, 2.16 mmol) was dissolved in DCM, then added to the

reaction mixture dropwise. After adding the EDC solution, TEA (0.3 ml, 2.16 mmol) was immediately added into the solution. The mixture was stirred for 4 h. The solvent was removed by a rotary evaporator. The product was purified by column chromatography using nHex: EA=1:1. The product was fully dried under a vacuum. The pink liquid was obtained (546 mg, 83 % yield). ^1H NMR (300 MHz, CDCl_3): δ =7.93-7.26 (m, phenyl, 5H), 4.19 (t, $-\text{OCH}_2-$, 2H), 3.41 (t, $-\text{CH}_2-\text{N}_3$, 2H), 2.73-2.36 (m, $-\text{CH}_2\text{CH}_2-$, 4H), 1.94-1.88 (m, $-\text{CH}_3$, $-\text{CH}_2-$, 5H). ^{13}C NMR (75MHz, CDCl_3): δ = 171.41, 144.54, 133.06, 128.93, 128.61, 126.70, 126.50, 118.47, 113.99, 62.01, 48.14, 45.73, 33.40, 29.76, 28.07, 24.20.

Synthesis of cobaltocenium-labeled CPPA

3-azidopropyl-CPPA (546 mg, 1.5 mmol) and ethynyl cobaltocenium (540 mg, 1.5 mmol) were dissolved in 55 mL of THF/ H_2O (3/2, v/v). Anhydrous CuSO_4 (239 mg, 1.5 mmol) was dissolved in 1.5 mL of H_2O and added into the mixture. With stirring the mixture, a freshly prepared 1.0 M solution of sodium ascorbate aqueous solution was added dropwise. The reaction mixture was stirred overnight. The solvent was removed by a rotary evaporator. Residual liquid was dissolved in DCM and extracted with sat. NaHCO_3 soln., H_2O , and sat. NaCl soln. The organic layer was collected and dried by anhydrous MgSO_4 . The residual solid was dissolved in 1.0 mL of DCM and precipitated in cold ether. Pink solid was obtained (371 mg, 34 % yield). ^1H NMR (300 MHz, acetone- d_6): δ = 8.60 (s, triazole, 1H), 8.00-7.50 (m, phenyl, 5H), 6.43 (s, **Cp**, 2H), 6.00 (s, **Cp**, 2H), 5.76 (s, **Cp**, 5H), 4.64 (t, $-\text{OCH}_2-$, 2H), 4.22 (t, $-\text{CH}_2-$, 2H), 2.73-2.36 (m, $-\text{CH}_2\text{CH}_2-$, 6H), 1.94-1.88 (m, $-\text{CH}_3$, 3H). MS(ESI) m/z calculated for $\text{C}_{28}\text{H}_{28}\text{CoN}_4\text{O}_2\text{S}_2^+$ (M^+) 575.61, found 575.

Synthesis of cobaltocenium-labeled PMMA

Cobaltocenium-labeled CPPA (50 mg, 0.07 mmol), MMA (1.39 g, 13.9 mmol), and AIBN (3.5 mg, 0.021 mmol) were dissolved in 1.0 mL of degassed DMF. The reaction mixture was stirred at 75 °C for 4 h. The polymer was precipitated in cold methanol three times. White solid was obtained.

Synthesis of 1-butene-4-cyclopentadiene

Freshly distilled cyclopentadiene (6.99 g, 105.8 mmol) was dissolved in THF (200 mL). The solution was cooled down to -78°C with N₂ bubbling. 2.0 M LDA (53 mL, 105.8 mmol) was added by dropwise addition. The reaction mixture was stirred at -78 °C for 2 h. 4-Bromo-1-butene (15.0 g, 111 mmol) was diluted with 10 mL of THF and added to the reaction mixture. The reaction mixture was stirred overnight. The reaction was quenched by sat. NH₄Cl soln. The mixture was extracted with ether and sat. NaHCO₃ soln. The organic layer was collected and washed with water and sat. NaCl soln. The organic layer was dried by anhydrous MgSO₄. The solvent was removed by evaporation. The dark orange liquid was obtained (14.67 g). Further purification was performed by fractional vacuum distillation. Light yellow liquid was obtained as a product (3.7 g, 29 % yield). ¹H NMR (300 MHz, CDCl₃): δ= 6.51-6.08 (m, Cp, 3H), 5.88 (m, -CH=CH₂, 1H), 5.04 (m, =CH₂, 2H), 3.00 (d, -CH₂-, 2H), 2.51 (m, -CH₂-, 2H), 2.36 (m, -CH₂-, 2H).

Synthesis of 1

Freshly prepared butenyl cyclopentadiene (3.7 g, 30.8 mmol) was dissolved in 200 mL of THF. The solution was cooled down to -78°C. 2.0 M LDA (15.4 mL, 30.8 mmol) was added. The reaction mixture was stirred at -78°C for 2 h. The reaction solution becomes

orange in color. CoBr_2 (3.36 g, 15.4 mmol) was added. The reaction mixture was stirred overnight at rt. The solution becomes dark purple. The solvent was removed by evaporation. The liquid residue was dissolved in 80 °C water. The aqueous solution was air-bubbled for 4 h. The aq. solution was added by activated charcoal and boiled for 30 min. The solution was filtered through the celite and washed by 80 °C water. The solution was reduced to ca. 100 mL and NaPF_6 were added. The mixture was extracted by DCM, and the organic layer was dried by anhydrous MgSO_4 . The solvent was removed by evaporation, and the solid was fully dried under vacuum. Yellow solid was obtained (3.7g, 54 % yield). $^1\text{H NMR}$ (300 MHz, acetone- d_6): δ = 5.99-5.79 (m, $-\text{CH}=$, **Cp**, 10 H), 5.3 (t, $=\text{CH}_2$, 4H), 2.70 (t, $-\text{CH}_2-$, 4H), 2.38 (q, $-\text{CH}_2-$, 4H). $^{13}\text{C NMR}$ (75MHz, acetone- d_6): δ = 136.87, 115.56, 107.84, 84.26, 84.06, 33.96, 26.83. MS(ESI) m/z calculated for $\text{C}_{18}\text{H}_{22}\text{Co}^+$ (M^+) 297.31, found 297.

Synthesis of 2

1,1'-(di-(1-propen-3-yl)) cobaltocenium hexafluorophosphate (442 mg, 1.0 mmol) was dissolved in 600 mL of DCM. The reaction mixture was stirred under N_2 atmosphere at 40 °C for 20 min. Grubbs II catalyst (42 mg, 0.05 mmol) was dissolved in 0.5 mL DCM and added to the reaction mixture. The reaction mixture was stirred at 50 °C for 2.5 h. The reaction mixture was cooled down to rt then the solvent was removed by evaporation. Brown solid was dissolved in DCM. The product was purified by column chromatography using basic aluminum oxide. DCM was used first after an impurity was removed, then the eluent was changed to acetone. The solvent was removed and dried under a vacuum. Yellow solid was obtained (240 mg, 58 % yield). $^1\text{H NMR}$ (300 MHz, acetone- d_6): δ =5.89-5.68 (m, $-\text{CH}=\text{CH}-$, **Cp**, 10H), 2.69-2.57 (m, $-\text{CH}_2-\text{CH}_2-$, 8H). $^{13}\text{C NMR}$ (75MHz,

acetone-d₆): δ = 131.90, 130.66, 83.96, 82.30, 81.40, 25.79, 25.10, 24.64. MS(ESI) m/z calculated for C₁₆H₁₈Co⁺ (M⁺) 269.07, found 269.

Synthesis of main-chain cobaltocenium-containing polymer

Cyclic cobaltocenium monomer (68 mg, 0.165 mmol) and 5-methoxy-1-cyclooctene (439 mg, 3.135 mmol) were dissolved in 1.0 mL of Acetone/DCM (1/1, v/v). Grubbs III catalyst (1mg, 1.37 μ mol) was dissolved in 0.2 mL DCM and added into the reaction mixture. The reaction mixture was stirred at room temperature for 3 h. The polymerization was quenched by adding few drops of EVE. The polymer was precipitated in cold methanol three times.

4.4 Results and Discussion

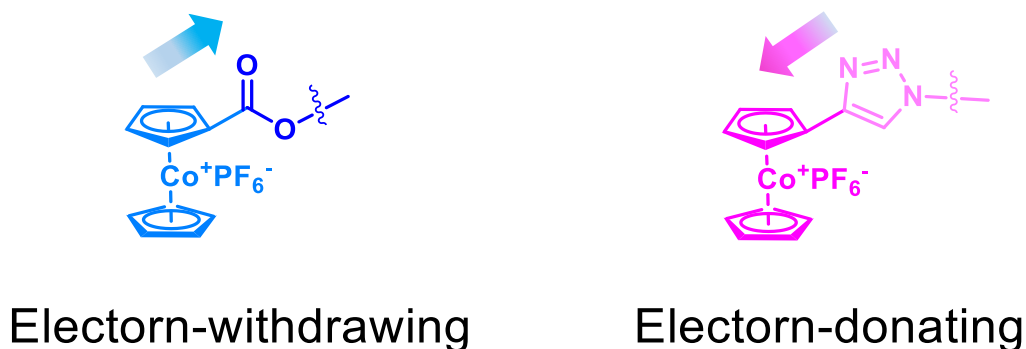


Figure 4.2 Structural variation of substituted cobaltocenium.

Design Principle and Synthesis of Main-Chain Cobaltocenium-Containing Polymers

The synthesis of main-chain cobaltocenium-containing polymers initially began with the similar design of ferrocene and ruthenocene-labeled polymers, which would involve metallocene substituted with esters. It was surprising that these derivatives (either

mono- or di-esters) are not stable under sonication (**Figure 4.3**). It came to our attention that electron-withdrawing groups such as esters destabilize cobaltocenium due to the reduced electron density of Cp rings with the presence of a positive metal center.^{38, 45} This hypothesis was further tested by designing a weak electron-donating group (EDG) of triazole attached to cobaltocenium. This new derivative was not observed noticeable change prior to and after sonication, indicating the importance of installing EDGs to maintain intrinsic chemical stability (**Figure 4.4**). This is in stark contrast with neutral metallocenes.

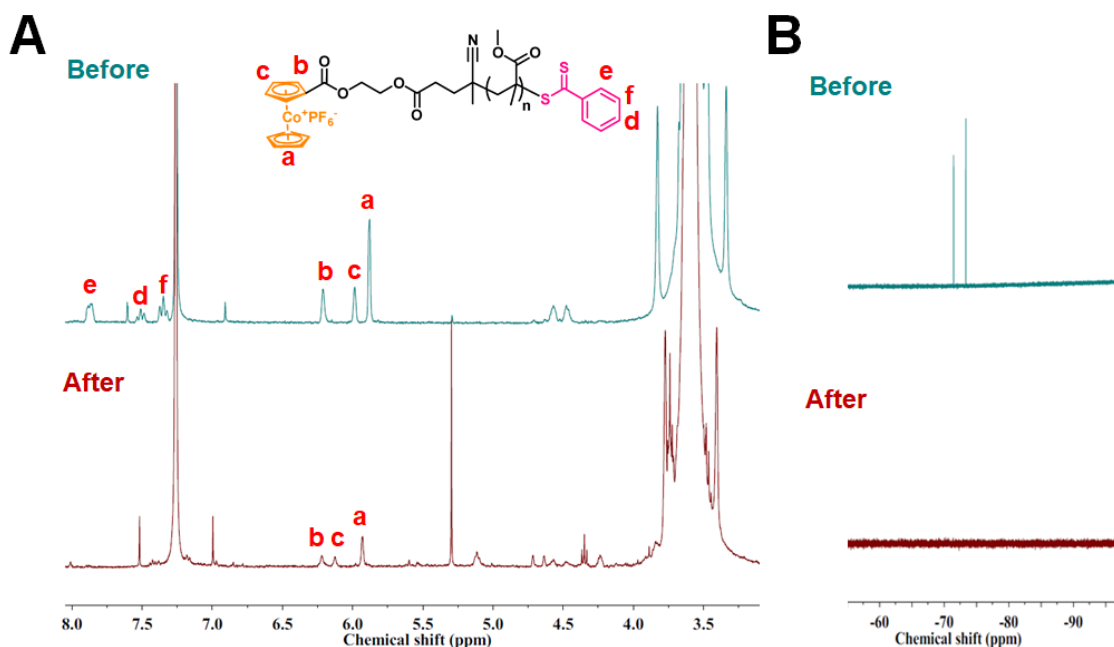


Figure 4.3. (A) ^1H NMR; and (B) ^{19}F NMR of cobaltocenium end-labeled PMA with ester linker before (green) and after (red) sonication.

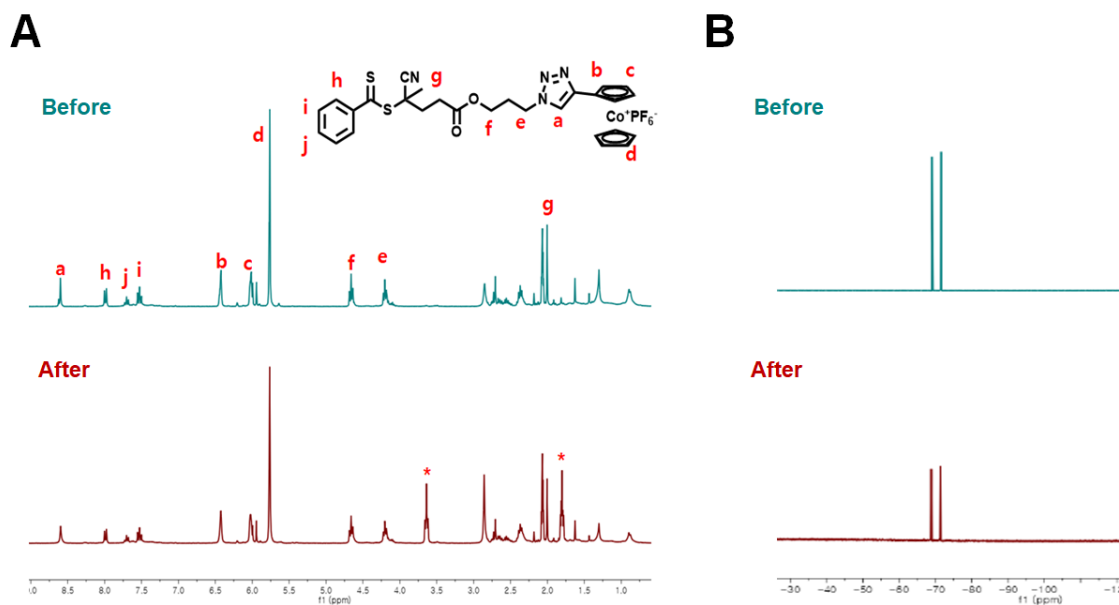


Figure 4.4. (A) ^1H NMR; and (B) ^{19}F NMR of cobaltocenium end-labeled RAFT agent with triazole linker before (green) and after (red) sonication.

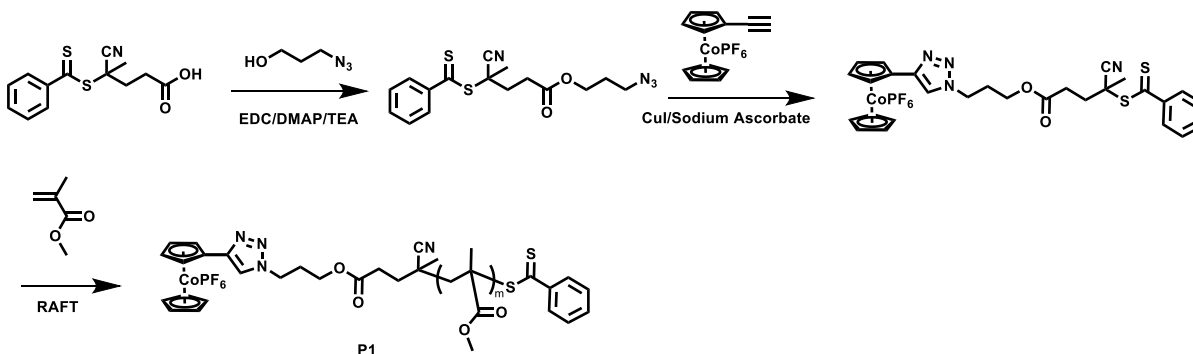


Figure 4.5. Synthesis of cobaltocenium end-labeled PMMA by RAFT polymerization.

To further confirm the mechanical lability of cobaltocenium, we synthesized cobaltocenium-labeled polymers. End-labeling of cobaltocenium was achieved by click reaction of ethynyl cobaltocenium and azide-modified chain transfer agent.⁴¹ Then, we carried out reversible addition-fragmentation chain-transfer (RAFT) polymerization of using methyl methacrylate to afford the cobaltocenium end-labeled poly(methyl methacrylate) (PMMA) with molecular weight of 60,000 g/mol (**Figure 4.5**). The

cobaltocenium end-labeled PMMA was exposed to an acoustic field for 2 h and characterized by ^1H and ^{19}F NMR. The results showed that the cobaltocenium was not dissociated under sonication (**Figure 4.6**). Moreover, the counterion of PF_6^- was also intact. Based on these results, it was confirmed that cobaltocenium is stable under ultrasonication, when it is located at the end of a polymer chain.

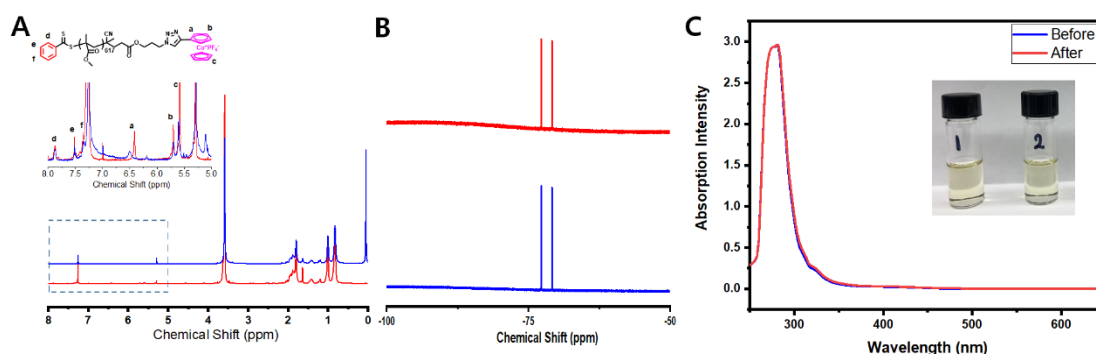


Figure 4.6. (A) ^1H NMR spectrum; (B) ^{19}F NMR spectrum (blue: before sonication; red: after sonication); and (C) UV-vis absorption spectrum of **P1**.

Following these initial investigations, a class of main-chain cobaltocenium-containing polymers was conceptualized using a simple polyethylene-like chain as the framework. This design considers (1) alkyl group as an EDG and (2) the elimination of unnecessary complications from other functional groups. A combination of ring-closing metathesis (RCM) and ring-opening metathesis polymerization (ROMP) was executed toward the synthesis of multiple cobaltocenium-containing polymers. Multi mechanophore labeling is more sensitive than a single mechanophore in mechanochemistry.⁴⁶ First, a diene compound **1** was prepared from lithium 1-butene-4-cyclopentadienide and CoBr_2 (**Figure 4.7**). Cyclic cobaltocenium monomer **2** was prepared by RCM of **1**. The cobaltocenium-containing polymer ($M_n = 67,000$ g/mol, $D = 1.03$) was synthesized by

copolymerization of **2** and 5-methoxycyclooctene in a similar approach to previous reports of our work.^{25, 26}

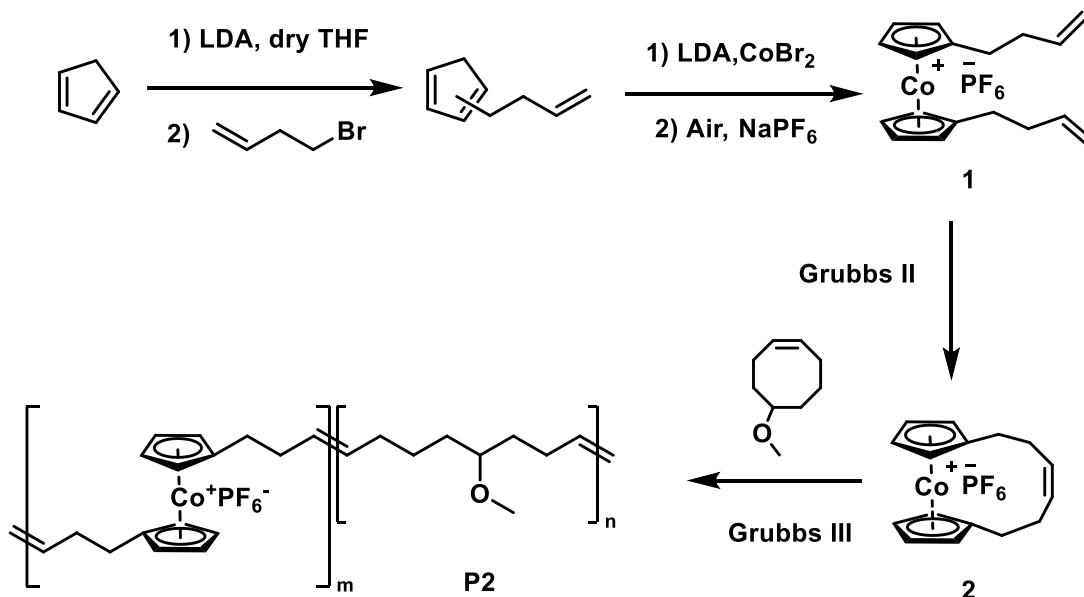


Figure 4.7. Synthetic scheme of a main-chain cobaltocenium-containing polymer.

Mechanochemistry of Cobaltocenium Polymers

Sonication of P2 was conducted in DCM with a concentration of 2.5 mg/mL. Two-hour sonication led to a decrease of molecular weight from 67,000 g/mol to 46,000 g/mol (**Figure 4.8A**). The susceptibility of cobaltocenium was further quantified by the change in ^1H NMR. The relative integration changes around 5.58 and 5.28 ppm, responding to the Cp of cobaltocenium, showed that 30% of cobaltocenium has disappeared (**Figure 4.8B**). In addition, ^{19}F NMR also showed the reduction of PF_6^- , also indicating the destroy of the cobaltocenium (**Figure 4.9**). These results demonstrated that cobaltocenium is the preferential scission site in the polymer chain.

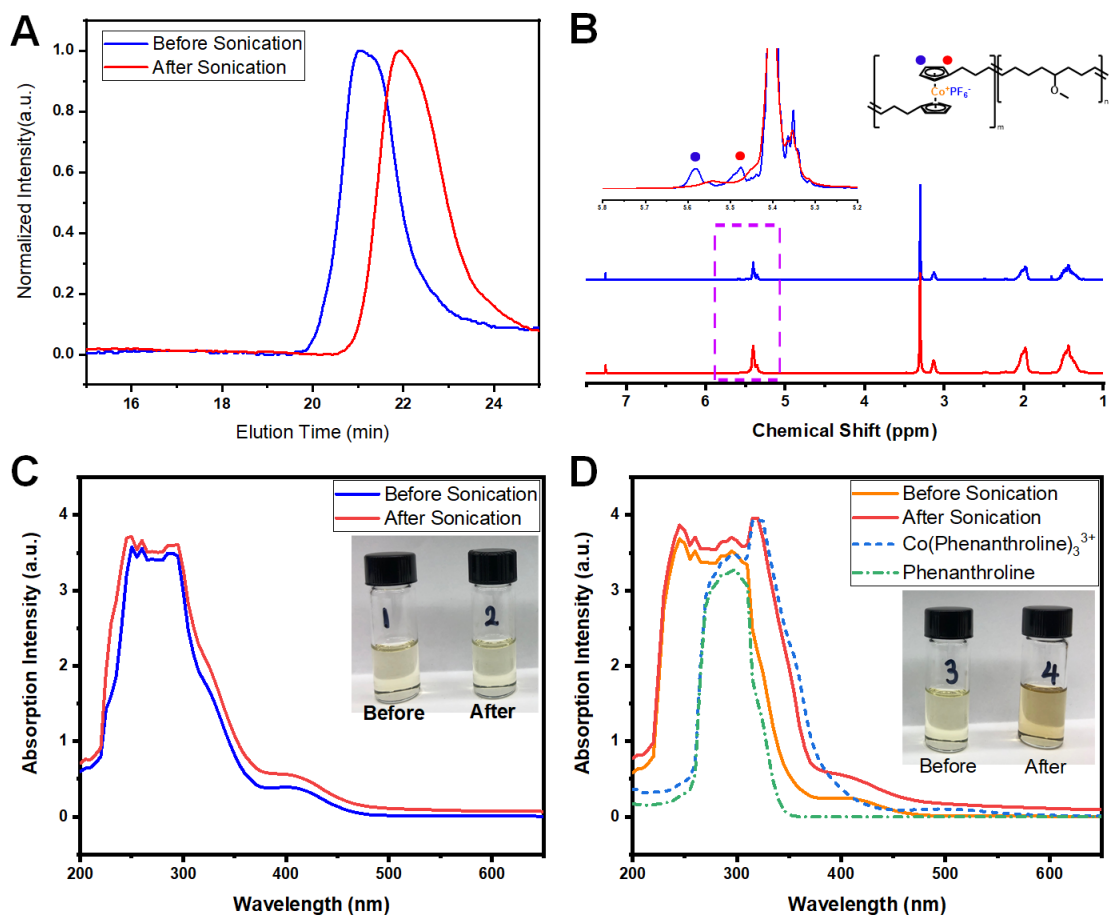


Figure 4.8. (A) GPC trace of **P2** before and after sonication for 2 h; (B) ^1H NMR spectrum; UV-vis absorption spectrum of **P2** (C) with 1,10-phenanthroline (D) without 1,10-phenanthroline.

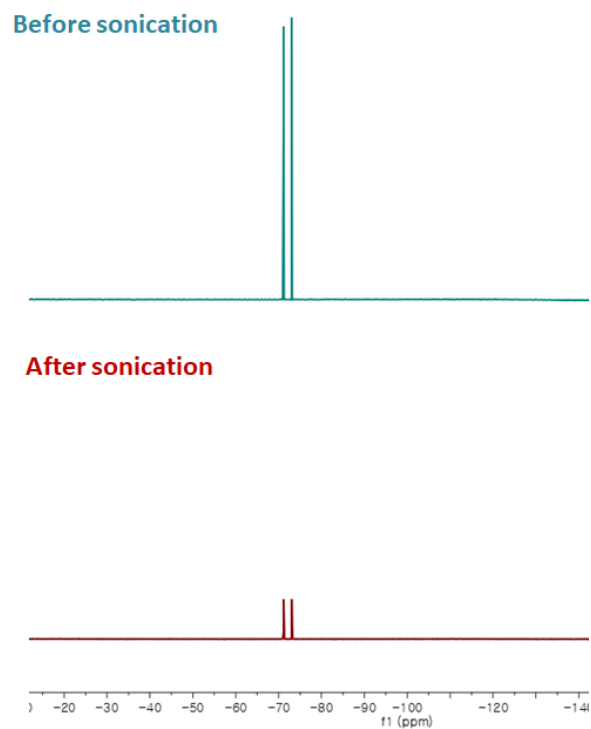


Figure 4.9. ^{19}F NMR spectrum of P2 before and after sonication for 2 h in DCM at a concentration of 2.5 mg/mL.

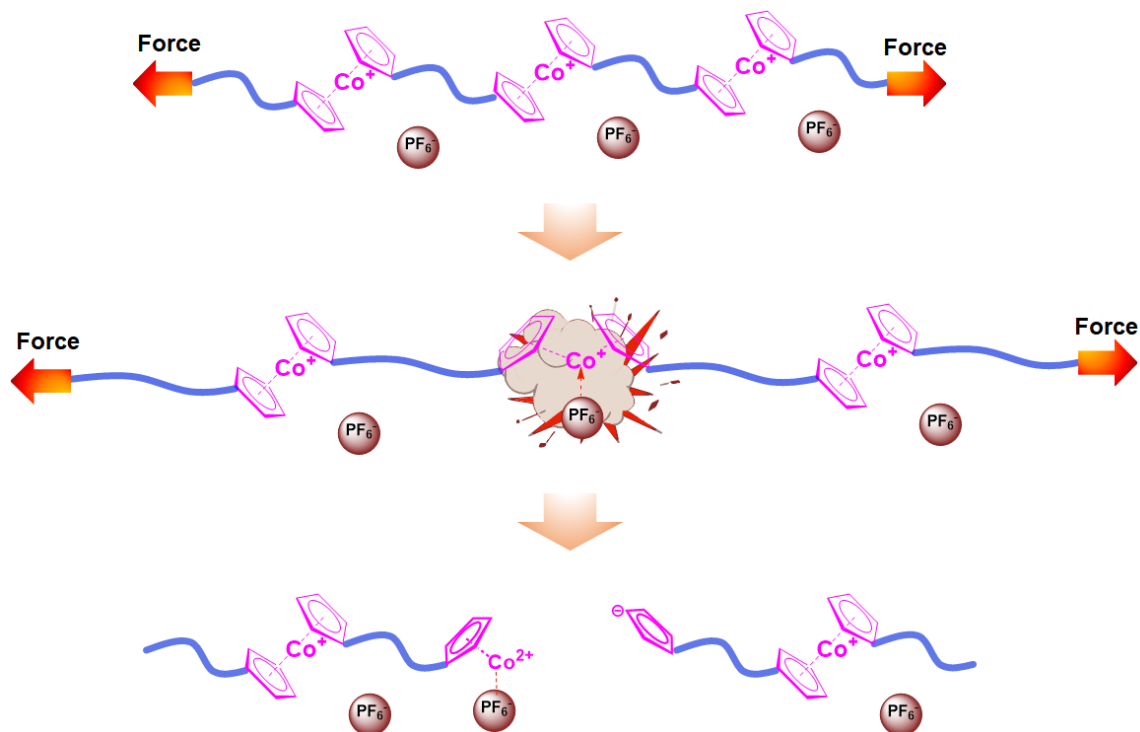


Figure 4.10. Schematic illustration of cobaltocenium dissociation under ultrasonication

Given that the scission mechanism of ferrocene and ruthenocene is quite similar to the heterolytic one, we anticipated that the scission of cobaltocenium would resemble that of ferrocene and ruthenocene. As illustrated in **Figure 4.10**, the dissociation of cobaltocenium might produce cobalt cation or its half-sandwich. From the earlier work, 1,10-phenanthroline is a useful molecule to trap the dissociated metal ions, resulting in UV absorption changes. Moreover, the trapping of released metal ions provides insight into the dissociation mechanism of the metallocene.^{24, 25, 47} Therefore, we expected that this method could be valid for cobaltocenium. P2 was dissolved in 3.0 mM of 1,10-phenanthroline solution in DCM, followed by the same sonication condition. The UV-vis absorption was compared between before sonication and after sonication. The results revealed that a new absorption peak at 325 nm appeared (**Figure 4.9D, solid red line**), which is assigned to the ligand to metal charge transfer. By contrast, sonication without 1,10-phenanthroline did not show any new absorption peak (**Figure 4.9C**). In order to further confirm this result, we prepared $[\text{Co}(\text{phenanthroline})_3]^{3+}$,⁴⁸ and compared UV-vis absorption. As shown in **Figure 4.9D (blue dashed line)**, the result was consistent with that of polymer sonication. This result supports that the dissociation of cobaltocenium produces Co^{3+} or $[\text{CoCp}]^{2+}$, which might be originated from the heterolytic dissociation of cobaltocenium.

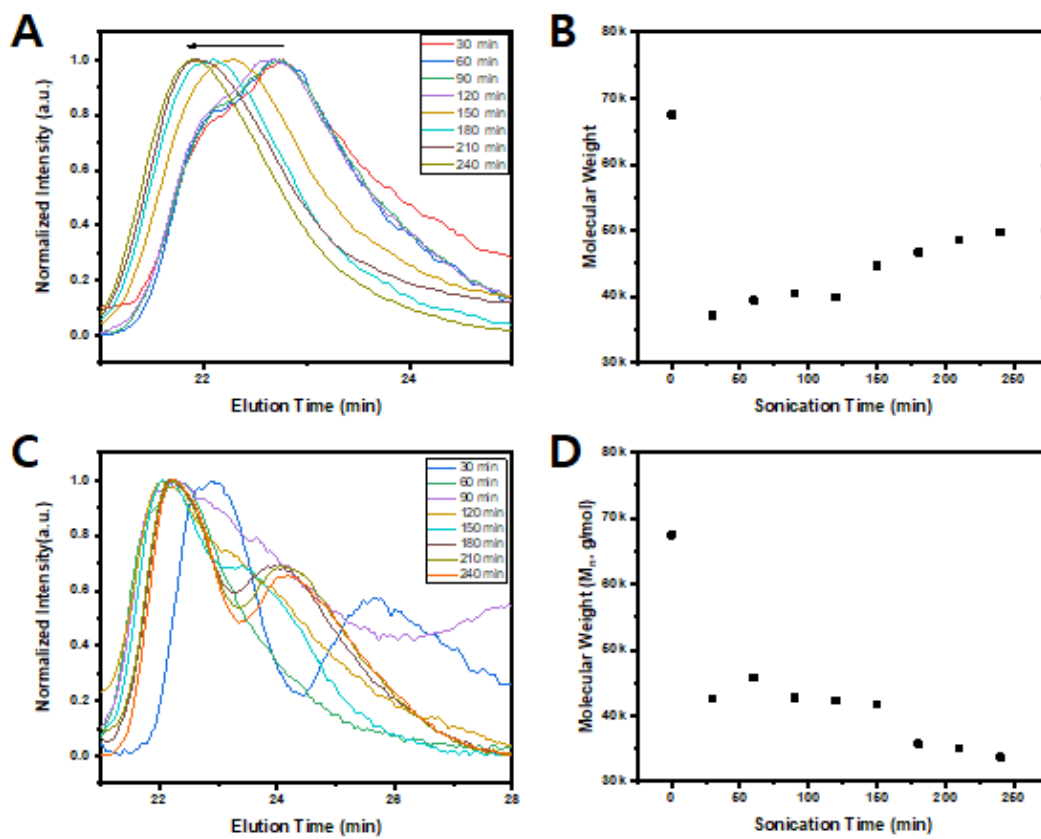


Figure 4.11. (A) GPC trace; (B) Plot of M_n vs. sonication time of P2 in DCM; (C) GPC trace; and (D) Plot of M_n vs. sonication time of P2 in DCM/MeOH (9/1, v/v) after sonication 30, 60, 90, 120, 150, 180, 210, and 240 min.

We next further investigated the molecular weight changes during sonication. It is quite reasonable that the molecular weight of the main-chain cobaltocenium-containing polymer should decrease during sonication due to the chain scission. We conducted the same experiment, but a longer sonication time was applied. At each interval, the aliquot of the solution was taken, and molecular weight was monitored. We found some strange results. As shown in **Figure 4.11A and 4.11B**, the sonication of **P2** initially reduced the molecular weight from 67,000 g/mol to 37,000 g/mol. However, the molecular weight started to increase after 30 min sonication, reaching finally 49,000 g/mol. This result is

quite counterintuitive to our expectation because the sonication reduces the molecular weight of the polymer.²⁵

We speculated that this change might be attributed to the back complexation of the Co(III) and Cp⁻. If these adducts can form an ionic bond, the increased molecular weight can be reasonably explained by that a back complexation of these adducts might increase the molecular weight. Therefore, this phenomenon might be suppressed by the protonation of Cp⁻. To test this, the **P2** was dissolved in DCM/MeOH (9:1, v/v) solution at a concentration of 2.5 mg/mL, then exposed to the pulsed ultrasonication (MeOH can protonate the Cp⁻). The sonication under protic solvent revealed the decrease of molecular weight of polymers during the sonication (**Figure 4.11D**). As shown in **Figure 4.11C**, the molecular weight at 60 min increased when compared to that at 30 min, indicating that back complexation is dominant at this point. Further sonication and protonation of Cp⁻ afforded smaller segments and larger segments, leading to the decrease in molecular weight. However, it still contains a large portion of high molecular weight. This might be attributed to the characteristics of Co(III). Co(III) can form a thermodynamically more stable complex.⁴⁹⁻⁵¹ And it has a slower ligand exchange rate compared to Co(II).⁵² The formation of a stable complex might result in the back complexation.

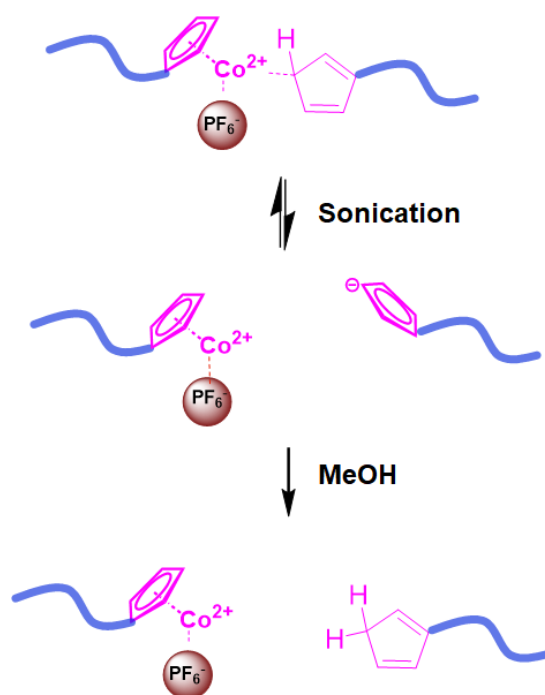


Figure 4.12. proposed mechanism of back complexation during sonication.

DFT calculation of cobaltocenium mechanophore

To further explore the stretching and breaking of cobaltocenium mechanophore, we carried out DFT calculation with constrained geometry simulating external force (COGEF), a well-known method for mechanochemistry mechanophore.^{53, 54} 1,1'-diethyl cobaltocenium hexafluorophosphate was chosen as a model compound due to its similarity of the mechanophore core structure. To mimic the elongation of the polymer backbone, we varied the end-to-end distance of the model cobaltocenium mechanophore (**Figure 1**). As shown in **Figure 4.13B**, the Cp rings are aligned in a slightly staggered geometry at the most energetically favored state when fully relaxed. As the cobaltocenium is stretched, two Cp rings rotate to form the anti-position of two ethyl groups (2 Å). The aligned two Cp rings start to slip with the increased end-to-end distance, resulting in the increase of the energy of the system. This step resembles that of ferrocene.²⁵ However, subsequent

stretching of cobaltocenium shows different structural evolution. As shown in **Figure 4.13A**, stretching of cobaltocenium induces the rupture of the sandwich structure at 3.8 Å, similar to the dissociation of ferrocenophane mechanophore.²⁷ Further stretching of this structure causes elongation of the Co-Cp bond and opens the ruptured structure with increased potential. Clearly, the full dissociation of Cp takes place when the stretching distance reaches 6.5 Å, producing Cp⁻ and [CpCo]²⁺PF₆⁻. COGEF potential also reveals deviation from those of ferrocene. The COGEF potential increases until it reaches the first potential peak at 3.7 Å because of the distorted bond angle and bond distance. When the stretching distance of cobaltocenium reaches 3.8 Å, COGEF potential abruptly decreases. Another potential decrease also occurs at 5.6 Å. Compared with geometries at these points, potential decreases are likely related to the structural evolutions. We hypothesized that this difference might be originated from the counterion. In contrast to ferrocene, cobaltocenium is coupled with a counterion, which can stabilize the molecule. Therefore, the counterion effect might affect the dissociation mechanism and potential changes of cobaltocenium mechanophore.

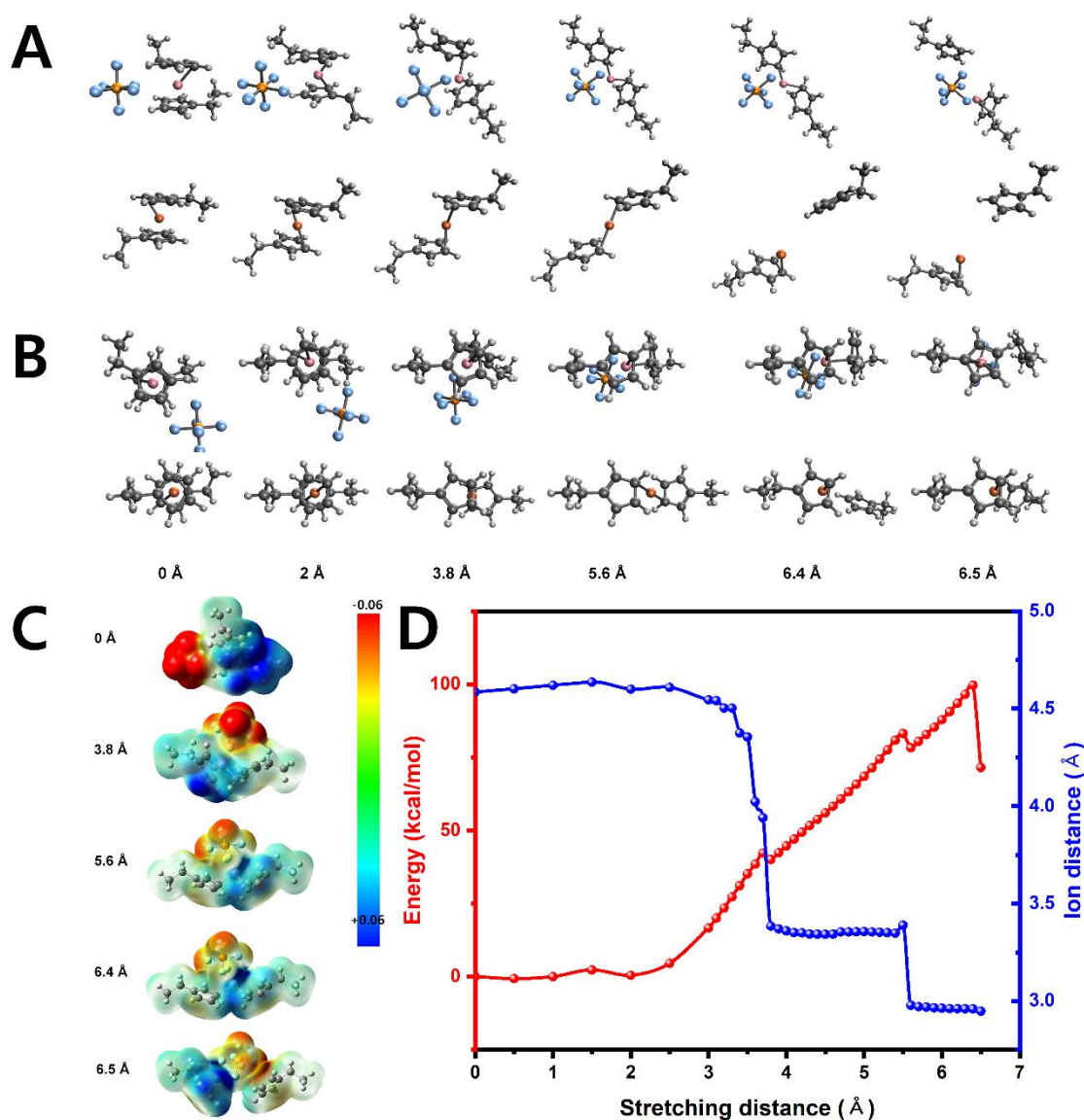


Figure 4.13. (A) Side view; (B) top view for the structural evolution of cobaltocenium model compound with stretching distance; (C) representative electrostatic potential map (The contour surface is described based on van der Waals surface with an electron density of 0.001 e/Bohr³ proposed by Bader⁵⁵; (D) COGEF potential (red symbol) and ion distance (blue symbol) with stretching of end-to-end distance.

To examine the counterion effect, the distance of cobalt to PF₆⁻ was measured and compared to the COGEF potentials. As shown in **Figure 4.13D**, the distance dramatically decreased at each transition point, demonstrating that interaction between cobalt and PF₆⁻ has a critical impact on the dissociation of cobaltocenium. With the stretching of

cobaltocenium, Cp rings are slipping along with the force direction, making more space for cobalt to interact with PF_6^- . The Coulumbic attraction between cobalt cation and PF_6^- might be increased as the stretching proceeds. As a result, the cobaltocenium sandwich structure is ruptured. The attraction guides the dissociation of cobaltocenium through a peeling-like pathway rather than slipping. One of the differences is that the maximum force calculated over the stretching is slightly reduced compared to that of ferrocene. F_{max} is 2.73 nN and 3.18 nN for cobaltocenium and ferrocene, respectively (**Figure 4.15**). Given that these metallocenes have comparable BDE, it might be concluded that counterion can facilitate the bond dissociation in the case of cobaltocenium.

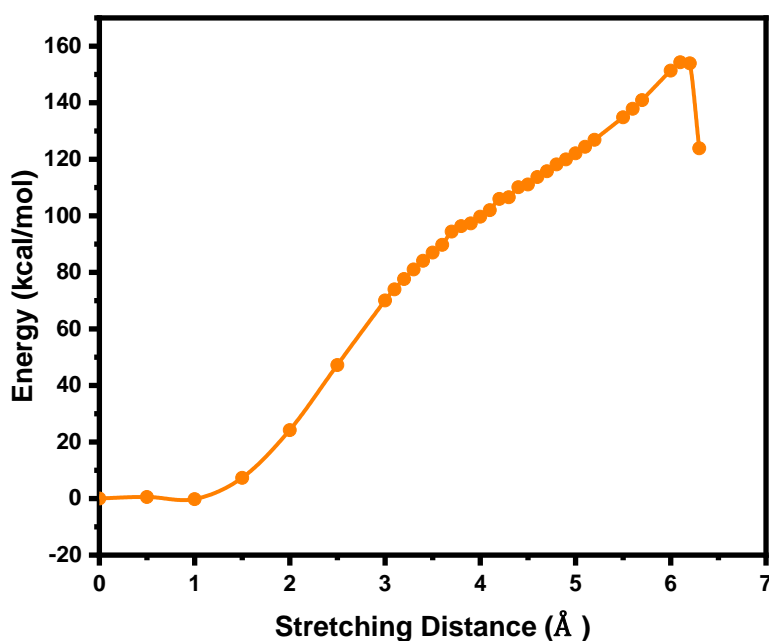


Figure 4.14. COGEF potential of ferrocene model compound with stretching of end-to-end distance.

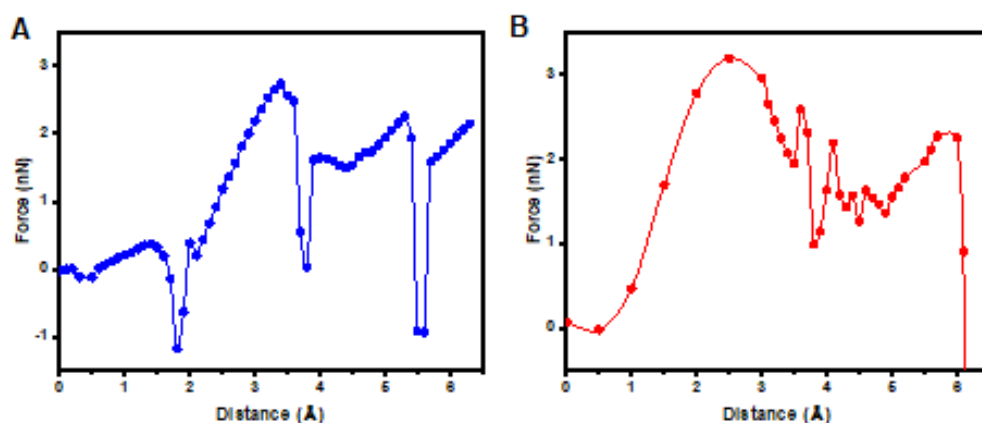


Figure 4.15. COGEF force of (A) cobaltocenium; and (B) ferrocene with stretching distance.

To further examine the bond cleavage mechanism, a molecular electrostatic potential (ESP) was used to depict the charge distribution during dissociation.⁵⁶ The representative ESP maps of the cobaltocenium model were shown as a function of distance in **Figure 4.13C**. Before chain elongation, the charge distribution was biased on cobaltocenium and PF_6^- . When it was stretched to 3.8 Å, where the sandwich structure ruptures, the negative charge on PF_6^- starts to diminish. With the decreased distance between cobalt and PF_6^- , the charge distribution along the molecule is delocalized, stabilizing the charge separation. After complete dissociation, half-sandwich cobaltocenium holds a more positive charge, and the negative charge density is distributed on PF_6^- and dissociated Cp^- . The ESP map also supports the heterolytic dissociation of cobaltocenium mechanophore, with separated charge density after dissociation.

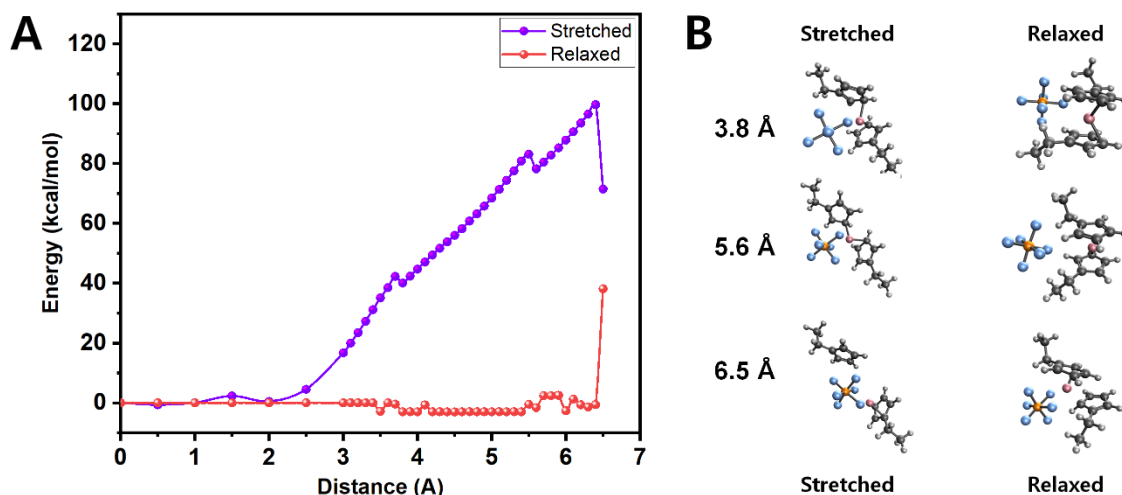


Figure 4.16. (A) COGEF potential of cobaltocenium model compound with stretching and relaxing; (B) optimized geometries at 3.8 Å, 5.6 Å, and 6.5 Å.

Next, we proposed that the back complexation might induce the molecular weight increase during sonication. For further insight into this phenomenon, we conducted a simple simulation to mimic the post-sonication. The optimized geometries of each intermediate obtained from stretching were re-optimized to get potential and geometry (**Figure 4.16A**). As shown in **Figure 4.16B**, the optimized geometries obtained from 3.8 Å and 5.6 Å show the recovery of their stable sandwich structures, indicating that the stretching of the mechanophore is reversible unless dissociation is completed. However, the fully dissociated structure at 6.5 Å shows the complex structure of half-sandwich cobaltocenium and Cp. This study suggested that the dissociated Cp can rebind to cobalt, leading to the increased molecular weight as experimentally observed.

4.5 Conclusion

In summary, we prepared the cobaltocenium derivatives and the main-chain cobaltocenium-containing copolymers via RCM and ROMP. Although the cobaltocenium possesses high thermodynamic stability, it showed a selective chain scission under the

acoustic field. In contrast to neutral metallocene, cobaltocenium has a different chain scission mechanism confirmed by computational mechanistic studies. Mechanical susceptibility and dissociation mechanism of cobaltocenium are likely dependent on counterion. Moreover, the chemical characteristic of cobalt affords unique back complexation that is probably useful for material applications, such as mechanical self-strengthening. We speculate that this discovery might put a stepping stone to further expand the mechanochemistry of metallocene.

4.6 References

1. Li, J.; Nagamani, C.; Moore, J. S. Polymer Mechanochemistry: From Destructive to Productive. *Accounts. Chem. Res.* **2015**, *48*, 2181-2190.
2. Davis, D. A.; Hamilton, A.; Yang, J.; Cremar, L. D.; Van Gough, D.; Potisek, S. L.; Ong, M. T.; Braun, P. V.; Martínez, T. J.; White, S. R.; Moore, J. S.; Sottos, N. R. Force-induced activation of covalent bonds in mechanoresponsive polymeric materials. *Nature* **2009**, *459*, 68-72.
3. Wang, T.; Zhang, N.; Dai, J.; Li, Z.; Bai, W.; Bai, R. Novel Reversible Mechanochromic Elastomer with High Sensitivity: Bond Scission and Bending-Induced Multicolor Switching. *Acs Appl. Mater. Interfaces* **2017**, *9*, 11874-11881.
4. Sagara, Y.; Karman, M.; Verde-Sesto, E.; Matsuo, K.; Kim, Y.; Tamaoki, N.; Weder, C. Rotaxanes as Mechanochromic Fluorescent Force Transducers in Polymers. *J. Am. Chem. Soc.* **2018**, *140*, 1584-1587.
5. Wang, Z.; Ma, Z.; Wang, Y.; Xu, Z.; Luo, Y.; Wei, Y.; Jia, X. A Novel Mechanochromic and Photochromic Polymer Film: When Rhodamine Joins Polyurethane. *Adv. Mater.* **2015**, *27*, 6469-6474.
6. Piermattei, A.; Karthikeyan, S.; Sijbesma, R. P. Activating catalysts with mechanical force. *Nat. Chem.* **2009**, *1*, 133-137.

7. Groote, R.; Jakobs, R. T. M.; Sijbesma, R. P. Performance of Mechanochemically Activated Catalysts Is Enhanced by Suppression of the Thermal Effects of Ultrasound. *ACS Macro Lett.* **2012**, *1*, 1012-1015.
8. Jakobs, R. T. M.; Sijbesma, R. P. Mechanical Activation of a Latent Olefin Metathesis Catalyst and Persistence of its Active Species in ROMP. *Organometallics* **2012**, *31*, 2476-2481.
9. Michael, P.; Binder, W. H. A Mechanochemically Triggered “Click” Catalyst. *Angew. Chem. Int. Ed.* **2015**, *54*, 13918-13922.
10. Wei, K.; Gao, Z.; Liu, H.; Wu, X.; Wang, F.; Xu, H. Mechanical Activation of Platinum–Acetylide Complex for Olefin Hydrosilylation. *ACS Macro Lett.* **2017**, *6*, 1146-1150.
11. Diesendruck, C. E.; Steinberg, B. D.; Sugai, N.; Silberstein, M. N.; Sottos, N. R.; White, S. R.; Braun, P. V.; Moore, J. S. Proton-Coupled Mechanochemical Transduction: A Mechanogenerated Acid. *J. Am. Chem. Soc.* **2012**, *134*, 12446-12449.
12. Lin, Y.; Kouznetsova, T. B.; Craig, S. L. A Latent Mechanoacid for Time-Stamped Mechanochromism and Chemical Signaling in Polymeric Materials. *J. Am. Chem. Soc.* **2020**, *142*, 99-103.
13. Hu, X.; Zeng, T.; Husic, C. C.; Robb, M. J. Mechanically Triggered Small Molecule Release from a Masked Furfuryl Carbonate. *J. Am. Chem. Soc.* **2019**, *141*, 15018-15023.
14. Ramirez, A. L. B.; Kean, Z. S.; Orlicki, J. A.; Champhekar, M.; Elsagr, S. M.; Krause, W. E.; Craig, S. L. Mechanochemical strengthening of a synthetic polymer in response to typically destructive shear forces. *Nat. Chem.* **2013**, *5*, 757.
15. Zhang, H.; Gao, F.; Cao, X.; Li, Y.; Xu, Y.; Weng, W.; Boulatov, R. Mechanochromism and Mechanical-Force-Triggered Cross-Linking from a Single Reactive Moiety Incorporated into Polymer Chains. *Angew. Chem. Int. Ed.* **2016**, *55*, 3040-3044.

16. Verstraeten, F.; Göstl, R.; Sijbesma, R. P. Stress-induced colouration and crosslinking of polymeric materials by mechanochemical formation of triphenylimidazolyl radicals. *Chem. Commun.* **2016**, 52, 8608-8611.
17. Encina, M. V.; Lissi, E.; Sarasúa, M.; Gargallo, L.; Radic, D. Ultrasonic degradation of polyvinylpyrrolidone: Effect of peroxide linkages. *J. Polym. Sci. Polym. Lett. Ed.* **1980**, 18, 757-760.
18. Berkowski, K. L.; Potisek, S. L.; Hickenboth, C. R.; Moore, J. S. Ultrasound-Induced Site-Specific Cleavage of Azo-Functionalized Poly(ethylene glycol). *Macromolecules* **2005**, 38, 8975-8978.
19. Li, Y.; Nese, A.; Matyjaszewski, K.; Sheiko, S. S. Molecular Tensile Machines: Anti-Arrhenius Cleavage of Disulfide Bonds. *Macromolecules* **2013**, 46, 7196-7201.
20. Shiraki, T.; Diesendruck, C. E.; Moore, J. S. The mechanochemical production of phenyl cations through heterolytic bond scission. *Faraday. Discuss.* **2014**, 170, 385-394.
21. Lenhardt, J. M.; Black, A. L.; Craig, S. L. gem-Dichlorocyclopropanes as Abundant and Efficient Mechanophores in Polybutadiene Copolymers under Mechanical Stress. *J. Am. Chem. Soc.* **2009**, 131, 10818-10819.
22. Chen, Y.; Spiering, A.; Karthikeyan, S.; Peters, G. W.; Meijer, E.; Sijbesma, R. P. Mechanically induced chemiluminescence from polymers incorporating a 1, 2-dioxetane unit in the main chain. *Nat. Chem.* **2012**, 4, 559.
23. Gossweiler, G. R.; Hewage, G. B.; Soriano, G.; Wang, Q.; Welshofer, G. W.; Zhao, X.; Craig, S. L. Mechanochemical Activation of Covalent Bonds in Polymers with Full and Repeatable Macroscopic Shape Recovery. *ACS Macro Lett.* **2014**, 3, 216-219.
24. Di Giannantonio, M.; Ayer, M. A.; Verde-Sesto, E.; Lattuada, M.; Weder, C.; Fromm, K. M. Triggered Metal Ion Release and Oxidation: Ferrocene as a Mechanophore in Polymers. *Angew. Chem. Int. Ed.* **2018**, 57, 11445-11450.

25. Sha, Y.; Zhang, Y.; Xu, E.; Wang, Z.; Zhu, T.; Craig, S. L.; Tang, C. Quantitative and Mechanistic Mechanochemistry in Ferrocene Dissociation. *ACS Macro Lett.* **2018**, *7*, 1174-1179.
26. Sha, Y.; Zhang, Y.; Xu, E.; McAlister, C. W.; Zhu, T.; Craig, Stephen L.; Tang, C. Generalizing metallocene mechanochemistry to ruthenocene mechanophores. *Chem. Sci.* **2019**, *10*, 4959-4965.
27. Zhang, Y.; Wang, Z.; Kouznetsova, T. B.; Sha, Y.; Xu, E.; Shannahan, L.; Fermen-Coker, M.; Lin, Y.; Tang, C.; Craig, S. L. Distal conformational locks on ferrocene mechanophores guide reaction pathways for increased mechanochemical reactivity. *Nat. Chem.* **2021**, *13*, 56-62.
28. Yan, Y.; Pageni, P.; Kabir, M. P.; Tang, C. Metallocenium chemistry and its emerging impact on synthetic macromolecular chemistry. *Synlett* **2016**, *27*, 984-1005.
29. Zhu, T.; Sha, Y.; Yan, J.; Pageni, P.; Rahman, M. A.; Yan, Y.; Tang, C. Metallo-polyelectrolytes as a class of ionic macromolecules for functional materials. *Nat. Commun.* **2018**, *9*, 4329.
30. Haaland, A. Molecular structure and bonding in the 3d metallocenes. *Accounts. Chem. Res.* **1979**, *12*, 415-422.
31. Opitz, J. Electron impact ionization of cobalt-tricarbonyl-nitrosyl, cyclopentadienyl-cobalt-dicarbonyl and biscyclopentadienyl-cobalt: appearance energies, bond energies and enthalpies of formation. *Int. J. Mass. Spectrom.* **2003**, *225*, 115-126.
32. Rowland, T. G.; Sztaray, B.; Armentrout, P. B. Metal–Cyclopentadienyl Bond Energies in Metallocene Cations Measured Using Threshold Collision-Induced Dissociation Mass Spectrometry. *J. Phys. Chem. A* **2013**, *117*, 1299-1309.
33. Zhang, J.; Chen, Y. P.; Miller, K. P.; Ganewatta, M. S.; Bam, M.; Yan, Y.; Nagarkatti, M.; Decho, A. W.; Tang, C. Antimicrobial Metallopolymers and Their Bioconjugates with Conventional Antibiotics against Multidrug-Resistant Bacteria. *J. Am. Chem. Soc.* **2014**, *136*, 4873-4876.

34. Zhang, J.; Yan, J.; Pageni, P.; Yan, Y.; Wirth, A.; Chen, Y.-P.; Qiao, Y.; Wang, Q.; Decho, A. W.; Tang, C. Anion-Responsive Metallopolymer Hydrogels for Healthcare Applications. *Sci. Rep.* **2015**, *5*, 11914.
35. Yang, P.; Bam, M.; Pageni, P.; Zhu, T.; Chen, Y. P.; Nagarkatti, M.; Decho, A. W.; Tang, C. Trio Act of Boronolactin with Antibiotic-Metal Complexed Macromolecules toward Broad-Spectrum Antimicrobial Efficacy. *ACS Infect. Dis.* **2017**, *3*, 845-853.
36. Pageni, P.; Yang, P.; Chen, Y. P.; Huang, Y.; Bam, M.; Zhu, T.; Nagarkatti, M.; Benicewicz, B. C.; Decho, A. W.; Tang, C. Charged Metallopolymer-Grafted Silica Nanoparticles for Antimicrobial Applications. *Biomacromolecules* **2018**, *19*, 417-425.
37. Cha, Y.; Jarrett-Wilkins, C.; Rahman, M. A.; Zhu, T.; Sha, Y.; Manners, I.; Tang, C. Crystallization-Driven Self-Assembly of Metallo-Polyelectrolyte Block Copolymers with a Polycaprolactone Core-Forming Segment. *ACS Macro Lett.* **2019**, *8*, 835-840.
38. Zhu, T.; Xu, S.; Rahman, A.; Dogdibegovic, E.; Yang, P.; Pageni, P.; Kabir, M. P.; Zhou, X.-d.; Tang, C. Cationic Metallo-Polyelectrolytes for Robust Alkaline Anion-Exchange Membranes. *Angew. Chem. Int. Ed.* **2018**, *57*, 2388-2392.
39. Musgrave, R. A.; Choi, P.; Harniman, R. L.; Richardson, R. M.; Shen, C.; Whittell, G. R.; Crassous, J.; Qiu, H.; Manners, I. Chiral Transmission to Cationic Polycobaltocenes over Multiple Length Scales Using Anionic Surfactants. *J Am Chem Soc* **2018**, *140*, 7222-7231.
40. Yan, Y.; Zhang, J.; Qiao, Y.; Tang, C. Facile Preparation of Cobaltocenium-Containing Polyelectrolyte via Click Chemistry and RAFT Polymerization. *Macromol. Rapid Commun.* **2014**, *35*, 254-259.
41. Sha, Y.; Zhu, T.; Rahman, M. A.; Cha, Y.; Hwang, J.; Luo, Z.; Tang, C. Synthesis of site-specific charged metallopolymers via reversible addition-fragmentation chain transfer (RAFT) polymerization. *Polymer* **2020**, *187*, 122095.
42. Shao, Y.; Gan, Z.; Epifanovsky, E.; Gilbert, A. T. B.; Wormit, M.; Kussmann, J.; Lange, A. W.; Behn, A.; Deng, J.; Feng, X.; Ghosh, D.; Goldey, M.; Horn, P. R.;

Jacobson, L. D.; Kaliman, I.; Khaliullin, R. Z.; Kuś, T.; Landau, A.; Liu, J.; Proynov, E. I.; Rhee, Y. M.; Richard, R. M.; Rohrdanz, M. A.; Steele, R. P.; Sundstrom, E. J.; Woodcock, H. L.; Zimmerman, P. M.; Zuev, D.; Albrecht, B.; Alguire, E.; Austin, B.; Beran, G. J. O.; Bernard, Y. A.; Berquist, E.; Brandhorst, K.; Bravaya, K. B.; Brown, S. T.; Casanova, D.; Chang, C.-M.; Chen, Y.; Chien, S. H.; Closser, K. D.; Crittenden, D. L.; Diedenhofen, M.; DiStasio, R. A.; Do, H.; Dutoi, A. D.; Edgar, R. G.; Fatehi, S.; Fusti-Molnar, L.; Ghysels, A.; Golubeva-Zadorozhnaya, A.; Gomes, J.; Hanson-Heine, M. W. D.; Harbach, P. H. P.; Hauser, A. W.; Hohenstein, E. G.; Holden, Z. C.; Jagau, T.-C.; Ji, H.; Kaduk, B.; Khistyayev, K.; Kim, J.; Kim, J.; King, R. A.; Klunzinger, P.; Kosenkov, D.; Kowalczyk, T.; Krauter, C. M.; Lao, K. U.; Laurent, A. D.; Lawler, K. V.; Levchenko, S. V.; Lin, C. Y.; Liu, F.; Livshits, E.; Lochan, R. C.; Luenser, A.; Manohar, P.; Manzer, S. F.; Mao, S.-P.; Mardirossian, N.; Marenich, A. V.; Maurer, S. A.; Mayhall, N. J.; Neuscamman, E.; Oana, C. M.; Olivares-Amaya, R.; O'Neill, D. P.; Parkhill, J. A.; Perrine, T. M.; Peverati, R.; Prociuk, A.; Rehn, D. R.; Rosta, E.; Russ, N. J.; Sharada, S. M.; Sharma, S.; Small, D. W.; Sodt, A.; Stein, T.; Stück, D.; Su, Y.-C.; Thom, A. J. W.; Tsuchimochi, T.; Vanovschi, V.; Vogt, L.; Vydrov, O.; Wang, T.; Watson, M. A.; Wenzel, J.; White, A.; Williams, C. F.; Yang, J.; Yeganeh, S.; Yost, S. R.; You, Z.-Q.; Zhang, I. Y.; Zhang, X.; Zhao, Y.; Brooks, B. R.; Chan, G. K. L.; Chipman, D. M.; Cramer, C. J.; Goddard, W. A.; Gordon, M. S.; Hehre, W. J.; Klamt, A.; Schaefer, H. F.; Schmidt, M. W.; Sherrill, C. D.; Truhlar, D. G.; Warshel, A.; Xu, X.; Aspuru-Guzik, A.; Baer, R.; Bell, A. T.; Besley, N. A.; Chai, J.-D.; Dreuw, A.; Dunietz, B. D.; Furlani, T. R.; Gwaltney, S. R.; Hsu, C.-P.; Jung, Y.; Kong, J.; Lambrecht, D. S.; Liang, W.; Ochsenfeld, C.; Rassolov, V. A.; Slipchenko, L. V.; Subotnik, J. E.; Van Voorhis, T.; Herbert, J. M.; Krylov, A. I.; Gill, P. M. W.; Head-Gordon, M. Advances in molecular quantum chemistry contained in the Q-Chem 4 program package. *Mol. Phys.* **2015**, *113*, 184-215.

43. Pritchard, B. P.; Altarawy, D.; Didier, B.; Gibson, T. D.; Windus, T. L. New Basis Set Exchange: An Open, Up-to-Date Resource for the Molecular Sciences Community. *J. Chem. Inf. Model.* **2019**, *59*, 4814-4820.

44. Tesch, M.; Kudruk, S.; Letzel, M.; Studer, A. Orthogonal Click Postfunctionalization of Alternating Copolymers Prepared by Nitroxide-Mediated Polymerization. *Chem. Eur. J.* **2017**, *23*, 5915-5919.
45. Zhu, T.; Sha, Y.; Firouzjaie, H. A.; Peng, X.; Cha, Y.; Dissanayake, D. M. M. M.; Smith, M. D.; Vannucci, A. K.; Mustain, W. E.; Tang, C. Rational Synthesis of Metallo-Cations Toward Redox- and Alkaline-Stable Metallo-Polyelectrolytes. *J. Am. Chem. Soc.* **2020**, *142*, 1083-1089.
46. Bowser, B. H.; Craig, S. L. Empowering mechanochemistry with multi-mechanophore polymer architectures. *Polym. Chem.* **2018**, *9*, 3583-3593.
47. Sha, Y.; Zhang, Y.; Xu, E.; McAlister, C. W.; Zhu, T.; Craig, Stephen L.; Tang, C. Generalizing metallocene mechanochemistry to ruthenocene mechanophores. *Chem. Sci.* **2019**, *10*, 4959-4965.
48. Riordan, A. R.; Jansma, A.; Fleischman, S.; Green, D. B.; Mulford, D. R. Spectrochemical series of cobalt (III). An experiment for high school through college. *Chem. Educator* **2005**, 115-119.
49. Wegner, S. V.; Schenk, F. C.; Spatz, J. P. Cobalt(III)-Mediated Permanent and Stable Immobilization of Histidine-Tagged Proteins on NTA-Functionalized Surfaces. *Chem. Eur. J.* **2016**, *22*, 3156-3162.
50. Kou, S.; Yang, X.; Yang, Z.; Liu, X.; Wegner, S. V.; Sun, F. Cobalt-Cross-Linked, Redox-Responsive Spy Network Protein Hydrogels. *ACS Macro Lett.* **2019**, *8*, 773-778.
51. Wegner, S. V.; Schenk, F. C.; Witzel, S.; Bialas, F.; Spatz, J. P. Cobalt Cross-Linked Redox-Responsive PEG Hydrogels: From Viscoelastic Liquids to Elastic Solids. *Macromolecules* **2016**, *49*, 4229-4235.
52. Helm, L.; Merbach, A. E. Inorganic and Bioinorganic Solvent Exchange Mechanisms. *Chem. Rev.* **2005**, *105*, 1923-1960.

53. Klein, I. M.; Husic, C. C.; Kovács, D. P.; Choquette, N. J.; Robb, M. J. Validation of the CoGEF Method as a Predictive Tool for Polymer Mechanochemistry. *J. Am. Chem. Soc.* **2020**, *142*, 16364-16381.
54. Beyer, M. K. The mechanical strength of a covalent bond calculated by density functional theory. *J. Chem. Phys.* **2000**, *112*, 7307-7312.
55. Bader, R. F. A quantum theory of molecular structure and its applications. *Chem. Rev.* **1991**, *91*, 893-928.
56. Bulat, F. A.; Toro-Labbé, A.; Brinck, T.; Murray, J. S.; Politzer, P. Quantitative analysis of molecular surfaces: areas, volumes, electrostatic potentials and average local ionization energies. *J. Mol. Model.* **2010**, *16*, 1679-1691.

CHAPTER 5
SUMMARY AND OUTLOOK

6.1 Dissertation Summary

In this dissertation work, two major research frontiers were explored. First, crystallization-driven self-assemblies of block copolymers consist of crystallizable block and cationic metallo block were developed. These block copolymers were prepared by carefully designed sequential polymerization techniques. The novel combination of metallo polyelectrolyte and crystalline polymer showed 2D platelet formation in protic solvent. The composition effect on the resultant micelle's morphologies was quite unprecedented: an increase in corona-forming block induced the morphological transition from the elongated hexagon to diamond-shaped 2D platelet. Their morphological transformation was further demonstrated by the blending of homo-PCL. Moreover, the ionic strength-dependent stabilization in the aqueous system was elucidated. The cationic characteristics of cobaltocenium have a critical role in micelle stabilization. This feature suggests that the 2D platelets obtained here may open up new possibilities for biomedical applications.

In the second part, the development of mechanical-responsive copolymers was achieved. First cyclic cobaltocenium olefin monomer was designed and synthesized. 1,1'-diallyl cobaltocenium was synthesized as a precursor for the cyclic cobaltocenium olefin monomer. Interestingly, this compound showed unexpected thermal isomerization. The RCM of these isomers resulted in two different cyclic cobaltocenium monomers: [3]-*ansa* cobaltocenium and [4]-*ansa* cobaltocenium hexafluorophosphate. The ring strain energy played a critical role in the formation of cyclic cobaltocenium. The cyclic cobaltocenium olefin monomers were used to synthesize main-chain cobaltocenium-containing copolymers. The results showed that these cyclic monomers were successfully

incorporated into the polymer backbone via ROMP. With the effort to synthesis main-chain cobaltocenium-containing polymers, mechano-responsiveness was also examined. Metallocene mechanophore recently has gained considerable attention due to its sensitivity toward external force. Unlike neutral metallocene, cationic cobaltocenium mechanophore showed a unique counterion-dependent dissociation mechanism. The computational study revealed that the chain scission of cobaltocenium underwent peeling-like dissociation. Moreover, ultrasonication of polymer solution showed unexpected back complexation, leading to increased molecular weight. This behavior might be a useful tool for material application, such as self-strengthening.

6.2 Outlook

Cobaltocenium with cationic charge and its self-assembly ability can be further developed to prepare antimicrobial micelles. As shown in this dissertation, the stability of the resultant micelles is quite dependent on their shell structures. Shell-crosslinking can be utilized to improve the micelle stability in the aqueous system. For example, thiol-ene click chemistry can be used via post-CDSA (**Figure 6.1A**). Shell-Crosslinking would afford the stable 2D micelles, which can be further used as a new type of antimicrobial agent.

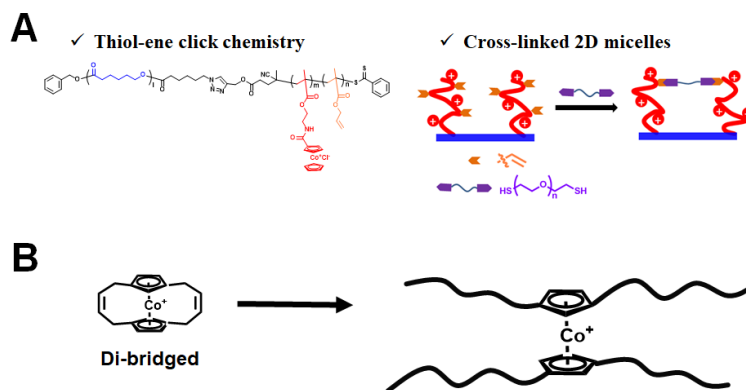










Figure 5.1. Schematic illustration of (A) Shell-crosslinking of 2D micelle and (B) application of di-bridged cobaltocenium for cross-linking of polymers.

The new cyclic cobaltocenium olefin monomer can be expanded to its application. The mechanical susceptibility and its post-dissociation behavior of cobaltocenium moiety can be combined to produce self-strengthening material. Cobaltocenium di-bridge can be utilized to construct a crosslinking system in hydrogel via ROMP (**Figure 6.1B**). The mechanical stress-induced damage can be healed by the back complexation of the dissociated adducts. Moreover, the ion-complex ability can be further developed for the stress-responsive color change, called mechanochroism. Although this dissertation demonstrated promising studies regarding the performance of cationic cobaltocenium-containing polymers as self-assembled nano-objects and mechano-responsive polymer, further investigations are required to expand its potential for biomedical and stimulus-responsive materials.

APPENDIX A
PERMISSION TO REPRINT

 Home
  Help
  Email Support
  Sign in
  Create Account



Stability of the Gyroid Phase in Diblock Copolymers at Strong Segregation. Volume 39, Number 7, March, 14, 2006, pp 2449–2451.
 Author: Eric W. Cochran, Carlos J. Garcia-Cervera, Glenn H. Fredrickson
 Publication: Macromolecules
 Publisher: American Chemical Society
 Date: Jun 1, 2006
Copyright © 2006, American Chemical Society

PERMISSION/LICENSE IS GRANTED FOR YOUR ORDER AT NO CHARGE

This type of permission/license, instead of the standard Terms & Conditions, is sent to you because no fee is being charged for your order. Please note the following:



- Permission is granted for your request in both print and electronic formats, and translations.
- If figures and/or tables were requested, they may be adapted or used in part.
- Please print this page for your records and send a copy of it to your publisher/graduate school.
- Appropriate credit for the requested material should be given as follows: "Reprinted (adapted) with permission from (COMPLETE REFERENCE CITATION). Copyright (YEAR) American Chemical Society." Insert appropriate information in place of the capitalized words.
- One-time permission is granted only for the use specified in your request. No additional uses are granted (such as derivative works or other editions). For any other uses, please submit a new request.





If credit is given to another source for the material you requested, permission must be obtained from that source.

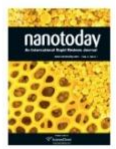
BACK
CLOSE WINDOW

© 2021 Copyright - All Rights Reserved | Copyright Clearance Center, Inc. | Privacy statement | Terms and Conditions
 Comments? We would like to hear from you. E-mail us at customer@copyright.com

Figure A. 1. Permission to reprint Figure 1.6.

 Home
  Help
  Email Support
  Yujin Cha



Block copolymer nanostructures

Author: Thomas Smart,Hannah Lomas,Marzia Massignani,Miriam V. Flores-Merino,Lorena Ruiz Perez,Giuseppe Battaglia

Publication: Nano Today

Publisher: Elsevier

Date: June–August 2008

Copyright © 2008 Elsevier Ltd. All rights reserved.

Order Completed

Thank you for your order.

This Agreement between Mr. Yujin Cha ("You") and Elsevier ("Elsevier") consists of your license details and the terms and conditions provided by Elsevier and Copyright Clearance Center.

Your confirmation email will contain your order number for future reference.

License Number 5034800564205 [Printable Details](#)

License date Mar 23, 2021

Licensed Content

Licensed Content Publisher	Elsevier
Licensed Content Publication	Nano Today
Licensed Content Title	Block copolymer nanostructures
Licensed Content Author	Thomas Smart,Hannah Lomas,Marzia Massignani,Miriam V. Flores-Merino,Lorena Ruiz Perez,Giuseppe Battaglia
Licensed Content Date	June–August 2008
Licensed Content Volume	3
Licensed Content Issue	3-4
Licensed Content Pages	9
Journal Type	S&T

Order Details

Type of Use	reuse in a thesis/dissertation
Portion	figures/tables/illustrations
Number of figures/tables/illustrations	1
Format	electronic
Are you the author of this Elsevier article?	No
Will you be translating?	No

About Your Work

Title	CATIONIC METALLO-POLYELECTROLYTE AND THEIR APPLICATION IN SELF-ASSEMBLY AND POLYMER MECHANOCHEMISTRY
Institution name	university of south carolina
Expected presentation date	Apr 2021

Additional Data

Portions	Figure 1.6
----------	------------

Tax Details

Publisher Tax ID	98-0397604
------------------	------------

Requestor Location

Mr. Yujin Cha	751 Mallet hill road 15208
Requestor Location	COLUMBIA, SC 29223 United States Attn: Mr. Yujin Cha

Price

Total	0.00 USD
-------	----------



Total: 0.00 USD


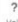


[CLOSE WINDOW](#)
[ORDER MORE](#)


© 2021 Copyright - All Rights Reserved | Copyright Clearance Center, Inc. | [Privacy statement](#) | [Terms and Conditions](#)
Comments? We would like to hear from you. E-mail us at customer@copyright.com

Figure A.2. Permission to reprint Figure 1.7.

137

 Home
  Help
  Email Support
  Yujin Cha



Polymer mechanochemistry: the design and study of mechanophores
 Author: Christopher W Bielawski, Kelly M Wiggins, Johnathan N Brantley
 Publication: Polymer International
 Publisher: John Wiley and Sons
 Date: Sep 6, 2012
 © 2012 Society of Chemical Industry

Order Completed

Thank you for your order.

This Agreement between Mr. Yujin Cha ("You") and John Wiley and Sons ("John Wiley and Sons") consists of your license details and the terms and conditions provided by John Wiley and Sons and Copyright Clearance Center.

Your confirmation email will contain your order number for future reference.

License Number: 5038400113279 [Printable Details](#)

License date: Mar 29, 2021

Licensed Content

Licensed Content Publisher: John Wiley and Sons

Licensed Content Publication: Polymer International

Licensed Content Title: Polymer mechanochemistry: the design and study of mechanophores

Licensed Content Author: Christopher W Bielawski, Kelly M Wiggins, Johnathan N Brantley

Licensed Content Date: Sep 6, 2012

Licensed Content Volume: 62

Licensed Content Issue: 1

Licensed Content Pages: 11

Order Details

Type of use: Dissertation/Thesis

Requestor type: University/Academic

Format: Print and electronic

Portion: Figure/table

Number of figures/tables: 1

Will you be translating?: No

About Your Work

Title: CATIONIC METALLO-POLYELECTROLYTE AND THEIR APPLICATION IN SELF-ASSEMBLY AND POLYMER MECHANOCHEMISTRY

Institution name: university of south carolina

Expected presentation date: Apr 2021

Additional Data

Portions: Figure 1.12

Tax Details

Publisher Tax ID: EUR26007151

Requestor Location

Mr. Yujin Cha
751 Mallet hill road 15208

Requestor Location

COLUMBIA, SC 29223
United States
Attn: Mr. Yujin Cha

Price

Total: 0.00 USD

Would you like to purchase the full text of this article? If so, please continue on to the content ordering system located here: [Purchase PDF](#)

If you click on the buttons below or close this window, you will not be able to return to the content ordering system.



[CLOSE WINDOW](#)
[ORDER MORE](#)





Total: 0.00 USD


© 2021 Copyright - All Rights Reserved | Copyright Clearance Center, Inc. | [Privacy statements](#) | [Terms and Conditions](#)

Comments? We would like to hear from you. Email us at customerscare@copyright.com.

Figure A.3. Permission to reprint Figure 1.12.

 Home
  Help
  Email Support
  Yujin Cha



Crystallization-Driven Self-Assembly of Metallo-Polyelectrolyte Block Copolymers with a Polycaprolactone Core-Forming Segment
 Author: Yujin Cha, Charles Jarrett-Wilkins, Md Anisur Rahman, et al
 Publication: ACS Macro Letters
 Publisher: American Chemical Society
 Date: Jul 1, 2019
Copyright © 2019, American Chemical Society

PERMISSION/LICENSE IS GRANTED FOR YOUR ORDER AT NO CHARGE

This type of permission/license, instead of the standard Terms & Conditions, is sent to you because no fee is being charged for your order. Please note the following:

- Permission is granted for your request in both print and electronic formats, and translations.
- If figures and/or tables were requested, they may be adapted or used in part.
- Please print this page for your records and send a copy of it to your publisher/graduate school.
- Appropriate credit for the requested material should be given as follows: "Reprinted (adapted) with permission from (COMPLETE REFERENCE CITATION). Copyright (YEAR) American Chemical Society." Insert appropriate information in place of the capitalized words.
- One-time permission is granted only for the use specified in your request. No additional uses are granted (such as derivative works or other editions). For any other uses, please submit a new request.

BACK
CLOSE WINDOW

© 2021 Copyright - All Rights Reserved | Copyright Clearance Center, Inc. | [Privacy statement](#) | [Terms and Conditions](#)
 Comments? We would like to hear from you. E-mail us at customerscare@copyright.com

Figure A.4. Permission to reprint Chapter 2.